Mapping the relationship between the subjective response of jurors to fan blade parameters

by

Sung bok Chung

Thesis presented in partial fulfilment of the requirements for the degree of Master of Engineering (Mechatronic) in the Faculty of Engineering at Stellenbosch University

Supervisor: Dr. J. Muiyser
Co-supervisor: Dr. M.P. Venter

March 2020

Declaration

By submitting this thesis elecronically, I declare that the entirety of the work contained therein is my own, original work, that I am the sole author thereof (save to the extent explicitly otherwise stated), that reproduction and publication thereof by Stellenbosch University will not infringe any third party rights and that I have not previously in its entirety or in part submited it for obtaining any qualification.

Date: .....

UNIVERSITEIT·STELLENBOSCH·UNIVERSITY
jou kennisvennoot • your knowledge partner

Plagiaatverklaring / Plagiarism *Declaration*

1 Plagiaat is die oorneem en gebruik van die idees, materiaal en ander intellektuele eiendom van ander persone asof dit jou eie werk is.
Plagiarism is the use of ideas, material and other intellectual property of another's work and to present it as my own.

2 Ek erken dat die pleeg van plagiaat 'n strafbare oortreding is aangesien dit 'n vorm van diefstal is.
I agree that plagiarism is a punishable offence because it constitutes theft.

3 Ek verstaan ook dat direkte vertalings plagiaat is.
I also understand that direct translations are plagiarism.

4 Dienooreenkomstig is alle aanhalings en bydraes vanuit enige bron (ingesluit die internet) volledig verwys (erken). Ek erken dat die woordelikse aanhaal van teks sonder aanhalingstekens (selfs al word die bron volledig erken) plagiaat is.
Accordingly all quotations and contributions from any source whatsoever (including the internet) have been cited fully. I understand that the reproduction of text without quotation marks (even when the source is cited) is plagiarism.

5 Ek verklaar dat die werk in hierdie skryfstuk vervat, behalwe waar anders aangedui, my eie oorspronklike werk is en dat ek dit nie vantevore in die geheel of gedeeltelik ingehandig het vir bepunting in hierdie module/werkstuk of 'n ander module/werkstuk nie.
I declare that the work contained in this assignment, except where otherwise stated, is my original work and that I have not previously (in its entirety or in part) submitted it for grading in this module/assignment or another module/assignment.

Studentenommer / *Student number*	**Handtekening / *Signature***
Voorletters en van / *Initials and surname*	**Datum / *Date***

Abstract

The noise generated by computer cooling fans is known to be a factor which may cause discomfort in the workplace. Aerodynamic noise caused by fan blades has been identified to be a significant factor which contributes largely to noise emission by fans. Fan parameters used in the design of fan blades are known to affect noise emission levels significantly. Considerations made for fan noise are known to be centred around taking unweighted and A-weighted sound pressure readings, with fan designs often being designed to limit sound pressure levels. The analysis made towards the unweighted and A-weighted sound pressure levels in the temporal and frequency domain alone is known to sufficiently define objective measures for fan noise. It is of interest to consider whether the subjective evaluation of noise made by jurors can also be accounted for.

The presented work is focused on identifying the feasibility of mapping the relationship between fan blade parameters to the subjective response of jurors, using the interim step of psychoacoustic analysis to make predictions for an expected level of annoyance towards fan noise emissions. Three blade parameters were selected for investigation, consisting out of blade chord, blade angle and sweep; these are considered to have significant effects on noise emissions produced by fan blades. Fifteen prototype models with varied blade parameters were created to investigate the effect which blade parameters have on the subjective evaluation of noise. Prototype models were created by 3D scanning and recreating a reference commercial fan, altering its blade parameters by using mesh morphing techniques.

Jury evaluation tests were used to collect data towards the perceived annoyance for fan noise using a forced pairwise comparison test, and a bipolar semantic differential test. The jury tests were used to obtain a ranking for prototype models, giving a relative measure of perceived preference, and also a description for noise, as experienced by jurors. Statistical analysis methods were used to fit simple, well-defined regression models, which were used to learn about the interaction effects present. One model, deemed adequate for making predictions on jury preferences, was selected and used for optimisation purposes. This model was optimised to determine the best expected performance, for a specific set of blade parameters. A final model using optimised blade param-

eters was 3D printed and used as a validation set to evaluate for the model. The optimised model was ranked 3^{rd} in the final, forced pairwise comparison test, where 20 jurors were asked to partake in the test. The presented work determined the relationship between blade parameters, psychoacoustic metrics and data obtained from subjective jury test results to determine the feasibility of determining jury preference from the parameters of a fan blade alone.

Opsomming

Die geraas wat 'n rekenaar se waaier genereer, is 'n faktor wat ongemak in die werkplek kan veroorsaak. En hoe harder die waaier werk, hoe groter is die ongewenste geraasvlakke dikwels ook. Aërodinamiese geraas, wat deur waaierlemme veroorsaak word, is geïdentifiseer as 'n belangrike faktor wat grootliks bydra tot die geraas wat 'n waaier vrystel. Die waaierparameters wat in die ontwerp van waaierlemme gebruik word, is bekend daarvoor dat dit 'n beduidende invloed het op die vlak van geraas wat gemaak word. Dit is bekend dat die oorwegings vir waaiergeraas, op die neem van ongeweegde en A-geweegde klankdruklesings berus, met waaiers wat dikwels ontwerp word om klankdrukvlakke te beperk. Die ontleding wat van die ongeweegde en A-geweegde klankdrukvlak gemaak word, in die tydelike en frekwensie-domein alleen, is bekend daarvoor dat dit op voldoende wyse objektiewe maatstawwe vir waaiergeraas omskryf. 'n Vraag van belang is egter of die subjektiewe evaluering van geraas deur 'n persoon wat dit beoordeel, ook verantwoord kan word.

Die werk wat hier aangebied word, fokus daarop om te bepaal hoe haalbaar dit is om die verband tussen die parameters van waaierlemme en die subjektiewe respons van beoordelaars te karteer, deur middel van psigo-akoestiese analise as tussenstap te gebruik om voorspellings te maak oor die irritasievlak wat 'n waaier se geraas na verwagting sal veroorsaak. Vir die ondersoek is drie parameters van 'n waaierlem geselekteer: naamlik die koord, die hoek en die swiep van die lem, wat geïdentifiseer is as elemente wat 'n aansienlike invloed het op die geraas wat waaierlemme maak. Vyftien prototipiese modelle, met verskillende lemparameters, is geskep om die effek te ondersoek wat lemparameters het op die subjektiewe evaluering van geraasuitset, soos waargeneem deur die beoordelaars. Die prototipiese modelle is geskep deur 3D-skandering en die herskepping van 'n kommersiële waaier as verwysing deur sy lemparameters, deur middel van sogenaamde mesh morphing-tegnieke te verander.

Tweeledige beoordelaarsevalueringstoetse is gebruik om data te versamel oor die werklik waargenome ergernis weens waaiergeraas: naamlik, 'n gedwonge paargewys-vergelykende toets en 'n bipolêre semantiese differensiaaltoets. Die beoordelaarstoetse is gebruik om 'n rangorde vir die prototipiese modelle te bepaal, deur 'n relatiewe maatstaf van waargenome voorkeur te gee, asook

'n beskrywing van die geraas, soos deur die beoordelaars ervaar. Statistiese ontledingsmetodes is daarna gebruik om 'n eenvoudige, goed gedefiniëerde regressiemodel op die data toe te pas, en die model is gebruik om meer te wete te kom oor die wisselwerking tussen lemparameters, psigo-akoestiese maatstawwe en die subjektiewe reaksie van beoordelaars. Die sensitiwiteit vir modelle is bepaal en 'n model, wat met behulp van lemparameters, voorspellings oor beoordelaarsvoorkeur kon maak, is geselekteer en geoptimaliseer vir 'n stel lemparameters wat na verwagting die beste prestasie sou gee. 'n Finale model met lemparameters wat uit die optimalisering voortgespruit het, is 3D gedruk en as 'n valideringstel gebruik om die model te evalueer. In die finale, gedwonge paargewys-vergelykende toets, waarin 20 beoordelaars gevra is om aan die toets deel te neem, is die optimeerde model derde geplaas. Die werk wat hier aangebied word, het die verband bepaal tussen lemparameters, psigo-akoestiese maatstawwe en data, wat uit subjektiewe beoordelaarstoetse verkry is, om te bepaal hoe haalbaar dit is om beoordelaarsvoorkeur op grond van die parameters van 'n waaierlem alleenlik, te bepaal.

Acknowledgements

I would like to express my sincere gratitude to the following people who helped me and provided me with support. I would first like to thank my family for their encouragement and prayers, always looking after me in times of distress and need. Secondly, I would like to thank my supervisors Dr Muiyser and Dr Venter, for their continuous support and guidance. Lastly I would like to thank God for his continuous guidance and peace, being the pillar who I rely on regardless of the circumstances.

Contents

List of Figures

List of Tables

Nomenclature

Due to the study being multidisciplinary, the nomenclature will be separated based on appropriate chapters and sections in which the symbols can be found. This is to allow field-specific symbols to be used whenever applicable.

Abbreviations

PA	Psychoacoustic Annoyance
SPV	Scaled Prediction Variance
SLA	Stereolithography
RSM	Response Surface Methodology
SPL	Sound Pressure Level
GUI	Graphic User Interface
BFP	Blade Pass Frequency
FFD	Free Form Deformations
RSM	Response Surface Methodology
3D	Three Dimensional
USB	Universal Serial Bus
CCD	Central Composite Design
CPU	Central Processing Unit
DAC	Digital to Analogue Converter
FDM	Fused Deposition Modelling
AMD	Air Moving Device
PWM	Pulse Width Modulation
2AFC	Two Alternative Forced Comparison

Chapter 2

n_{b}	Number of blades	[−]
v_{rot}	Rotational velocity	[rpm]
C_L	Coefficient of lift	[−]
η	Sweep	[degrees]
δ	Blade skew	[degrees]

F	Fluctuation strength	[vacil]
p	Position of maximum camber	[−]
R	Roughness	[asper]
PA	Psychoacoustic annoyance	[−]
ν	Dihedral angle	[degrees]
ζ	Stagger angle	[degrees]
β	Blade angle	[degrees]
$\Delta\beta$	Change in blade angle	[degrees]
s	Pitch spacing	[m]
c	Chord length	[m]
r_m	Mean radius	[m]
r_h	Fan blade inner (hub) radius	[m]
r_t	Fan blade tip radius	[m]
z	Critical bands	[Bark]
g	Weighting factor	[−]
N	Total loudness	[Sone]
N_5	Five percentile loudness	[Sone]
N'	Specific loudness	[Sone/Bark]
S	Sharpness	[acum]
ΔL	Level difference for temporal masking pattern	[−]
f_{mod}	Modulation frequency	[Hz]
G	Total number of comparisons for 2AFC	[−]
h	Total number of variables considered in 2AFC	[−]
A	Single example design variable used in 2AFC	[−]
B	Single example design variable used in 2AFC	[−]
C	Single example design variable used in 2AFC	[−]
D	Single example design variable used in 2AFC	[−]
E	Single example design variable used in 2AFC	[−]

Chapter 3 and Appendix A

θ	Angle of rotation	[degrees]
ϕ	Surface elevation angle	[degrees]
r	Radius/ vertex radius length	[m]
$\Delta\beta_{\text{max}}$	Maximum angle of rotation for blade tip vertex	[degrees]
a	Stacking line equation coefficient ($a = 0.0431426$)	[−]
b	Stacking line equation coefficient ($b = 0.1589838$)	[−]
θ_{out}	Fan blade outer ring maximum angle change	[degrees]

x	Spatial x co-ordinate	[m]
y	Spatial y co-ordinate	[m]
y'	Change in spatial y co-ordinate system (derivative)	[−]
x'	Change in spatial x co-ordinate system (derivative)	[−]
x_{ref}	Spatial reference aerofoil scaling direction	[m]
x_{new}	New vertex node x co-ordinate with altered sweep	[m]
y_{new}	New vertex node y co-ordinate with altered sweep	[m]
x_{node}	vertex node x co-ordinate with a radius r_{node}	[m]
y_{node}	vertex node y co-ordinate with a radius r_{node}	[m]
$\Delta\theta_{calc}$	Change in vertex node degree of rotation	[degrees]
k	Number of design variables considered in CCD	[−]
σ	Standard deviation	[−]
α	Design threshold	[−]
F	CCD Design parameter used in RSM	[−]
$\hat{y}$	Predicted statistical dependent variable	[−]
n_c	Number of center runs in CCD	[−]
$\boldsymbol{x}$	Vector of design variables used in CCD	[−]
C	Chord length	[m]
B	Blade angle	[degrees]
S	Blade sweep	[degrees]
a_1	Length measure equivalent to an α value of 1	[−]
b_1	Length measure equivalent to an α value of 1.414	[−]
V	Variable representing either C, B or S	[−]
V+	Marginally increased variable	[−]
V−	Marginally decreased variable	[−]
VM	Variable value set to maximum value	[−]
Vm	Variable value set to minimum value	[−]

Chapter 4

$q_{V,max}$	Maximum flow rate of the scaled plenum	[m^3/s]
V_0	nominal air volume of the full size plenum	[m^3]
V	nominal air volume of the scaled plenum	[m^3]
x	Spatial x co-ordinate	[m]
y	Spatial y co-ordinate	[m]
z	Spatial z co-ordinate	[m]
r	Hemi-spherical measurement surface radius	[m]
D_{IAi}	Directivity index	[dBA]

L_{pAi}	Background noise corrected SPL	[dBA]
i	Measured microphone position number	[−]
$\overline{L_{pA}}$	Mean surface SPL over the hemispherical dome	[dBA]
N_M	Number of microphone positions	[−]
L_{pAi}	Background noise corrected time-averaged SPL	[dBA]
L'_{pAi}(ST)	Time averaged A-weighted SPL	[dBA]
K_{1Ai}	Background noise correction value	[dBA]
L_{pAi}(B)	Time averaged SPL for background noise	[dBA]
L_{cal}	Calibration SPL reading	[dB]
P_{meas}	Measured pressure reading during calibration	[Pa]
N_1	Initial fan speed reading	[rpm]
Q_1	Initial airflow reading at N_1	[m^3/s]
H_1	Initial static pressure reading at N_1	[m^3/s]
N_2	Scaled fan speed reading	[rpm]
Q_2	Scaled airflow reading at N_2	[m^3/s]
H_2	Scaled static pressure reading at N_2	[m^3/s]
N_5	Five percentile loudness	[Sone]
F	Fluctuation strength	[vacil]
S	Sharpness	[acum]
R	Roughness	[asper]
PA	Psychoacoustic annoyance	[−]
w_S^2	PA adjustment co-efficient influenced by S	[−]
w_{FR}^2	PA adjustment co-efficient influenced by F and R	[−]

Chapter 5

n	Row index	[−]
n	Column index	[−]
x_n	nth sound stimuli	[−]
x_m	mth sound stimuli	[−]
a_{nm}	Comparison made between the nth and mth sound stimuli	[−]
Q	Quartiles	[−]
$Q0$	Lower limit for quartile range	[−]
$Q1$	Lower quartile	[−]
$Q2$	Median	[−]
$Q3$	Upper quartile	[−]
$Q4$	Upper limit for quartile range	[−]

Chapter 6

ϵ	Error term	[−]
β_a	ath coefficient	[−]
x_n	nth statistical independent variable	[−]
$\hat{y}$	statistical dependent/ predictor variable	[−]
p	p-value used in ANOVA	[−]
α_c	p-value criterion threshold	[−]
H_0	Null hypothesis	[−]
H_1	Alternate hypothesis	[−]
$\mathbf{C}$	variable representing blade chord	[−]
$\mathbf{S}$	variable representing blade circumferential sweep/sharpness	[−]
$\mathbf{B}$	variable representing blade angle	[−]
$\mathbf{F}$	variable representing fluctuation strength	[−]
$\mathbf{R}$	variable representing roughness	[−]
$\mathbf{L}$	variable representing loudness	[−]
A	Coefficient	[−]
B	Coefficient	[−]
C	Coefficient	[−]
r	Pearson's r value	[−]
$f(\boldsymbol{x})$	Maximisation problem	[−]
$F(\boldsymbol{x})$	Minimisation problem	[−]
$\boldsymbol{x}$	Vector of independent variables	[−]

Chapter 1

Introduction

1.1 Background and problem statement

The design of small fans typically used in the cooling of electronic components is driven not only by their performance, in terms of airflow and pressure rise, but also the noise that they generate. These fans are often used in close proximity to people, making the subjective response that people have to the noise generated important to consider.

Figure 1.1.1: Baseline fan model (Corsair, 2018)

The main focus of this project was to conduct experiments that could be used to map the subjective response of fan noise directly to fan blade parameters. The primary fans in consideration consisted of a 120 mm×120 mm computer cooling fans with a select baseline fan shown in Figure 1.1.1. As the noise emitted from fan blades was of interest, it was beneficial to mitigate as much noise as possible from other fan noise sources. This baseline fan was selected as it used magnetic levitation bearings, reducing motor to bearing noise (Corsair, 2018).

Psychoacoustic metrics, as well as jury evaluation tests, were used to evaluate the subjective response to fan noise. Previous work by Schneider (2015:2) has quantified the sound quality of computer fans in terms of the standardized psychoacoustic metrics. These metrics include loudness, sharpness, roughness and fluctuation strength (Fastl, 2013). These metrics are typically used to indicate whether a person would find a sound pleasant or not, with higher values of loudness and sharpness, leading to a less pleasant sound. In addition to these psychoacoustic metrics, jury testing has also been used to determine the subjective response to fan noise (Schneider and Feldmann, 2015). Here several jurors are subjected to a set of stimuli and asked to rank the fan noises from most to least pleasant as well as classify each noise in terms of several semantic adjectives, such as 'powerful' or 'calming'. This subjective response can then be mapped to the objective psychoacoustic parameters to provide information regarding people's preference in the specific context.

It is proposed that the subjective response of a jury can be predicted directly from the parametric design of the fan, without the opaque intermediate steps of relating the blade parameters to noise metrics, the jury result to noise metrics and then relating the psychoacoustic metrics to the blade parameters. The research makes use of statistical analysis to predict preference between recorded sounds generated by prototype rotor models. The novel contribution of this project is shown as a block diagram in Figure 1.1.2 with blade parameters mapped to the subjective response.

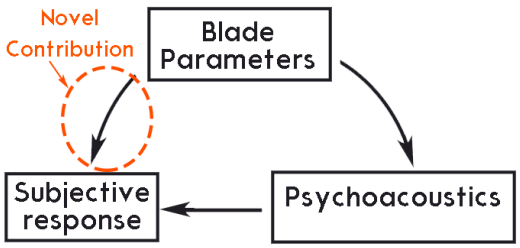

Figure 1.1.2: Block diagram showing correlation between datasets

1.2 Research objectives and overview

The aim of this project was to conduct experiments used to map the subjective response of fan noise to fan blade parameters. The project was focused on collecting data used to correlate between blade parameters, psychoacoustic measures and the subjective response for jurors. The main objectives for this project are listed as follows:

1. Create fan prototype models used to determine the effect of varying blade parameters.
2. Collecting data through prototype model noise measurements and jury evaluation tests.
3. Fit statistical models using blade parameter and the subjective response data.
4. Create an optimized fan model and evaluate the performance of the select model.

The diagram showing the main flow of the project is represented in Figure 1.2.1. Performance tests for fans were considered outside the scope of this project, but measurements for the airflow and static pressure were still considered to assess whether or not certain fan designs were more feasible than others.

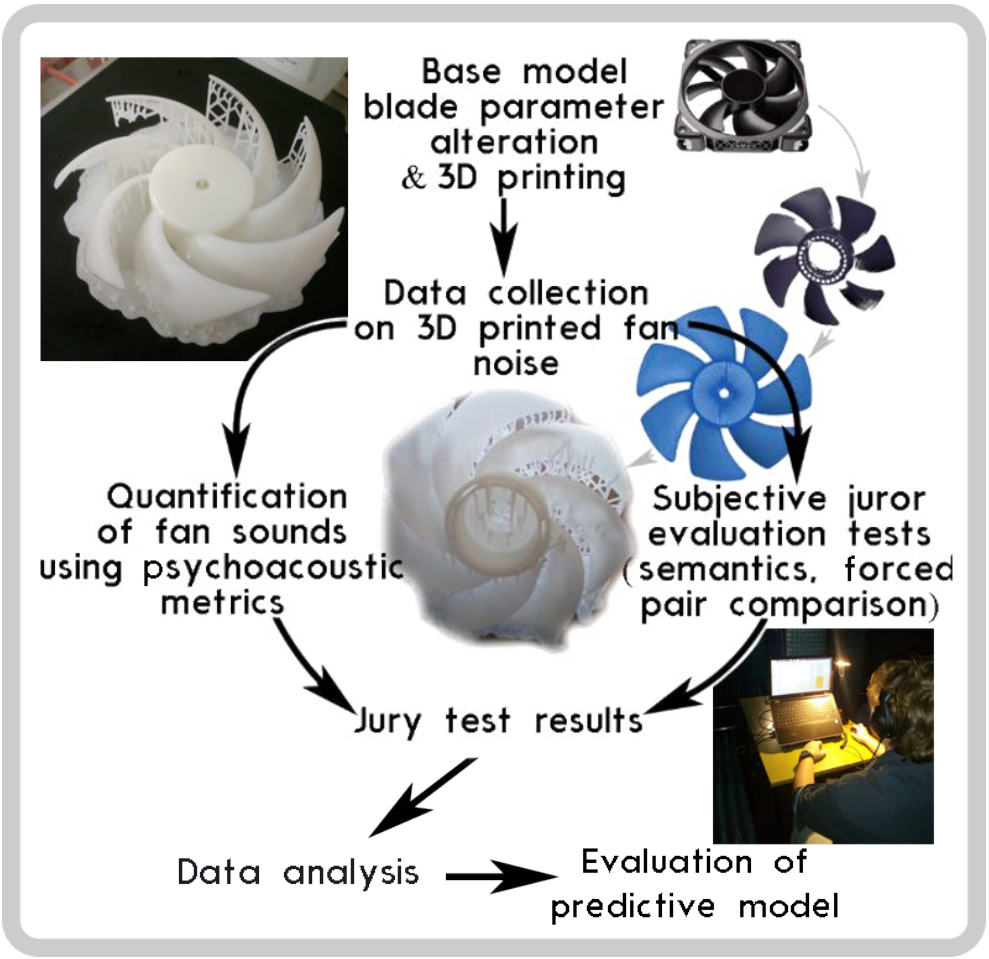

Figure 1.2.1: Flow diagram presenting the main project flow

Chapter 2

Literature study

The literature study conducted will be discussed in this chapter. The study was aimed at identifying relevant information necessary to provide motivation and insight on the data which will be collected. Literature, as found relevant to the select fan parameters, psychoacoustic metrics, subjective jury responses, and data analysis methods, will be mentioned. In addition, necessary terminology providing background, with relevant research contributions will also be discussed.

2.1 Computer cooling fan

The design of small fans typically used in the cooling of electronic components consists mainly of low-pressure axial fans. The performance of axial fans, as well as its reduction in noise, influence a large portion of how a fan is designed. For many electronic components, the cooling unit is known to have the greatest influence on the noise generated, more specifically, the blade profile (Bies *et al.*, 2017). Figure 2.1.1 shows a disassembled axial fan describing fan components. For an axial computer fan, the profile of the fan blade is of major importance. This is due to the blade being the major component for noise generation for fans (Sharland, 1964). A list of a few common parameters used in fan design includes the number of blades, camber, blade angle, sweep, and chord length distributions.

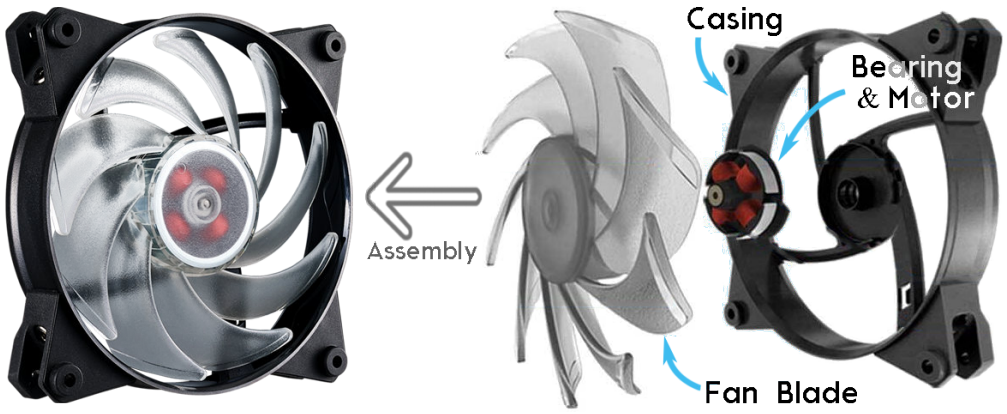

Figure 2.1.1: Axial computer cooling fans

For a given fan blade, an aerofoil blade profile is used to characterise the dimensions of the fan blade (Gudmundsson, 2013). The aerofoil profiles at the hub and tip often describe the maximum and minimum deviations for aerofoil geometry, with varied aerofoil distributions present in the design of profiled blades. The hub is the base on which fan blades are mounted, while the tip is the furthest region of the blade from the hub. Blade parameters often used to describe aerofoil geometry consists of blade angle, chord, and camber. The blade angle is described as the angle which the blade aerofoil makes with the direction of rotation or movement of the blade. The blade angle is often called the angle of attack for aerofoil profiles. The chord is the distance between the leading and trailing edge and the camber is defined as the distance between the camber and chord line. The parameters which characterise important dimensions for a fan aerofoil is given in Figure 2.1.2. Aerofoil sections are commonly taken as tangential cutouts for a given radius with each profile considered being parallel to one another. Tangential aerofoil sections denote the profiled blade with sweep removed as described by Vad (2008).

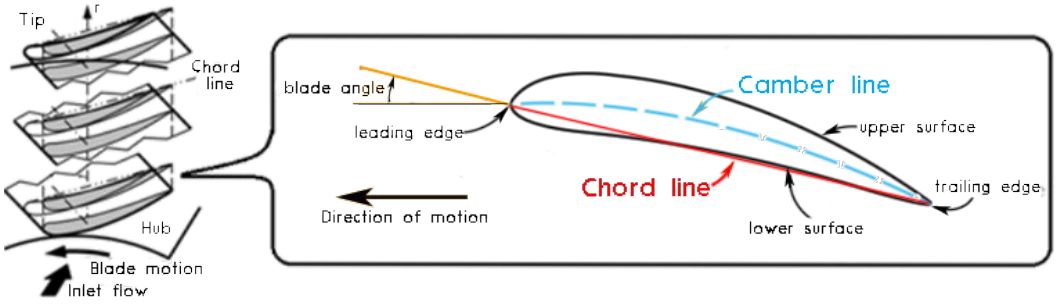

Figure 2.1.2: Fan blade aerofoil (Vad, 2008)

2.2 Blade design parameters affecting noise

A major contribution to the acoustic power for noise is associated with its broadband SPL component (Anghinolfi *et al.*, 2016: 1) with tonal noise also identified to cause annoyance levels. The following study was conducted to identify parameters which have the largest influence to fan noise as identified in literature. The focus was aimed at identifying parameters which are primarily considered in the design for blade aerodynamics and noise. A selection will be made from identified parameters used to conduct experimental research.

2.2.1 Fan noise spectrum analysis

Analysis, as made by Wright and Simmons (1990) towards noise emissions for fans, will be discussed. Wright and Simmons (1990) identify an important analysis of the spectral content of fan noise. Figure 2.2.1 shows the various spectral content plot over a log frequency plot. By analysing the spectral noise characteristics, noise associated with random, periodic or steady forces was identified from fan blades. Wright and Simmons (1990:2) made contributions to examining blade sweep aimed to alleviate the dominant source of noise. The benefits for sweep angle was further supported by Metzger and Rohrback (1986) as well as Hanson (1985). The studies were directed in reducing blade tonal noise through phase shift cancellation methods incorporating blade-to-blade interference. As shown in Figure 2.2.1 different causes for noise sources are present; classified as noise emission from steady thrust radiation, excess noise, laminar shedding noise and turbulent shedding noise as suggested by Wright and Simmons (1990:2).

The main critical source of noise was identified to be the 'Excess noise' category, as shown in Figure 2.2.1. According to Wright and Simmons (1990:2), the mentioned 'Excess noise' group emits noise most sensitive as seen on a dBA-scaled weighting curve; closely depicting sensitivity for human hearing. The use of large axial separation methods from turbulent sources; as well as the use of skewing blade alignment is identified to be two methods which have been used to minimize the identified noise category of concern (Wright and Simmons, 1990:2). The more efficient method, as identified by Wright and Simmons (1990:2) includes the study of noise reduction related to how a change in blade sweep may alleviate problems associated with noise.

Wright and Simmons (1990) identifies that Cummings (1972) and Brown (1977) also supports the approach on varying sweep for a fan blade. More specifically, research as done by Envia and Kerschen (1986) provide a basis for selecting distributions of sweep angle. Envia and Kerschen (1984) also provide slight insight on selecting varying sweep angles aimed to cause phase shift cancellation for noise in theory. An interesting finding by Fukano *et al.* (1978) identifies that sweeping blades have considerably larger effects to noise with increased

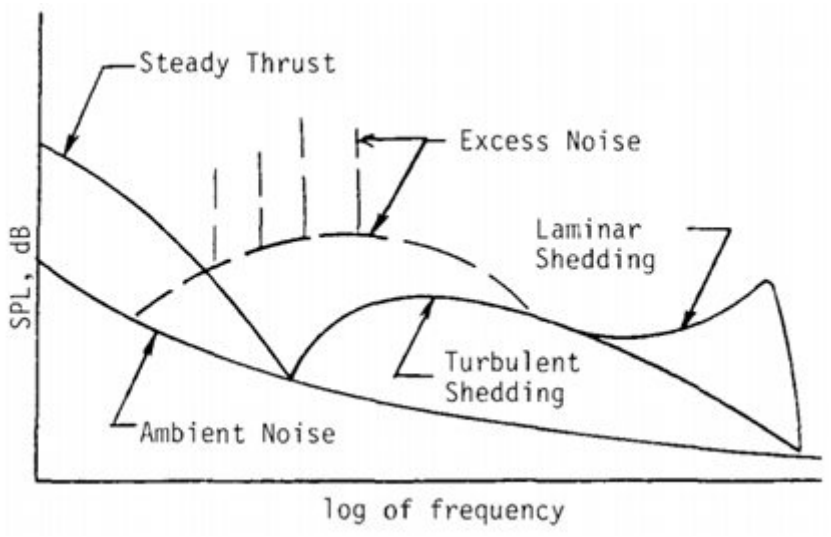

Figure 2.2.1: Fan noise spectrum over frequency (Wright and Simmons, 1990:2)

chord length. Blade sweep is commonly applied in blade design to reduce noise levels. With blade chord influencing the performance of sweep, both sweep and chord were identified to be relevant parameters which should be considered as parameters to be investigated.

Sweeping blades, as identified by Wright and Simmons (1990:7) is known to reduce the pure tone SPL level at blade pass frequency (BPF) given by equation 2.2.1.

$$BPF = v_{\text{rot}} \times n_{\text{b}}/60 \tag{2.2.1}$$

The variable v_{rot} denotes the rotational velocity measured in rpm and n_{b} the number of blades as given in equation 2.2.1. It is also discussed by Wright and Simmons (1990:7) that forward sweep should also decrease broadband noise for fans, but there is a degree of uncertainty as to this effect.

2.2.2 Influence of blade angle on noise

Sturm *et al.* (2015) made use of analytical models for the prediction of fan noise based on tonal and broadband analytical models. It was concluded that the main broadband noise created was due to the trailing edge noise source for isolated axial fans also supported by Blake (2017: 417). Hutcheson and Brooks (2006) studied the effect of blade angle and concluded that increased blade angle is mostly associated with increased trailing edge noise. Amiet (1976) identified the trailing edge noise to be a major contributing factor to fan noise, studying the effect of noise emission due to turbulent operating conditions. Glegg and Devenport (2008) noted that the trailing edge noise is often considered the main source of noise for rotor only noise emissions. A similar argument was made by Filleul (1966). Li *et al.* (2016) also identify that changes

to blade angle create notable effects on the aeroacoustic traits for axial flow fan, although an abnormal blade configuration was used. The investigation, as conducted by Li *et al.* (2016) was more beneficial in terms of identifying the influence which an abnormal blade angle has on the performance of a baseline fan.

The study, as conducted by Nashimoto (2008:369), gave a visual means to identify noise emissions for a fan as seen in Figure 2.2.2. The noise emissions present in the leading and trailing edge of the fan was identified to contribute largely to noise emission levels. Visually, the leading edge seemed to have a larger influence to noise levels as seen in Figure 2.2.2a (suction side); but Figure 2.2.2b showed motivation that noise emission near the trailing edge might also contribute largely when visualised from the side view orientation. Glegg and Devenport (2009) and Filleul (1966) identifies that a general trend increase over the whole frequency spectrum to be expected with increasing blade angle.

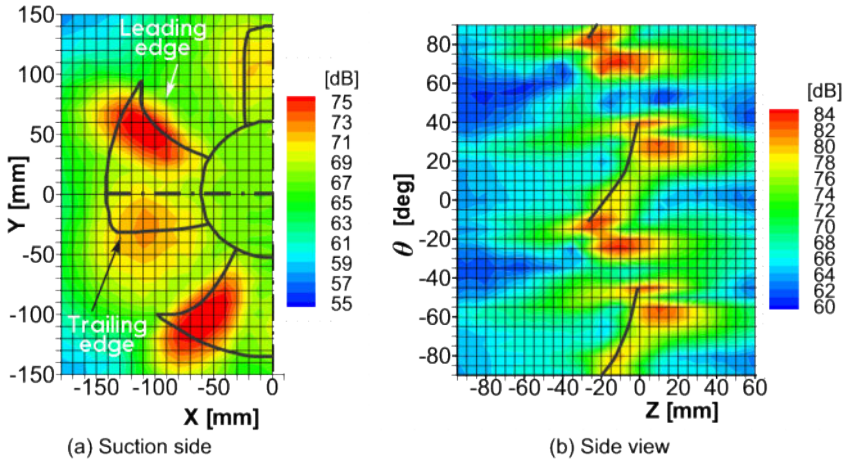

Figure 2.2.2: Visualisation for fan rotor noise region (Nashimoto, 2008:368)

Blade angle is identified as a parameter which is often considered critical to performance for fans due to its influence on the coefficient of lift (C_L). Increasing blade angle is commonly known to also increase lift for a fan blade (Clancy, 1975). In addition, increasing lift causes the amount of air being deflected from the fan blade to increase proportionally till a point is reached where fan blades no longer perform well. This point of operation for fans is commonly known as the stalling point. The stall is an important phenomenon which must be avoided as it drastically reduces performance for fans as the airflow will no longer follow the blade surface uniformly and begin to fall off. Increasing blade angle will equivalently increase the amount of air being deflected, and pressure generated until the stalling point is reached where the amount of pressure being generated stops increasing and normally falls off (Clancy, 1975). Blade angle has significant implications towards the noise level as well

as effects on performance. Therefore, blade angle was considered an important design parameter to be considered.

2.2.3 Influence of chord and other blade parameters on noise emission

Blade chord and additional blade parameters identified in literature to have an important influence on noise emissions will be mentioned. Additional parameters include blade thickness, camber and the number of blades. Fukano *et al.* (1978), as well as Quinlan and Bent (1998:184), studied the effects to altering blade thickness for a fan blades trailing edge as well the outer blade profile namely the blade tip. It was determined that turbulent noise could be reduced by thinning down the fan blade thickness towards the trailing edge (Fukano *et al.*, 1978). In relation to other parameters cambering a fan blade was determined to have lesser contributions to reducing the sound power but had considerable effects on the aerodynamic characteristic for fans. Wright and Simmons (1990) supported by Fukano *et al.* (1978) identifies the number of blades to influence fan noise emission. It is argued that with increasing blade number, the number of noise sources also increases. Wright and Simmons (1990:193), Cumpsty (1977) also identifies that a doubling of blade chord increases noise as it was determined that broadband noise is a function of blade chord and blade thickness. In comparison to Fukano *et al.* (1978:276) and Bianchi *et al.* (2009:1386), Wright and Simmons (1990) argues that blade thickness has a lesser influence as compared to blade chord.

2.3 Selection of blade parameter ranges of interest

Blade parameters select to conduct experimental research consisted out of sweep, chord and blade angle. The study, as found relevant in altering the parameters, will be addressed. With blade parameters selected, it was necessary to determine feasible parameter ranges to be used for experimental analysis. The terminology used for the three select blade parameters and relevant literature, will be addressed.

2.3.1 Sweep

Blade sweep as defined by Wright and Simmons (1990:2) can be explained by the angle which is created between the stacking line and radial line for a fan blade which has been altered to bend in a radial direction as shown in Figure 2.3.1. It is said that the fan is forward-swept when it is tilted in the direction of rotation and swept backwards when tilted against the direction of rotation. Work as mentioned by Fukano *et al.* (1977) concluded that forward sweep

shows significant enhancement on noise reduction as opposed to blades swept rearwards. Rearward sweep was also identified to reduce noise, but due to the inclusion of noise associated with higher-frequency broadband noise; it was identified to be less desirable. As such, the design study have been limited to only incorporating forward sweep.

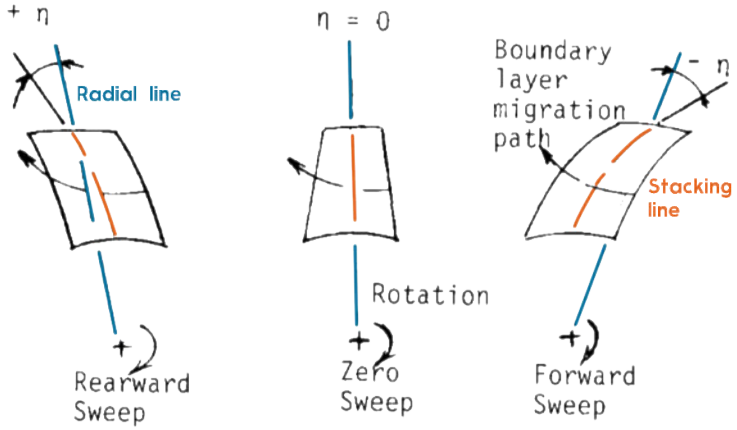

Figure 2.3.1: Definition of blade sweep (Wright and Simmons, 1990:3)

Many definitions for blade sweep exists a few examples as mentioned by Fukano *et al.* (1977) is shown in Figure 2.3.2 showing simple linear and circular transitions for sweep. A more complex design for blade sweep also exists for which sweep has been optimized and designed for optimum aerodynamic efficiency and operation (Van der Spuy *et al.*, 1997:17) but requires much more complex design procedures. As such, a more general definition of sweep as defined for Beiler et al. (1999) was used. Beiler *et al.* (1999) takes a similar definition for sweep as Wright and Simmons (1990). Both Beiler *et al.* (1999) and Wright and Simmons (1990) refer to the effects to sweep and dihedral effects for an axial fan. The only difference present is in the notation which Beiler *et al.* (1999) makes for which he defines the combinational effect of sweep and dihedral to be known as skew. Beiler *et al.* (1999) defines blade skew (δ) to be the interaction of both blade sweep (λ) and dihedral angle (ν) but with the dihedral angle being omitted blade skew will equate to blade sweep as described by Beiler *et al.* (1999). Beiler *et al.* (1999) discusses two methods for incorporating blade sweep consisting out of a variable change to blade sweep dependant on the blades radial position or a constant blade sweep incorporated in the design. A constant sweep angle was characterised by fan blades being tilted in the circumferential direction.

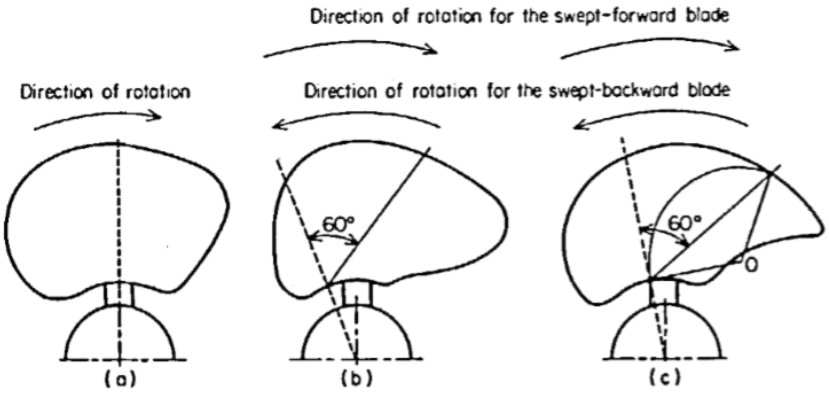

Figure 2.3.2: Examples of varying definition for blade sweep (Fukano *et al.*, 1977)

A design region for constant sweep considered by Beiler *et al.* (1999) was between 45° backwards sweep and 45° forward sweep. No mention was made of the select range for sweep to be the maximum and minimum values which should be considered. This is to say that higher values for sweep can also be considered further supported by Beiler *et al.* (1999) considering an additional fan design incorporating 60° forward sweep outside the select design region for sweep investigated. The same method incorporating constant blade sweep was used by Smith and Yeh (1963). The analogy used by Smith and Yeh (1963) was identified to be the same definition for constant sweep as used by Beiler *et al.* (1999). Smith and Yeh gave ranges for blade sweep which was even higher than 60° dependant on the Mach number of the fan, but due to uncertainties present for performance measures used, a maximum value of 60° forward sweep was considered. Although a set value for sweep is most commonly used in literature; studies as conducted by Mohammad and Raj (1977) also conclude that a higher sweep angle would be most desired but the main limiting factor for sweep would be due to mechanical considerations of the fan blade. Mohammad and Raj (1977) considered a lower range for sweep but regardless, came to the conclusion that including more sweep other than the select range in the study was identified to be beneficial. Specifics used to alter for sweep according to the definition of Beiler *et al.* (1999) will be discussed further in the section describing fan geometry morphing techniques.

2.3.2 Blade angle

McKensie (1997) notes that the blade angle (β) to be defined as 90°-ζ, where the stagger angle (ζ) of the blade is defined as the angle between the aerofoil chord line to the axis of rotation. With inspection to the original fan model, it was necessary to find an appropriate method to change for blade angle. A design region for blade angle needed to be selected. Therefore, the following literature review was conducted to select ranges for blade angle and also

methods used to alter for blade angle. In literature the blade angle is expected to range between 0° and 90° (Clancy, 1975) with design considerations made to avoid stall, and provide a value as desired for the coefficient of lift (C_L). Stall can be identified by referring to the static pressure performance values where a drastic drop in pressure rise will be seen. A study was conducted for which a maximum deviation in blade angle ranged between a change in angle of maximum change $\Delta\beta \leq 50°$ (Li *et al.*, 2016). The study as conducted by Li *et al.* (2016) was aimed at identifying the effect of an abnormal blade angle altered for a single blade affecting performance.

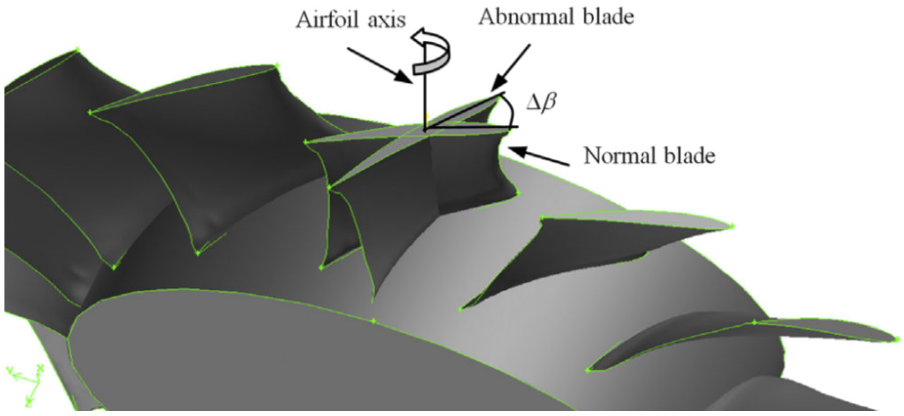

Figure 2.3.3: Study on the effect of an abnormal blade angle (Li *et al.*, 2016)

Although change to the blade angle was made to only one blade, the study shows how a change to a single blade can have great effects on the efficiency as well as performance when deviated from a baseline design. Li *et al.* (2016) shows that the effects to pressure rise only drops by 0.7% whereas efficiency notably declines by 7% when $\Delta\beta = 10°$. Once $\Delta\beta \geq 20°$ both pressure rise and efficiency for fan blades drop dramatically. When compared to normal conditions pressure rise declines by 25%, 46% and 53%, and efficiency was decreased by 25%, 33%, 36% and 40% for $\Delta\beta = 20°$, 30°, 40° and 50°. With performance and efficiency for fans decreasing drastically between design region above $\Delta\beta = 20°$; $\Delta\beta \leq 15°$ was select to be the maximum change for blade angle which should be considered. Other studies, as conducted by Van der Spuy *et al.* (1997) also investigate the use of blade angles between the range of 5° and 45°. Due to uncertainty being present for the select design criteria being feasible; measures of pressure rise need to be used to identify whether or not stall is present for fan designs. As long as pressure rise does not normally drop off due to stall, fan designs were considered relevant to be used for investigative purposes.

Different ways to change the blade angle are identified in literature focussing on the design for blade aerofoil profiles. A design method used to alter blade angles needed to be selected. Inspecting the orientation of aerofoils for a select

baseline fan was used as a reference to select the pivots for which blade angle for blade aerofoils was changed. The theory used by Eck (1972) was used to identify ways in which blade angle should be altered. As seen in Figure 2.3.4, two design approaches were used to alter for blade angle. Blade aerofoil sections were taken tangentially to radial positions as shown in Figure 2.3.4 with each aerofoil being parallel to each other. Aerofoil profiles were identified to have pivot points located either in line with the trailing edges interaction line of the fan blade as shown in Figure 2.3.4(a) or around the centre axis of the blade as shown in Figure 2.3.4(b), for a variable profiled fan blade.

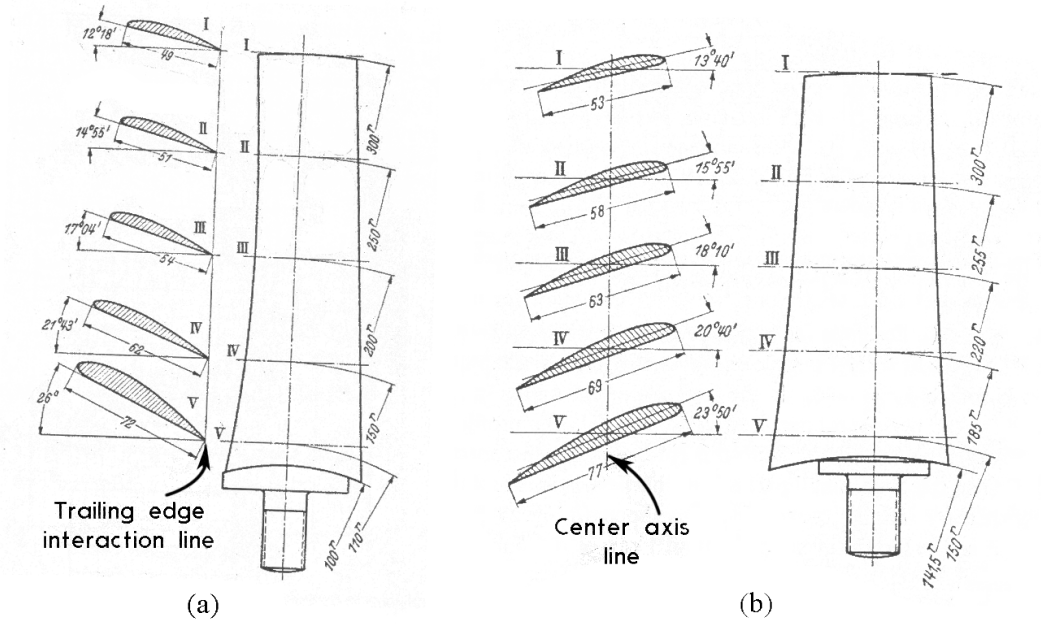

Figure 2.3.4: Profiled blade design (Eck, 1972:130)

2.3.3 Blade chord

Select methods as used to alter blade chord and to determine design ranges will be discussed. Considering aerofoil profiles for a given fan blade it is believed that aerofoils can be adequately defined by the blades maximum thickness, the position of the maximum blade thickness, the camber line, the position of the blade maximum camber and the thickness of the leading and trailing edges. As noted by Carter *et al.* (1960) these quantities do not completely define the profile, but given these quantities, the variations one would expect from manufacturing techniques are known to be sufficiently described. It was also noted that tests conducted in literature indicated that the effect of leading and trailing edge thickness only had a minor effect to the aerodynamic performance according to Carter *et al.* (1960); provided that the trailing edge thickness is not allowed to become excessive.

An adaptation to the parameters affecting aerofoil geometry is shown in Figure 2.3.5 (Huang and Gau, 2012). A small adjustment to the Figure was made rather using the British convention for aerofoil thickness where the thickness is measured perpendicular to the chord line rather than the camber line. The use of the British conventions allowed for better visualisation on how the camber distribution was kept constant as a percentage of chord with altered aerofoil chord. To alter blade chord while keeping other blade parameters for a given aerofoil constant, it was identified that scaling aerofoil profile only in the x axis direction as given in Figure 2.3.5 was most appropriate.

Although this method may change the ratio between blade thickness and chord which is often used as a parameter to define standardized aerofoil profiles which include NACA and F-series aerofoil profiles; the camber distribution and blade thickness remained constant in terms of position in terms of chord ratio; while keeping the majority of the dominant geometric factors constant which include the upper, lower and maximum camber thickness (t_a) and positions relative to percentage chord ('p' in Figure 2.3.5 denotes the position of maximum camber relative to percentage chord given as a ratio between 0 and 1).

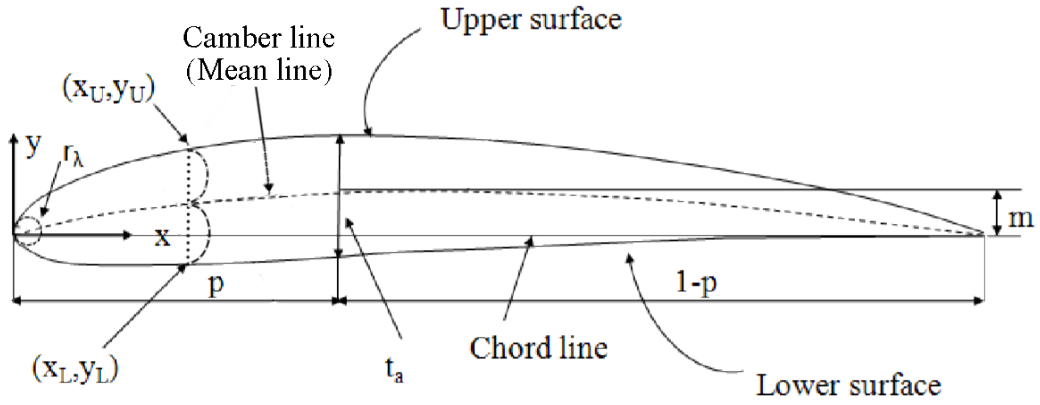

Figure 2.3.5: Blade aerofoil (Huang and Gau, 2012)

One of the most important design factors for axial fans is related to the blade solidity ratio which is defined as the ratio of blade chord length to pitch spacing between blades (blade solidity $= c/s$).

$$s = 2\pi \times r_m / n_b \tag{2.3.1}$$

$$r_m = [(r_t^2 + r_h^2)/2]^{0.5} \tag{2.3.2}$$

The equation for the pitch spacing (s) is determined by the equation 2.3.1 where r_m is the mean radius and n_b the number of blades. For the case of axial flow fans the mean radius r_m is calculated using equation 2.3.2 where r_h

is the inner radius of the fan blade at the hub and r_t the tip radius. Blade solidity has been identified to generally fall in the range of 0.4-1.1 (Peng, 2008) as such the design limits for alterations to chord length was chosen by ensuring that the alterations to chord do not influence blade solidity to reach unreliable regions of design.

2.4 Psychoacoustics

Fan models are often designed to limit levels of noise emission using blade parameters. It is proposed that the use of psychoacoustic measures of annoyance can be used to describe the quality of noise emissions for fans better. Studies, as conducted in the field of psychoacoustics, provided models which can be used to quantitatively measure the expected levels of annoyance as perceived by people (Fastl and Zwicker, 2006). By determining how well blade parameters correlate to psychoacoustic metrics; the feasibility for a model used to map blade parameters to psychoacoustic metrics can be determined. A Head Acoustic Squadriga (Head Acoustics, 2010) portable recording device was used to make noise recordings; with measures for psychoacoustic metrics determined using the program Artemis Suite from Head Acoustics.

2.4.1 Literature contributions

Relevant literature and contributions found will be discussed in this section relating studies for psychoacoustics to fan noise. Zenger *et al.* (2017) studied the effect which sweep has to the noise quality using psychoacoustic measures of sharpness and loudness (Fastl and Zwicker, 2006). Zenger *et al.* (2017) mentions that backwards skewed blades improve the acoustic emissions for blades at low flow rates while forward skewed blades show improvements to the hydraulic property, efficiency while reducing noise emissions.

Schneider and Feldmann (2015) conducted a study evaluating the noise sample for three different computer fans with varying number of blades and inflow conditions. The psychoacoustic characteristic for each noise sample for the different fans was determined, and juror testing was conducted to assess the character of each different noise source using semantic differentials and paired comparison tests. The paper concluded that psychoacoustic parameters are most necessary to take the subjective noise sensation of the juror into account.

Schneider and Feldmann (2015:2) make use of four psychoacoustic metrics consisting out of loudness, sharpness, roughness and fluctuation strength. These psychoacoustic metrics were used to predict what is called the psychoacoustic annoyance. The model for psychoacoustic annoyance as proposed by Fastl and Zwicker (2006:328) is used to determine expected levels of annoyance for measured noise. The study conducted by Schneider and Feldmann (2015) in-

vestigated the influence of various inflow conditions, fan speed and operating points on sound quality. Through jury testing and analysis of psychoacoustic metrics, a strong correlation between loudness and the subjective annoyance factor was determined; but a statement was also made that fluctuation strength and tonality can play an important role when considering fans operated near stall.

It was determined that psychoacoustic parameters of fan noise could be influenced by varying fan inflow conditions as well as the rotational speed and operating point where loudness has the greatest impact on annoyance levels. Schneider and Feldmann (2015) used the psychoacoustic parameters in conjunction with semantic differentials and paired comparison tests to create a modified formulation for the noise annoyance factor. A more recent study was conducted by Feldmann and Schneider (2017) evaluating the sound quality of fan systems using novel semantic differentials and a predictive model. It was determined that the perceived sound quality of fan systems is mainly determined by the loudness and tonality of the sound with no significant impact being noticed on the influence of sharpness as well as roughness.

Study as conducted by Yang and Zhu (2016a) also considered the subjective evaluation for fan noise using paired comparison tests and psychoacoustic measures. Yang and Zhu (2016a) collected sound samples by recording fan noise present for TV and radio signal transmission stations. The correlation between psychoacoustic metrics to data obtained from a pairwise comparison test was made. The psychoacoustic metrics of sharpness, loudness, fluctuation strength and roughness (Fastl and Zwicker, 2006) with the SPL readings and A-weighted sound levels were identified to be in high correlation with the subjective evaluation for responses as obtained from a paired comparison test. Results indicated that only tonality, articulation index and speech intelligibility were negatively relevant.

Muiyser *et al.* (2018) studied the effect which straight and swept blades have on sound quality metrics. The analysis was made using psychoacoustic metrics for loudness, sharpness, fluctuation strength, and roughness (Fastl and Zwicker, 2006) used to calculate the psychoacoustic annoyance metric. Muiyser *et al.* (2018) determined how annoyance values for fans were entirely dominated by the metric loudness with changes to sharpness having little effect across a range of operating points. The reduction in noise level generated by fans with forward swept fans has been identified to be a dominating factor when compared to fans with straight blades. Muiyser *et al.* (2018) also identified relevant literature from Novak *et al.* (2005), Sottek and Genuit (2007), Minorikawa *et al.* (2015), and Yang and Zhu (2016b) contributing to literature on the evaluation of fan noise using psychoacoustic analysis.

Novak *et al.* (2005) investigated the validity of using sound quality metrics to compare for three select computer fan designs. Novak *et al.* (2005) reported the loudness, sharpness, prominent tone and articulation index in terms of fan rotational speed. No description for fan designs were given, and only suggestions were made that psychoacoustic sound quality metrics should be used in analysis of product quality for computer cooling fans.

Yang and Zhu (2016b) performed a non-linear regression analysis on sound quality metrics, objective metrics and the results obtained from a pairwise comparison test; using data obtained from Yand and Zhu (2016a). The researchers presented regression models and determined that the subjective evaluation of stimulus is only a function of loudness, sharpness, sound pressure level and the A-weighted sound level. This result indicated that for specific fans being tested, tonality, speech intelligibility, articulation index, fluctuation strength and roughness did not influence the subjective evaluation.

Minorikawa *et al.* (2015) investigated the tonal components of small cooling fans. The study was conducted using the tone to noise ratio and prominence ratio metrics. After conducting jury testing, a strong correlation was identified by the tone to noise ratio, prominence ratio and the subjective response. This result obtained by Minorikawa *et al.* (2015) further supported the need to consider sound quality metrics with SPL analysis when analysing fan noise.

2.4.2 Critical band rate

To calculate for psychoacoustic metrics loudness and sharpness, the critical-band rate used to describe hearing sensations is important to consider as described by Zwicker (2008:158). This is due to critical bands describing the frequency bandwidth of the inner ears auditory filter describing frequency bands which will avoid interference effects caused by auditory masking (Fletcher and Munson, 1933). The critical band analogy is used most often in the analysis of psychoacoustics that a unit was defined leading to a so-called critical-band rate scale. This scale is based on the fact that our hearing system makes an analysis of a broad spectrum into parts that correspond to critical bands. The scale produces 24 abutting critical bands which have the unit 'Bark'. Figure 2.4.1a shows the critical bandwidth as a function of frequency from which the critical bandwidth scale is determined as shown in Figure 2.4.1b. As shown by 2.4.1b, each critical band corresponded to a unit of 'Bark' has an upper limit which corresponds to the lower limit of the next higher critical band.

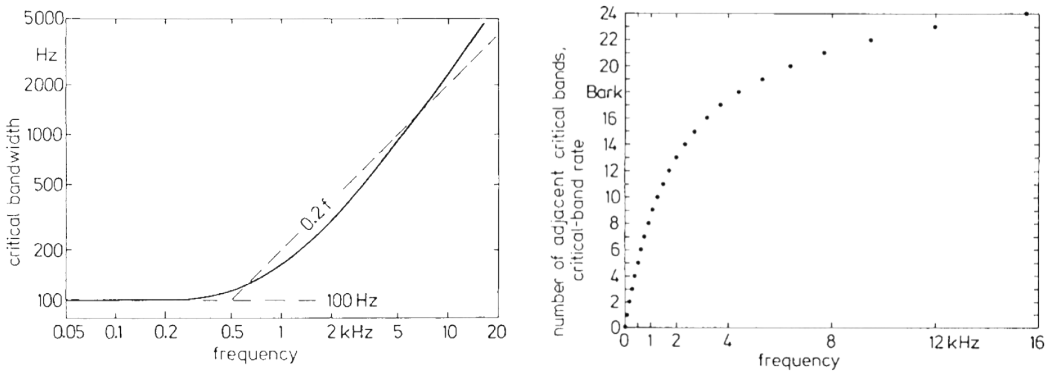

(a) Critical bandwidth as a function of frequency

(b) Numeral associated with the sequence of adjacent critical bands

Figure 2.4.1: Critical band rate (Fastl and Zwicker, 2006:159-161)

2.4.3 Loudness

Loudness, as defined in psychoacoustics, is characterized as the sensation of intensity for a sound stimulus (Fastl and Zwicker, 2006:220). Loudness is not characterised only by a magnitude value but belongs somewhere between sensational and physical value. In analysis of Zwicker's proposed analysis, loudness was measured according to the DIN 45631/A1 (DIN, 2010) standard applicable for stationary and transient loudness. The notation z denotes the selection of critical bands from 0 to 24 bark.

$$N = \int_0^{24\,\text{Bark}} N'.dz \tag{2.4.1}$$

Zwicker makes use of the critical band rate measured in 'Bark' to determine for total loudness (N) measured in units of 'Sone'. Analysis for loudness is also known to be made using units of Sone/Bark. The equation as given by Zwicker for the model of loudness, is shown by equation 2.4.1. The notation N denotes the total loudness as described by Zwicker and N' the specific loudness which is the loudness value determined over each Bark level. Using Zwicker's loudness model, a pure tone producing 40 dB at 1 kHz would equate to a measure of 1 Sone used as a reference value. When calculating for psychoacoustic annoyance, the five percentile loudness value is used (N_5). Percentile loudness describes a loudness value which is reached or exceeded for a select percentage of time. For a constant steady-state noise source, the percentile loudness value is known to be very close to the total loudness value. Fan noise sources considered will be operated in steady-state. Therefore the percentile loudness was determined to be equal to the total loudness considered for this study.

2.4.4 Sharpness

Sharpness, as defined in psychoacoustics, is characterised as a sensory trait which is most influential to sensory pleasantness for noise. With the increase in measures of sharpness, the level of expected sensory pleasantness is also predicted to decrease (Fastl, 2015:239). For steady-state noise, there has been a tendency to transfer everything not related to the sensation of loudness or pitch to a residual of sensation known as timbre. With this definition of timbre, the sensation of 'sharpness' is known to be contained as a subgroup which describes sound density. Sharpness, as described by Zwicker (2006:240), is measured in units of 'acum' where the reference sound producing 1 acum is known to be a narrow-band noise one critical-band wide at a centre frequency of 1kHz having a level of 60 dB.

Noise which contains high frequency content has been identified to be more annoying according to analysis made using critical-band wide narrowbands. Fastl and Zwicker (2006:240) describe that sharpness increases faster than the critical-band rate at the centre frequency for narrowband noise; which can be used as an explanation why high-frequency sounds produce a sensation that is dominated by their sharpness.

$$S = 0.11 \frac{\int_0^{24\,\text{Bark}} N' g(z) z . dz}{\int_0^{24\,\text{Bark}} N' . dz} \quad \text{acum} \tag{2.4.2}$$

The model of sharpness as given by Fastl and Zwicker (2006:240) is shown by equation 2.4.2 where the weighting factor $g(z)$ is determined by using Figure 2.4.2. Sharpness was measured using Aure's sharpness using DIN 45631/A1 (DIN, 2010) Specific loudness and Aure's algorithm for sharpness.

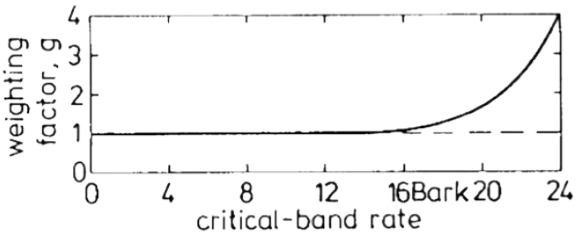

Figure 2.4.2: Weighting factor for sharpness as a function of critical-band rate (Fastl and Zwicker, 2006:240)

2.4.5 Fluctuation strength

Fluctuation strength used in the study of psychoacoustics is characterised by time-dependent modulation changes which influence the perceived sound quality for signals. Fluctuation strength is an objective metric that is dependant

on low modulation frequencies lower than 20 Hz. Units of 'vacil' are used to measure for fluctuation strength. The reference value for fluctuation strength is defined by a tone of 1 kHz at 60 dB with a 100% modulation at a modulation frequency of 4 Hz. Equation 2.4.3 gives a model which is used to determine the fluctuation strength using definitions as given by Fastl and Zwicker (2006:256). Figure 2.4.3 shows how certain parameters as given by 2.4.3 is determined on the temporal domain. The notation ΔL denotes the level difference between the maximum and minimum variation present for the temporal masking pattern. Masking to known to occur when the perception of one sound is affected by the presence of another sound stimuli (Fastl and Zwicker, 2006:61). The combination of various noise sources output from a fan is considered to create various masking patterns in the temporal domain. Measurements for fluctuation strength was made using a hearing model developed by Sottek and Genuit (2007).

$$F = \frac{0.008 \int_0^{24\,\text{Bark}} (\Delta L/\text{dB Bark}).dz}{(f_{\text{mod}}/4\,\text{Hz}) + (4\,\text{Hz}/f_{\text{mod}})} \quad \text{vacil} \tag{2.4.3}$$

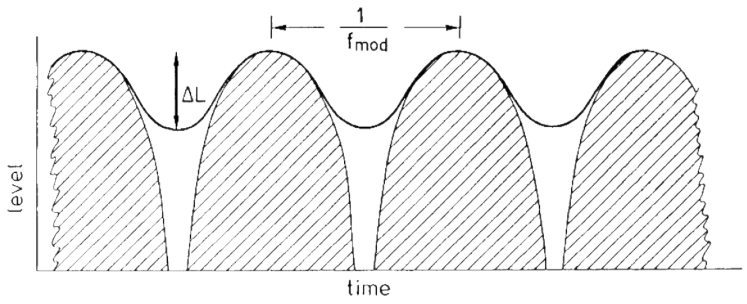

Figure 2.4.3: Model of fluctuation strength (Fastl and Zwicker, 2006:256)

2.4.6 Roughness

The model for roughness (R) as given by Fastl and Zwicker (2006:257) is measured in units of 'asper' and is characterised by the equation $R \approx f_{\text{mod}} \Delta L$. Both these values can be referred to by the Figure as seen by 2.4.3 shown for fluctuation strength. Similar to fluctuation strength, roughness is known to be induced due to factors contributing to modulation frequencies. Primary causes are known to be from either frequency or amplitude modulation. In contrast to fluctuation strength which is considered for very low modulation frequencies below 20 Hz, roughness considers frequency ranges between 20 to 300 Hz. For the purpose of sound measurements as made by Artemis the hearing model as developed by Sottek and Genuit (2007) was used to measures roughness.

2.5 Jury evaluation tests

Studies as conducted by Scheider and Feldmann (2015) make use of both psychoacoustic measures as well as jury testing procedures to evaluate the subjective response of fan noise. Psychoacoustic measures are used to estimate the expected level of pleasantness for sound stimuli while jury evaluation tests are used to clarify and determine the quality of noise as perceived by people. Measurement scales are necessary to distinguish ranking between fan noise. To rate the effect of different design parameters, Dieter and Schmidt (2013) mentions two scales of measurement which need to be understood, the ordinal and nominal scale; used to measure the response of people.

The nominal scale is a named category or identifier; making a comparison on whether a category is the same or not, such as when making a distinction between 'yes or no'. The ordinal scale is a measurement scale used to place items in rank order, first, second, third etc.; making comparison as to whether a stimulus considered is greater or less in terms of a measure of concern. A comparison made using the ordinal scale can determine whether two stimuli being compared is better, worse or equal when compared to each other. Still, it does not describe the magnitude of how much variables differ, making addition and subtraction infeasible (Dieter and Schmidt, 2013: 261).

Ranking as obtained from jury testing is determined using the ordinal scale, which calls for decisions based on subjective preferences. The following sections will describe jury testing procedures used to collect data on jurors preferences to fan noise; used with measures of psychoacoustics to evaluate the subjective response for fan noise. Two jury evaluation tests will be considered, namely the semantic differential test and pairwise forced comparison test; being the most commonly used tests to determine for sound characteristics (Kleiner, 2011). Both tests considered made use of the ordinal scale, respectively.

2.5.1 Bipolar semantic differential test

The semantic differential test (Schneider and Feldmann, 2015; Kleiner, 2011) is used to make an assessment using adjectives to describe specific isolated sound characteristics. Listeners are instructed to rate their impression on a given Likert scale; being a bipolar scaling method used to measure either a positive or a negative response. Figure 2.5.1 gives an example of a six-level bipolar semantic differential test, used for juror evaluation.

adjective scales	
loud	soft
deep	shrill
frightening	not frightening
pleasant	unpleasant
dangerous	safe
hard	soft
calm	exciting
bright	dark
weak	powerful

Figure 2.5.1: Example of a bipolar semantic differential test using a six-level Likert scale

An example adjective scale used as shown in Figure 2.5.1, which does not restrict a test person to specific points; having the advantage of an absence of numerical value, with the limited use of words minimizing word bias (Kleiner, 2011). Each adjective used to describe the sound will, in return, have a best and worst trait, giving a reflection on how stimuli were perceived.

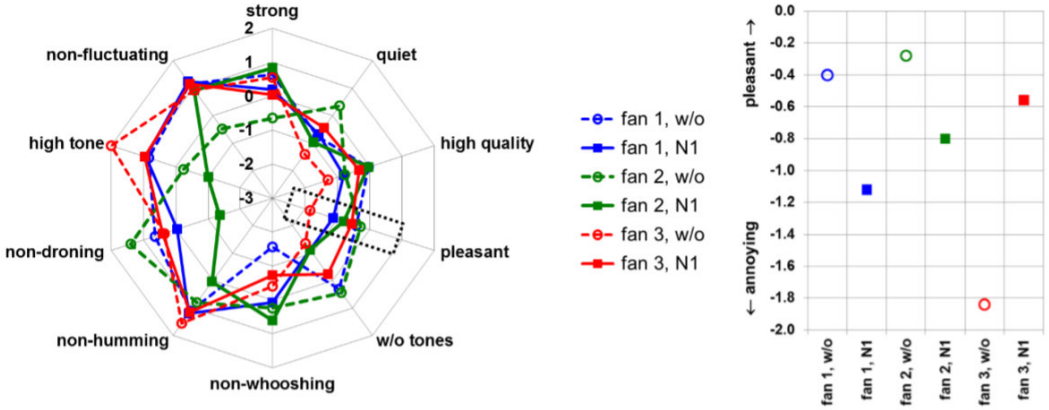

Figure 2.5.2: Bipolar semantic differential test results (Schneider and Feldmann, 2015)

A study as conducted by Schneider and Feldmann (2015) listed ten bipolar semantic adjectives which can be used to describe fan noise best, given in Figure 2.5.2. The adjectives consisted of strong, quiet, high quality, pleasant, without tone, non-whooshing, non-humming, non-droning, high tone and non-fluctuating. With fan noise being evaluated in this project, the suitability for the select adjectives as used by Schneider and Feldmann (2015) was relevant. Semantic adjectives, listed by Schneider and Feldmann (2015), were used to conduct bipolar semantic differential tests for this project.

2.5.2 Forced-choice pairwise comparison test

Ranking on an ordinal scale calls for decisions to be made based on subjective preferences for jurors. One method of ranking alternatives on an ordinal scale

is to make use of the method of pairwise comparisons (Dieter and Schmidt, 2013). Each design variable considered is listed and is compared to every other variable using pairs of two samples compared with one another. If the test conducted does not allow for a neutral selection between stimuli, the pairwise comparison is called a forced-choice comparison test (Bi, 2015:5). The juror is not allowed to indicate that two samples have no difference and as such is called the forced comparison or 2AFC (two-alternative forced-choice).

The method of forced pairwise comparison will be explained using the example table as given by Dieter and Schmidt (2013), shown by Table 2.5.1. The Design criterion, as given by table 2.5.1 describes the variables being considered, which for the purpose of this project would represent fan noise stimuli from prototype models. Each design criterion listed is compared to every other criterion, two at a time. With a comparison made, the criterion perceived to be less annoying is given a tally of 1 with the other criterion being compared given 0. The total number of comparisons (G) made is calculated using the equation $G = h(h-1)/2$ where h is the number of variables being considered.

Considering the case as given by Table 2.5.1, with five design variables A, B, C, D and E considered, a comparison of A being made to B will be used as an example for explanatory purposes. With A being select as the preferred stimuli, a tally of 1 is assigned to A and 0 to B. In building the matrix as given by Table 2.5.1 a value of 1 indicates that the criterion considered in the row is preferred to the criterion considered in the column. As such, with a single pairwise comparison being made, two values would be placed on the matrix; with a value of 0 and 1 placed on opposite ends from the main diagonal. To clarify, in comparing variable A to C, with C determined to be preferred; a value of 0 is placed in row A and column C, and a value of 1 in row C and column A. The ranking for each stimuli being compared is determined by adding the tally for each row, with a higher number of tally indicating higher preferences to the specific sound.

Table 2.5.1: Paired comparison test (Dieter and Schmidt, 2013)

Design Criterion	**A**	**B**	**C**	**D**	**E**	**Row Total**
A	—	1	0	0	1	2
B	0	—	1	1	1	3
C	1	0	—	0	0	1
D	1	0	1	—	1	3
E	0	0	1	0	—	1
						—
						10

Chapter 3

Geometry manipulation

3.1 Introduction

Prototype fan models need to be created with varied blade parameters to investigate the effect which blade parameters have on noise. This chapter focusses on the 3D scanning and printing steps used to create prototype fan models from a select commercial fan used as a baseline. The steps and procedures used to manipulate fan geometry; as well as the criterion used to select parameter values for final rotor models are discussed. The main process consisted of obtaining a 3D scan for a reference fan, and applying geometry manipulation to the model with blade parameters of interest. An HP 3D Structured Light Scanner Pro S2 was used to 3D scan a baseline fan blade profile (HP 3D Scan, 2019). Figure 3.1.1 shows the 3D scan model of a computer fan selected to be the base model. The final 3D scanned profile contained regions of discontinuity, as such it was necessary to redesign the fan rotor and clean up the fan model for it to be 3D printable.

Figure 3.1.1: 3D scanned model view

3.2 Mesh wrapping

A vertex meshing creation and fitting method was used to create a mesh which overlapped with the original 3D scanned profile using 3Ds Max. This software was used to clean the final model and create models with blade metrics varied from the base fan design. Geometry manipulation and warping techniques were used to alter relevant blade parameters as identified in the literature study. A method which could be used for the mesh wrapping process was needed. As such, the following section will explain the steps which were taken to create a mesh profile which is possible to 3D print as well as create other prototype fan models with varied blade parameters. A mesh wrapping process was used to create a cleaned and usable model from the base fan model which was 3D scanned. Initially, a coarse mesh was first wrapped around the 3D scanned model. Figure 3.2.1 shows the initial mesh plane, which was created to begin the mesh wrapping process.

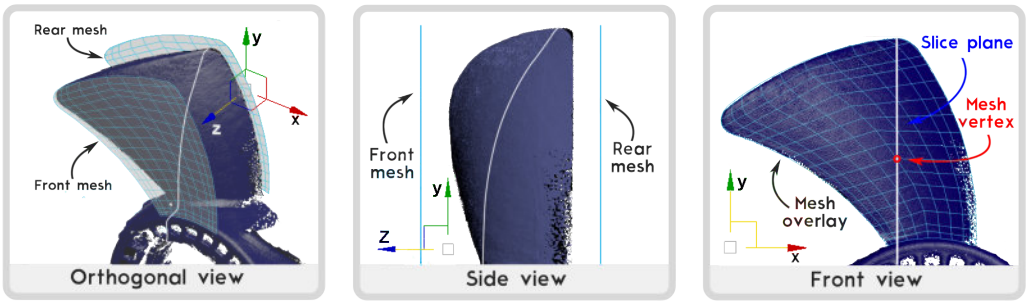

Figure 3.2.1: Mesh wrapping

Two-coarse mesh planes were positioned on either side of the fan blade. Using the coordinate system convention provided in Figure 3.2.1, the coarse mesh was first made to cover the fan mesh as seen from the x and y axis plane(front view). Two mesh planes were created for the fan blades front section as well as the backside. To determine the depth of each vertex, it was necessary to match each vertex to the 3D scanned model after making a sectioned view. Figure 3.2.2 shows a vertically sectioned blade at a vertex node of interest. Each node on the rear mesh and front mesh was aligned with the position of the 3D scanned model positions. This process was repeated for all vertex nodes for the coarse mesh to create an initial matching profile to the 3D scan. After aligning the 'Rear mesh' and 'Front mesh' to the original profile, the two mesh profiles were connected to complete the course mesh, as shown in Figure 3.2.3. The red section, as shown in Figure 3.2.3 shows the region which was formed by connecting the back and front mesh.

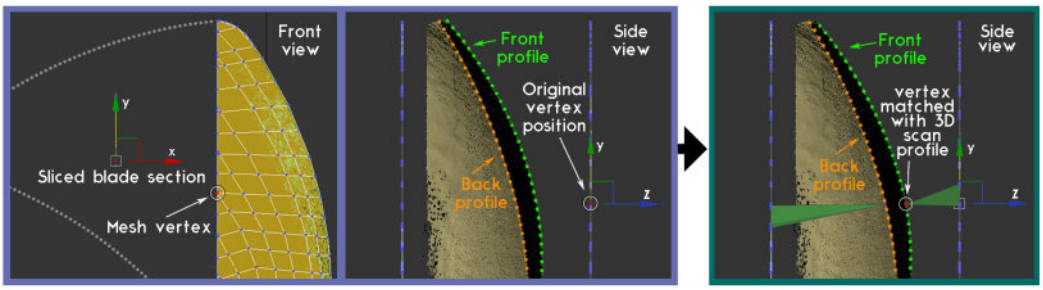

Figure 3.2.2: Mesh vertex relocation in z-axis direction

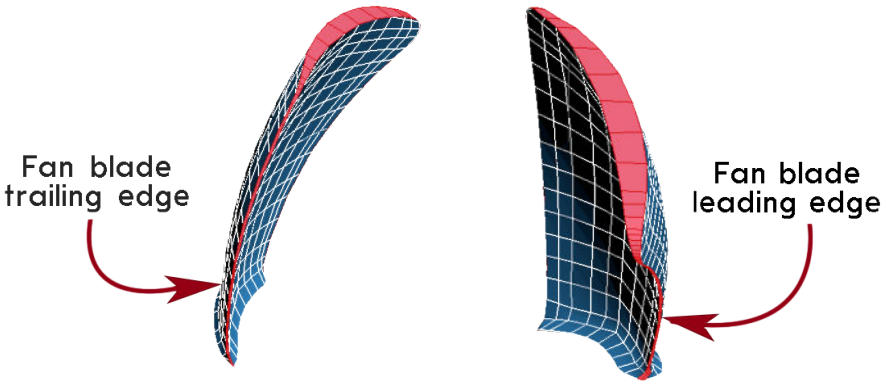

Figure 3.2.3: Coarse mesh creation

The full profiled view of the coarse mesh can be seen in Figure 3.2.4, which displays the front and side views for the fan blade. As the course mesh only provides a simplified representation of the 3D scan model, it was necessary to refine the mesh. This process consisted of creating more subdivisions of the coarse mesh and matching each vertex position to the depth of the scanned profile. Additional vertex nodes were created by adding segments to the coarse mesh. The process which was used to match the nodes for each vertex as mentioned for the course mesh profile was used to edit each vertex nodes position for the refined mesh.

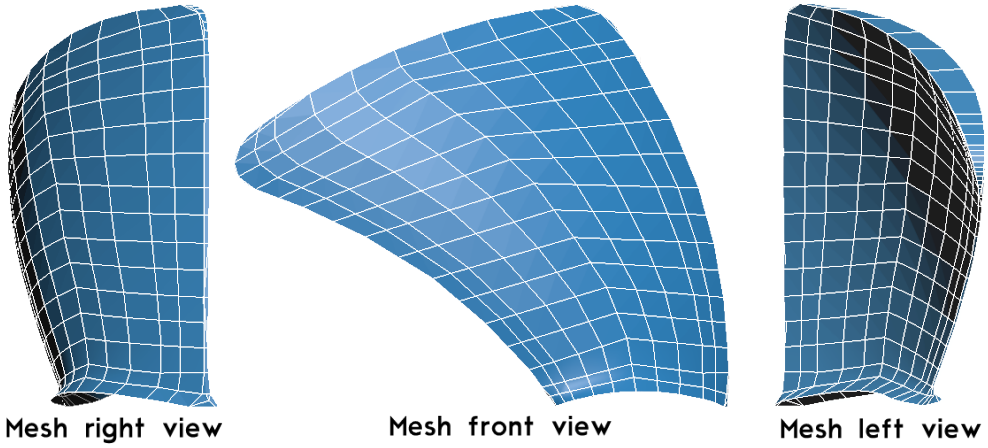

Figure 3.2.4: Coarse mesh overlay of base fan blade

3.3 Mesh refinement

A final reference model was created by increasing the number of vertex nodes and by applying a NURMS (Non-Uniform Rational Mesh Smooth) smoothing technique (Menus, 2014; Murdock, 2015). The NURMS method applies an algorithm which takes polygon geometry and applies an automated smoothing function. To ensure that the altered profile matches with the base profile, a crease operand was used in conjunction with the NURMS smoothing technique ensuring that vertex positions for smoothed surfaces would be maintained. The transition from a coarse mesh profile to the refined mesh is depicted in Figure 3.3.1.

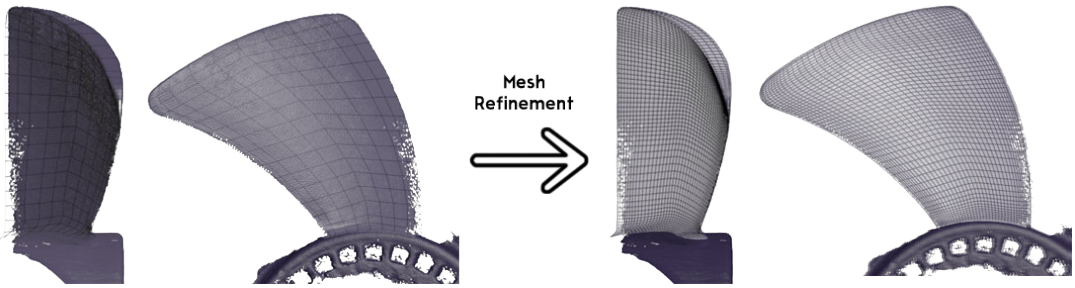

Figure 3.3.1: Coarse mesh refinement with (left) course mesh and (right) refined mesh

Figure 3.3.1 shows a comparison made between the base 3D scanned model with the mesh overlay. The NURMS tool was an equivalent tool which is comparable to the usage of NURBS surfaces which is an industry-standard used for designing and modelling surfaces (Derakhshani *et al.*, 2012). As such, the

recreated base mesh was determined to be a sufficient model representing the 3D scanned fan rotor.

With the redefined and cleaned base model, 3D morphing techniques could be applied to alter blade metrics to create fan blade variations. In an inspection of the original 3D scanned profile, the scanned mesh did portray sections of discontinuity characterised by empty disjointed locations but due to primary vertex points being present necessary to redefine fan geometry the identified concern did not impose a problem. As such, it was still possible to recreate the fan model as the vertexes characterising the edge profile of the fan was still present. An orthogonal view of the final base profile is given in Figure 3.3.2. The mesh overlay for the final model is given in figure 3.3.2a with the plain 3D view of the final model given in Figure 3.3.2b.

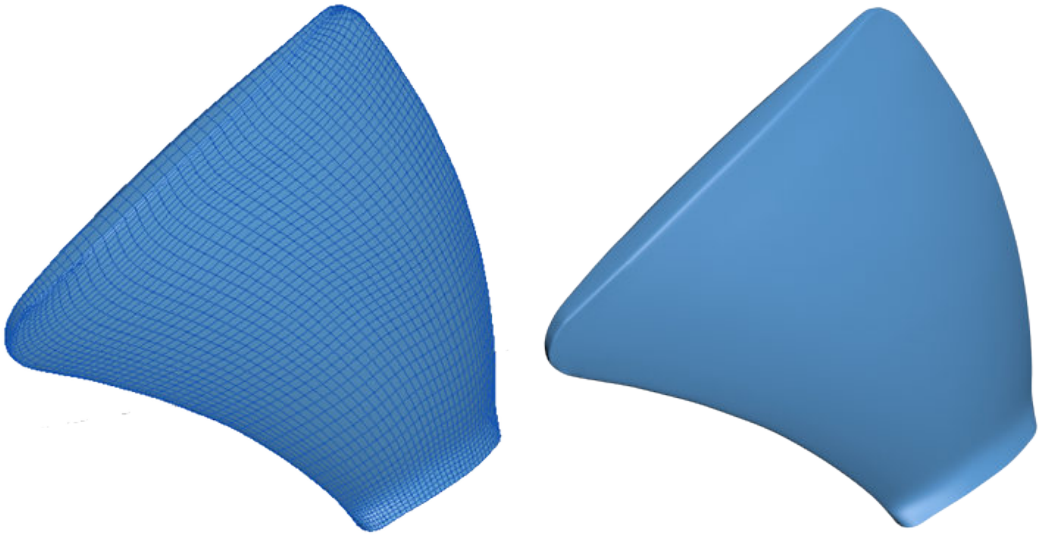

(a) (b)

Figure 3.3.2: (a) Base blade mesh orthogonal view and (b) base blade isometric view

The orientation of the fan blade was kept relative to the original 3D scan for which the final printable model was created by duplicating and revolving fan blades around the rotors axis of rotation with each blade being placed equidistant to one another. An orthogonal view of the final recreated base prototype model is given in Figure 3.3.3. The prototype model compared with the base 3D scanned profile is also given in Figure 3.3.3.

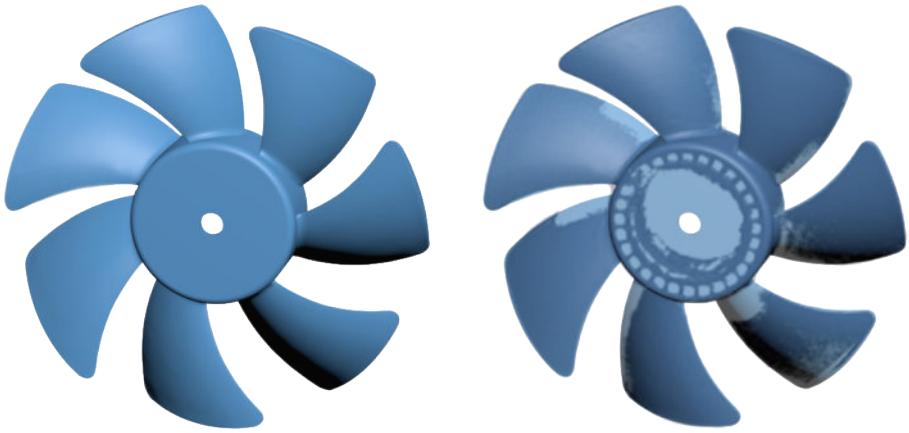

Figure 3.3.3: Isometric view for the final baseline fan (left) and a comparison made to the 3D scanned fan profile (right)

3.4 Fan geometry parameter alterations

The following sections describe the analogy used to alter the parameters to blade sweep, angle and chord length. Geometry near the blade hub and tip showed more complex shapes characteristic of adding cut-outs, fillet and chamfer sections. Methods used to address these regions which cant be described by blade parameters alone will also be discussed. One specific method to vary each parameter will be discussed, although numerous other approaches to altering blade parameters may exist.

3.4.1 Modification of circumferential blade sweep

Wright and Simmons (1990:4) mentions various approaches which have been made to alter sweep. The most well-known definition for blade sweep is the angle made between the stacking and radial line. A blade is known to be forward swept when it is swept in the direction of rotation and backwards swept when the blade is swept in the opposite direction of rotation. Wright and Simmons (1990:4) identifies forward sweep to have more beneficial implications to fan noise and efficiency in comparison to rearwards sweep. As such rearwards sweep has been omitted and considerations for forward sweep have only been made. The method to alter sweep, as outlined by Beiler *et al.* (1999) was used. Beiler *et al.* (1999) use the concept of skew (δ) as shown in Figure 3.4.1, which is described to be a combination of blade sweep (λ) and dihedral angle (ν). When considering the effect of blade sweep only, the dihedral angle can be removed, as mentioned by Beiler *et al.* (1999). With removing the effect of the dihedral angle, Beiler's definition of blade skew can be incorporated to design for blade sweep as blade skew becomes equal to blade sweep.

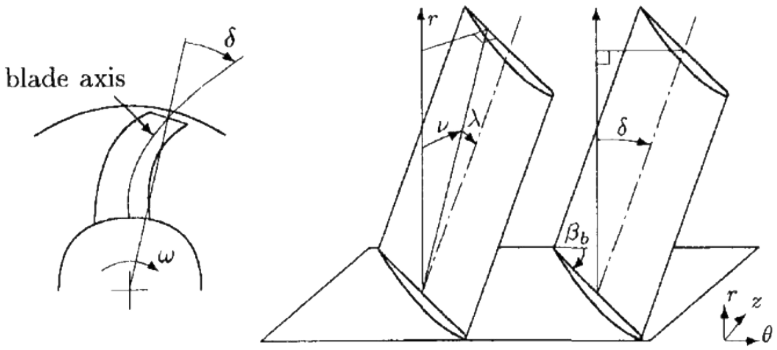

Figure 3.4.1: Blade sweep definition (Beiler *et al.*, 1999:2)

As shown in the coordinate system given in Figure 3.4.1, θ is denoted as the direction of rotation which is shown to be in the direction of the axis-symmetric surface. The profile as shown in Figure 3.4.1 shows the profile of a fan blade for which a constant blade sweep δ has been applied to the fan blade in the circumferential direction. This is to say that for each profile moving from the rotor hub (axis-symmetric surface) to the tip of the fan blade the profile along the aerofoil is rotated a set degree which is increased as the radial location is increased. The angle ϕ denotes the angle of elevation which the antisymmetric surface presents for the blade hub on which fan blades are mounted. For axial fans, this angle ϕ is equal to zero as mentioned by Beiler et al. (1999:60) as there is no angle of elevation present for the hub on which fan blades are mounted. The co-ordinate system which needs to be taken into account is denoted by the axes θ and r as given in Figure 3.4.2 which denote variables used in a polar coordinate system. The blade geometry is shown with sweep applied to a fan blade. For convenience, the stacking line is used as a reference where the shifting of position can be seen, with the original stacking line positioned in line with the r axis as given in Figure 3.4.2. The co-ordinate z was used to consider changes for the dihedral angle and thus can be neglected when only considering sweep. The axes, as used by Beiler *et al.* (1999) was used for convenience to explain how sweep should be altered. Figure 3.4.3 shows the method adaptation used to alter fan blade sweep as described by Beiler *et al.* (1999:60) with a constant varying fan blade sweep profile. In Figure 3.4.3, $\Delta\beta_{\max}$ denotes the maximum angle of rotation for the vertex profiles as located at the tip of the fan blade. The principle of altering fan blade sweep is shown using the stacking line as a reference. Each vertex node for the profile of the fan blade is rotated a set degree of rotation dependant on the radial distance of the node (r_{node}) relative to the tip radius($r_{\max}$) as given by the equation 3.4.1.

$$\Delta\beta_{\text{node}} = \Delta\beta_{\max} \times (r_{\text{node}}/r_{\max}) \tag{3.4.1}$$

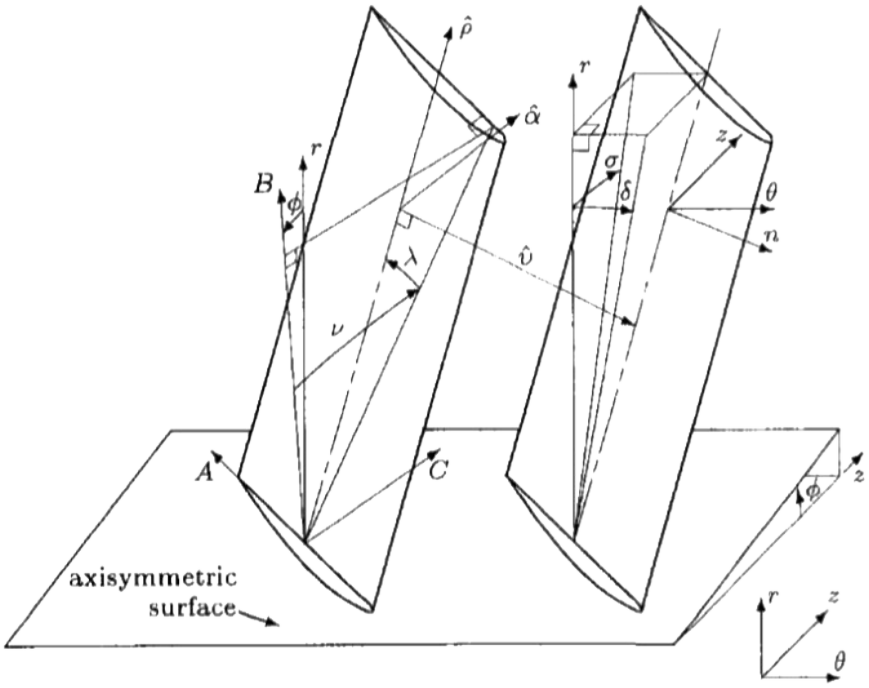

Figure 3.4.2: Axisymmetric flow surface with fan blades (Beiler *et al.*, 1999:60)

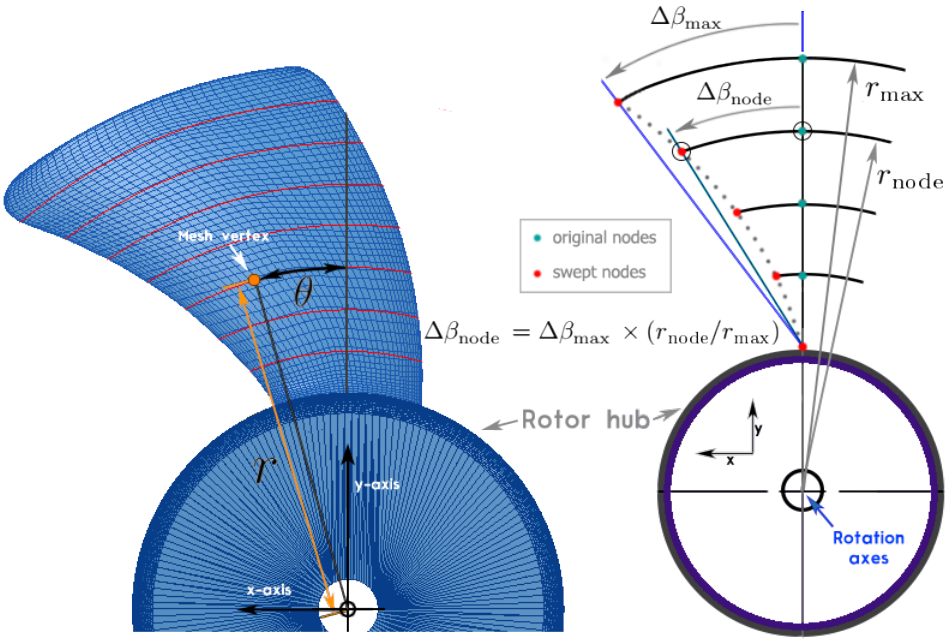

Figure 3.4.3: Constant change to sweep in the circumferential direction showing (left) polar co-ordinate system for θ and r uses as axes in Figure 3.4.2 and (right) sweep altered circumferentially for mesh vertices located on the stacking line

For blade sweep, the primary change to the geometry consisted out of a rotation of the object using a polar coordinate system as shown in Figure 3.4.3 for which the origin of the polar coordinate system is located at the centre of the fan or the position of the unswept blades stacking line position. On the polar coordinate system given in Figure 3.4.3 'r' denotes the radius length whereas 'θ' denotes the angle from the y-axis used to describe the position of points within the coordinate system. Starting from a rotation of 0° at the blade root the blade geometry is rotated to a maximum change to angle $\Delta\beta_{\max}$. Each mesh vertex point located in a concentric ring originating from the fan centre will be rotated with a set value. The values of rotation for each point located on a concentric ring will linearly change from the 0° to the maximum for rings with linearly increasing vertex radius length (r). The profile of the stacking line can be defined using the equation: $r(\theta) = a + b\theta$, where θ denotes the angle in radians measured from the y-axis on a polar coordinate system.

$$y(r,\theta) = r\cos\theta \tag{3.4.2}$$

$$x(r,\theta) = r\sin\theta \tag{3.4.3}$$

From equations (3.4.2) and (3.4.3) a point which is located on the stacking line will have the following co-ordinates as given in equations (3.4.4) and equation (3.4.5).

$$y(\theta) = r(\theta)\cos\theta = (a + b\theta)\cos\theta \tag{3.4.4}$$

$$x(\theta) = r(\theta)\sin\theta = (a + b\theta)\sin\theta \tag{3.4.5}$$

Differentiating the given equations (3.4.6) and (3.4.7) the rates of change for the Cartesian co-ordinates $y(\theta)$ and $x(\theta)$ can be determined given in equations (3.4.6) and (3.4.7).

$$y'(\theta) = b\cos\theta - (a + b\theta)\sin\theta \tag{3.4.6}$$

$$x'(\theta) = b\sin\theta + (a + b\theta)\cos\theta \tag{3.4.7}$$

$$\frac{x'(\theta_{out})}{y'(\theta_{out})} = \frac{b\sin(\theta_{out}) + (a + b\theta_{out})\cos(\theta_{out})}{b\cos(\theta_{out}) - (a + b\theta_{out})\sin(\theta_{out})} = \frac{b\tan(\theta_{out}) + (a + b\theta_{out})}{b - (a + b\theta_{out})\tan(\theta_{out})} \tag{3.4.8}$$

Using equations (3.4.6) and (3.4.7), the slope of the stacking lane can be determined necessary to calculate blade sweep. The notation θ_{out} denotes the maximum angle change which is equal to $\Delta\beta_{\max}$ located on the outer ring of the fan blade. The equation used to calculate for blade sweep is given by equation 3.4.9. For a desired sweep, the change in maximum angle need to be calculated using a desired value of sweep as given in equation 3.4.10.

$$\eta(deg) = 90° - \Delta\beta_{\max} - \arctan\left(\frac{y'(\theta_{out})}{x'(\theta_{out})}\right) \tag{3.4.9}$$

$$\Delta\beta_{\max} = 90° - \eta - \arctan\left(\frac{y'(\theta_{out})}{x'(\theta_{out})}\right) \tag{3.4.10}$$

Using equation 3.4.11 to calculate the amount of rotation necessary to obtain a desired sweep denoted as $\Delta\theta_{calc}$ for a single vertex node, the new co-ordinates of the vertex can be determined using equation 3.4.12 and 3.4.13. Equation 3.4.11, 3.4.12 and 3.4.13 will be applied to each and every vertex node of the fan to obtain a desired degree of sweep.

$$\Delta\theta_{calc} = \Delta\beta_{\max}\left(\frac{r_{\text{node}} - r_h}{r_t - r_h}\right) \tag{3.4.11}$$

$$x_{new} = x_{\text{node}}\cos(\Delta\theta_{calc}) - y_{\text{node}}\sin(\Delta\theta_{calc}) \tag{3.4.12}$$

$$y_{new} = x_{\text{node}}\sin(\Delta\theta_{calc}) + y_{\text{node}}\cos(\Delta\theta_{calc}) \tag{3.4.13}$$

Using the definition for constant sweep as defined by Beiler *et al.* (1999), Figure 3.4.4 shows how the blade sweep was removed for the final fan blade model. The stacking line for the fan blade was determined by taking the centre sections between each leading edge and trailing edge node and was interpolated to determine the profile for which sweep has been removed. It was necessary to first remove the sweep as the design for the blade chord, and blade angle depended on a base profile with no sweep.

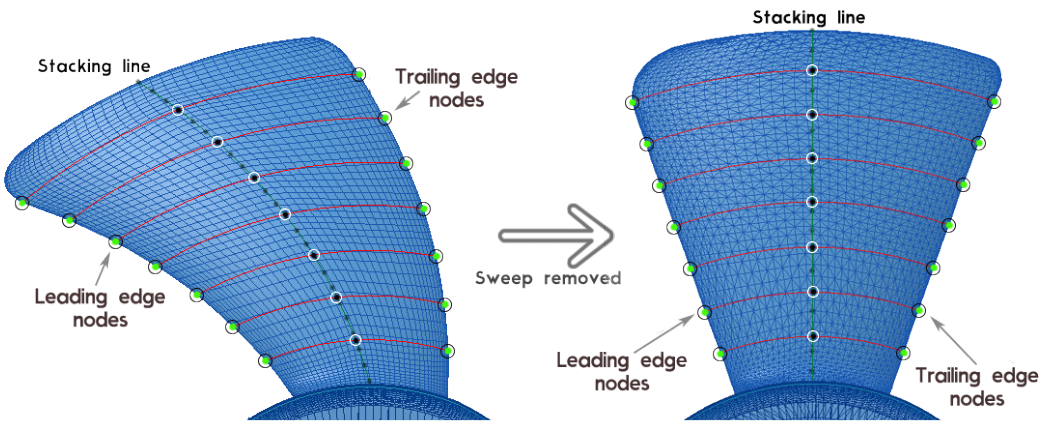

Figure 3.4.4: Base blade model with unaltered sweep (left) and with sweep removed (right)

Sweep can be altered from the base model as shown using the same method used to remove for sweep as shown in Figure 3.4.4. Sweep is usually applied to a base blade profile. This is to say that other parameters for the fan blade can not be determined before removing blade sweep due to radial distortions caused by blade sweep affecting blade parameters. The following sections describe the steps which were used to alter blade chord and angle after sweep has been removed.

3.4.2 Modification of blade angle

With the sweep removed, the parameters for the fan blade could be analysed using aerofoil cut outs for the fan blade. Aerofoil segments were used to change the blade angle as well as the chord length. Adaptations from Eck (1972) and Vad (2008) was used to determine the aerofoil sections consisting of tangential sections in the radial direction, as shown in Figure 3.4.5. The lines shown in Figure 3.4.5 show sections which were taken to obtain the aerofoil profiles as used by Vad (2008). The trailing edge line was identified to be aligned vertically, indicating that the fan blade may have used the trailing edge interaction line as a pivot to make alterations to blade angle.

Figure 3.4.6 shows an orthogonal view for aerofoil sections made to the base fan blade, as shown in Figure 3.4.5. The sectioned view (bottom view), showing the orientation for blade aerofoils is also given. The trailing edge line for aerofoil profiles were identified to be lined up vertically as seen in Figure 3.4.5. A fan blade incorporating a different form of skew was also identified to make use of this geometric feature as shown in Figure 3.4.7 (Eck, 1972).

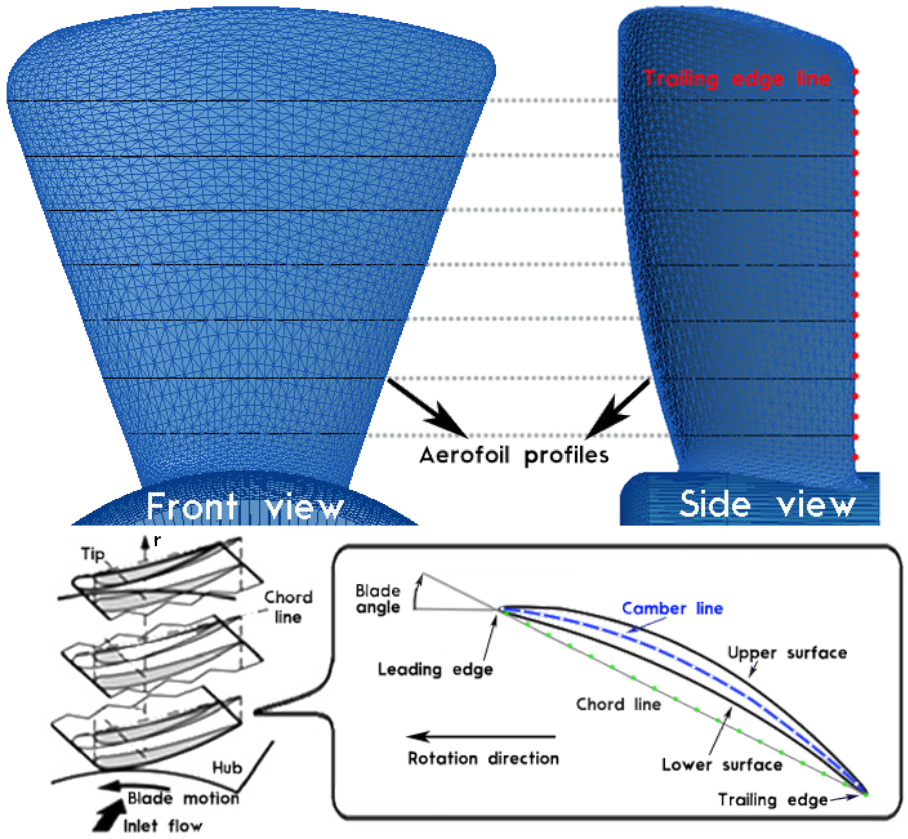

Figure 3.4.5: Unswept base blade aerofoil sections as seen taken from the front view (left), aerofoil sections taken from the side view (right) and the aerofoil definition as used by Vad (2008) showing the orientation and aerofoils with parameters mentioned (bottom)

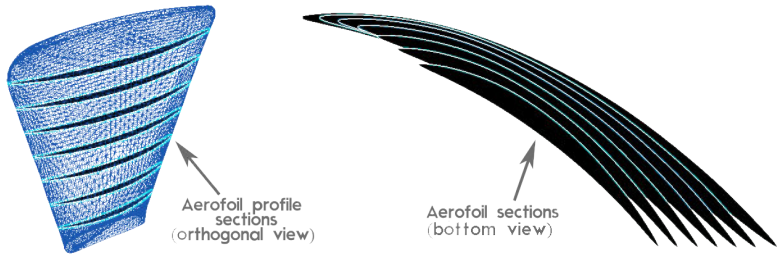

Figure 3.4.6: Aerofoil sections, (left) orthogonal view and (right) sectional view (bottom view)

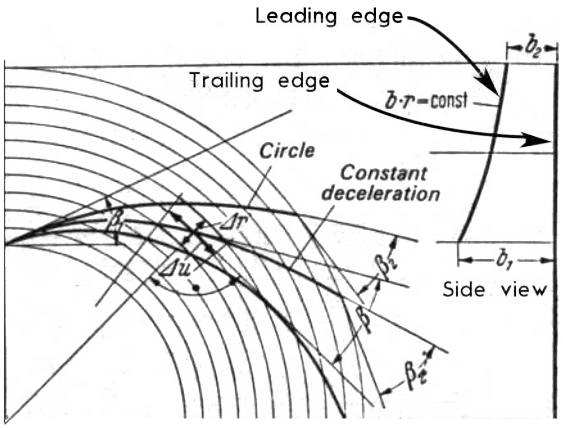

Figure 3.4.7: Configuration of a fan blade showing side view profiles for the leading and trailing edge section (Eck, 1972:103)

In contrast to changing blade angle around a central axis which goes through the midpoint of the fan; the vertical line-up of the trailing edge as identified from a number of fans from Eck (1972) gave motivation to rather use the trailing edge as a pivot point to alter for blade angle. As no considerations were made for the aerodynamic analysis of fans, only the possible methods used to alter for fan blades were identified and selected according to Eck (1972). No specifics were also mentioned by Eck (1972) why one method used to alter blade angle was select over another. Rather it was identified to be a selection made by fan designers. Due to uncertainty as to the selection criteria which needs to be made, it was rather aimed to preserve geometric traits as observed by the baseline fan. Figure 3.4.8 shows the analogy which was used to alter the blade angle per aerofoil segment. Profiles were rotated around aerofoil intersection points with the trailing edge line as given in Figure 3.4.8. In comparison to the alternative method or rotating the blade around the blades centre axis this allowed for the blade location to not interfere with the fans basic chassis structure.

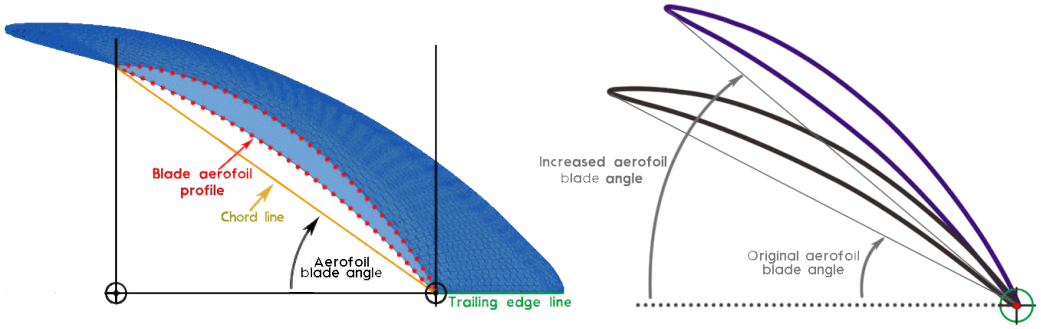

Figure 3.4.8: Definition for blade angle

By inspection of the profile and also referring to design analogy for Eck (1972) a constant trailing edge profile was used in the design which can also be observed for the base aerofoil profile. Thus each aerofoil was rotated about the trailing edge line to change the blade angle per aerofoil division for the fan.

3.4.3 Modification of blade chord

By overlaying the aerofoil profiles and scaling them down to all have the same chord length it was determined that the base aerofoil profile which was used to create the fan consisted out the aerofoil as given in Figure 3.4.9. The following sections will describe the alterations made to blade chord.

Figure 3.4.9: Base aerofoil profile

A scaling was applied in the direction of chord length for aerofoil profiles, to adjust the chord length for fan blades. This ensured that the maximum camber thickness stayed constant while maintaining blade camber thickness profiles over chord length. It must be noted that the camber distribution stayed constant in terms of percentage chord distribution rather than the actual chord length. Motivation to alter chord in this fashion was obtained from Carter *et al.* (1960). Figure 3.4.10 shows how scaling was applied in a reference direction denoted as x_{ref} which was positioned parallel to the chord length direction.

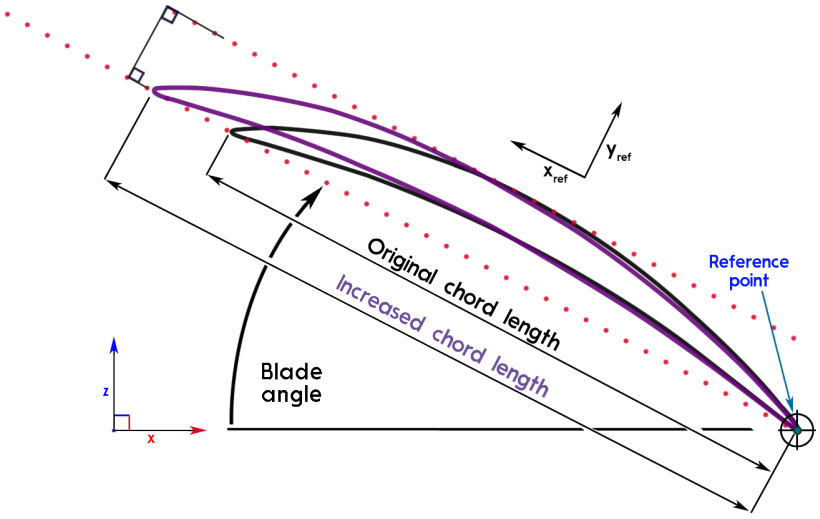

Figure 3.4.10: Alterations to blade chord length

As the fan blade had a variable profile from blade hub to tip, it was not possible to determine a single value for blade solidity. Rather, the approach as conducted by Osborn and Steinke (1974) was used for which the blade solidity was determined for the blade hub and blade tip profiles. A select range for blade solidity was used to determine design ranges for chord length. By ensuring that chord length measured from hub to tip maintains a solidity value between 0.4 and 1.1 (Peng, 2008), the maximum and minimum ranges permissible for blade chord could be determined.

Equation 2.3.1 and 2.3.2 was used to calculate the blade solidity. The calculations made will be discussed. The base computer cooling fan which considered had a tip radius (r_t) of 54.74 mm and a hub radius (r_h) of 21.55 mm. The mean radius (r_m), as determined by equation 2.3.2, was calculated to be 41.6 mm using the formulation $r_m = [54.74^2 + 21.55^2)/2]^{0.5}$. Using r_t, the pitch spacing ,calculated using equation 2.3.1, was determined to be 37.34 mm using the formulation ($s = 2\pi \times r_m/n_b$). The chord length (c) for the base blade tip was measured to be 34 mm, which equated to a solidity ratio of 0.91 calculated using the equation (blade solidity $= c/s$). Similarly, the chord length at the fan base was measured to be 19.94 mm, which equated to a solidity ratio of 0.534 at the fan hub. Two different approaches to altering blade chord have been identified in literature: varying relative to the percentage of chord length (Fukano *et al.*,1977) or linearly increasing the chord length from hub to tip with a specific length per aerofoil section. Due to the simplicity of implementation, the method of increasing blade chord linearly from hub to tip was chosen. After applying modifications to the blade i.t.o. blade angle and chord, some regions of the blade still had to be morphed to maintain the characteristics of the original fan. The methods used to further morph fan blades is given in Appendix A.1.

3.5 Design of experiments

To build an efficient design approach, the theory as used in Response Surface Methodology (RSM) by Myres (1976:297) will be incorporated in the design of experimental work, used to determine the influence of blade parameters. In many designs of experiments, the true response function is commonly unknown, as such the study of RSM provides a means of experimental study for exploring the unknown space using empirical statistical modelling to develop an approximation model. Many application of RSM involves fitting and assessing the adequacy for first and second-order systems. A highly efficient response design known as the central composite design (CCD) is commonly used to fit second-order models.

The main motivation for the use of CCDs is in the use of sequential experimentation involving $2k$ factorial designs combined with the use of $2k$ axial points

where k denote the number of independent variables considered. The factorial points represent a variance-optimal design considering first-order model interactions, mainly the +two-factor interactions. Inclusion of factorial points allows for estimation to be made towards interaction terms between variables in the design. Used in conjunction with a centre run information on the existing curvature can be found with the addition of axial points allowing for efficient estimation of pure quadratic terms (Myres, 1976:297). Center runs, or a single centre run incorporated in CCDs further provide an internal estimate of error and contribute to the estimate of quadratic terms providing a means to determine the predicted variance defined as $N\text{Var}[\hat{y}(\boldsymbol{x})]/\sigma^2$.

CCD's provide an area of flexibility in experimental design which resides in the selection of α the axial distance and n_c the number of centre runs. Common values for axial distance selected consist of values 1.0 and $\sqrt{k}$ where α=1 places axial points on the face of a cube or hypercube and α=$\sqrt{k}$ makes all points to be placed on a common sphere. Most often a design incorporating rotatability is recommended with an α value of $\alpha = \sqrt[4]{F} = 1.682$ for $k = 3$ where $F = 2^k = 8$ which is designed regardless of the number of center runs.

To consider the effects caused by rotatable designs a factor most often known as SPV (scaled prediction variance)is used to determine importance variance properties of an experimental design as determined by the nature of a moment matrix which characterises the variances and covariances of regression coefficients as well as prediction variance. Although rotatability itself as mentioned by Myres (1976: 305) does not ensure stability or even near-stability in the design region, it is used to provide useful guidelines for a choice of design parameters namely a margin of selection for parameters α and n_c.

The purpose of incorporating rotatability was noted to be an attempt at producing stability, in a sense maintaining constant SPV($\boldsymbol{x}$) on spheres where $\boldsymbol{x}$ denote a vector of independent variables (Myres, 1976:307). However the presence of a rotatable design does not imply stability throughout the design region where it was identified that spherical designs used for fitting second-order models actually have infinite SPV($\boldsymbol{x}$) with the design being singular as identified by Box and Hunter (1957), and Myres (1976). Including centre runs were identified to contribute to the stability of SPV($\boldsymbol{x}$) in the design region, which is beneficial for rotatable designs. It is not uncommon in practice to select α values which are different than proposed values as determined by the criterion which defines rotatability. This is to say that near rotatable designs are also quite applicable. With the tests in mind, considering numerous centre values was considered less meaningful since considering the centre run for the same fan model would output the same results for a base rotor model.

Due to a rotatable model usually being advised to have 3 to 5 centre runs although fewer centre runs can persist, a α value was select which leans towards a cuboidal design region which has an α value of 1. This was done as cuboidal design regions only require one centre run. An alpha value of 1.414 was rather select between ranges of 1 and 1.682. The Central Composite Design, used as a sampling method to collect data on the influence of blade parameters, is shown in Figure 3.5.1. The coordinate system of (C, B, S) was used where 'C' stands for the chord length, 'B' stands to blade angle and 'S' for blade sweep.

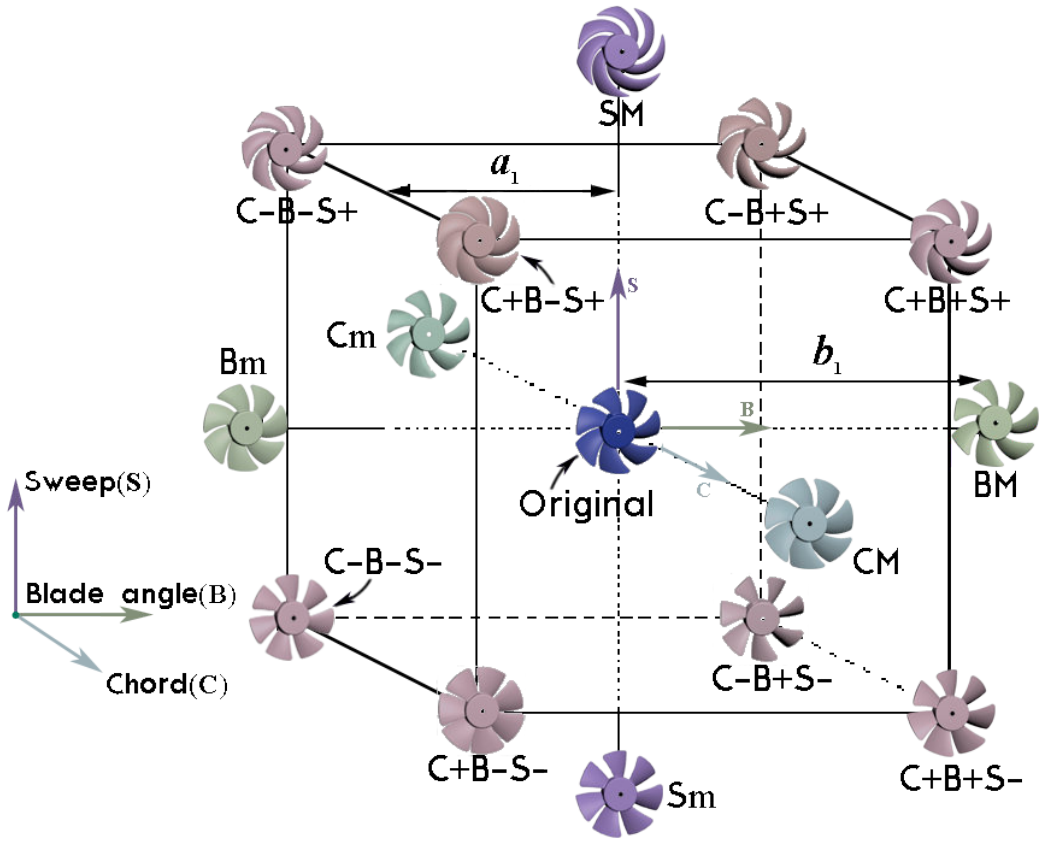

Figure 3.5.1: Central composite design (Myres, 1976)

All factorial and axial points were located in a spherical fashion around the centre point. Fan models were created with variations to blade metric parameters of sweep, blade angle and chord according to the CCD, with the original base fan model located in the centre of the CCD. The notation a_1 and b_1 were used to represent lengths for equivalent α values used in Figure 3.5.1. The value a_1 represented a length equivalent to an alpha value of 1 while b_1 represent a length equivalent to an alpha value of 1.414. A value which scaled from -1.414 to 1.414 was used for the co-ordinate system representing the alpha values for each variable. This was indicated by using a naming convention Vm($\alpha = -1.414$), V$-$($\alpha = -1$), V+($\alpha = 1$) and VM($\alpha = +1.414$) where

the notation V can stand for either C, B or S representing the three blade parameters. A total of 8 factorial points were considered with the co-ordinates (1,1,1); (-1,1,1); (-1,-1,1); (1,-1,1); (1,1,-1); (-1,1,-1); (-1,-1,-1) and (1,-1,-1). These points were characterised by corner points of the cube as shown in Figure 3.5.1, which have notations V+ or V– depending on the variable names. In addition to the midpoint having a co-ordinate of (0,0,0) 6 axial points were considered with co-ordinates (b_1,0,0); ($-b_1$,0,0); (0, b_1,0); (0, $-b_1$,0); (0,0,b_1) and (0,0,$-b_1$). A design region was selected by addressing relevant literature for blade parameters. Table 3.5.1 shows the changes which were made for each fan as seen by the CCD design in Figure 3.5.1 with the design ranges shown in Table 3.5.2. A number and name were assigned to each fan design with specified alterations made to blade parameters. The assigned naming system will be used to identify each relevant fan for convenience. The dimensions for the original fan blade is given in Appendix A.2, giving a mention towards the select design ranges for blade parameters.

Table 3.5.1: CCD design regions

Fan no.	**Fan name**	**Alterations made to blade metrics**		
		Chord(C)	Blade angle(B)	Sweep(S)
1	C+B+S−	+3.54 mm	+10.61°	−17.68°
2	C+B+S+	+3.54 mm	+10.61°	+17.68°
3	C−B+S−	−3.54 mm	+10.61°	−17.68°
4	Bm	0.00 mm	−15.00°	0.00°
5	C+B−S+	+3.54 mm	−10.61°	+17.68°
6	C+B−S−	+3.54 mm	−10.61°	−17.68°
7	Cm	−5.00 mm	0.00°	0.00°
8	Sm	0.00 mm	0.00°	−25.00°
9	Original	0.00 mm	0.00°	0.00°
10	SM	0.00 mm	0.00°	+25.00°
11	C−B+S+	−3.54 mm	+10.61°	+17.68°
12	CM	+5.00 mm	0.00°	0.00°
13	C−B−S+	−3.54 mm	−10.61°	+17.68°
14	C−B−S−	−3.54 mm	−10.61°	−17.68°
15	BM	0.00 mm	+15.00°	0.00°

Table 3.5.2: CCD design boundaries

Blade metrics	**Minimum change(Vm)** $\alpha = -1.414$	**Maximum change(VM)** $\alpha = 1.414$	**Reference**
Blade angle	−15°	+15°	Li *et al.* (2016)
Sweep	−25°	+25°	Beiler et al. (1999), Smith and Yeh (1989)
Chord	−5 mm	+5 mm	Peng (2008)

3.6 Fan 3D printing and design

The final 15 rotor models were printed using a Stereolithography (SLA) 3D printer which prints 3D parts by laser curing isotropic parts from a liquid photopolymer resin. Using an SLA printer allowed for objects to be printed in a higher resolution in comparison to FDM (Fused Deposition Modelling) techniques which is most often known to have less precise surface finish due to the resolution of the printer being a factor of the nozzle size and precision of the extruders movements. FDA printing is known to have a number of minor factors relating to surface warping, layer misalignment and issues relating to shrinkage. These problems commonly occur in FDM printing due to the bonding forces between layers being lower than SLA printing which may cause issues as the weight of upper layers may influence the form of lower layers. Although these effects are not critical, it does influence the precision for printed designs.

In contrast to FDM printers, the resolution for SLA printers are determined by optical spot size of the laser used to print objects and much less force is used due to a laser curing process being used to create objects as opposed to filament extrusion techniques as used in FDM printing. SLA printers also experience factors relating to surface warping and other problems which are experienced by 3D printing but is considered much less compared to FDM printing methods. A Form 2 resin printer using 'Engineering resin' more specifically, the 'Rigid resin' supplied by Formlabs was used to print fan models. The 'Rigid resin' selected to print fan models has been identified to be used to print fan blades due to beneficial material properties which include high stiffness and resistance to deformation over time ideal for printing fan blades. The rigid resin has been documented by Formlabs to have the highest modulus compared to all other Formlabs materials and has great resistance to heat and stability (Formlabs, 2019). The final set of prototype fan models are given in Figure 3.6.1 and Figure 3.6.2.

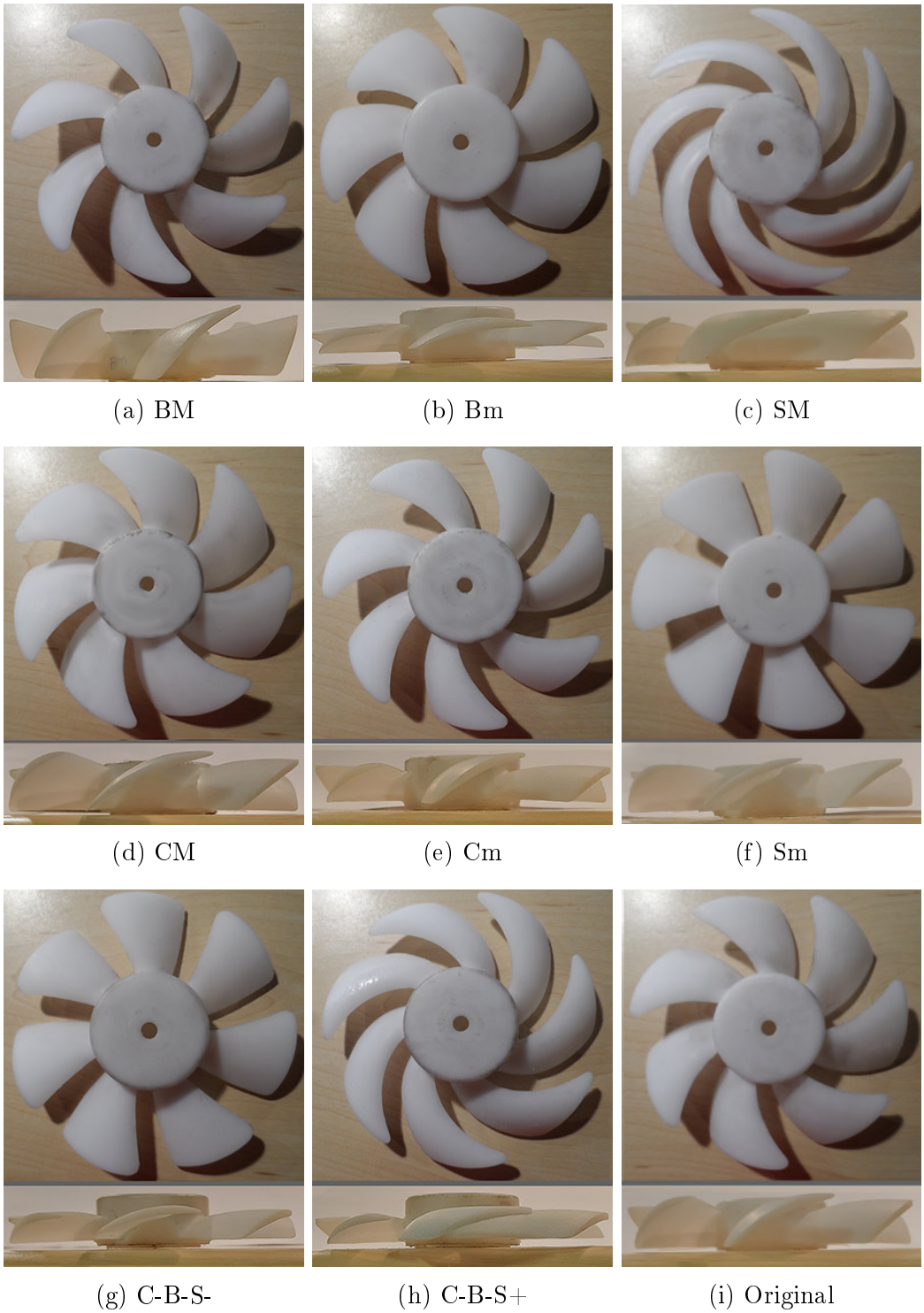

(a) BM (b) Bm (c) SM

(d) CM (e) Cm (f) Sm

(g) C-B-S- (h) C-B-S+ (i) Original

Figure 3.6.1: 3D printed prototype model variations with (a) maximum blade angle, (b) minimum blade angle, (c) maximum sweep, (d) maximum chord length, (e) minimum chord length, (f) minimum sweep, (g) C–B–S–, (h) C–B–S+ and (i) original baseline prototype

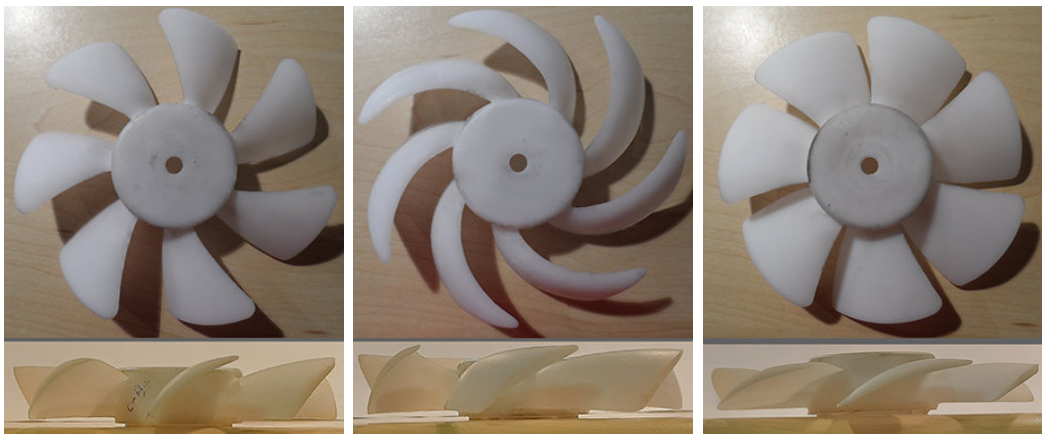

(a) C-B+S- (b) C-B+S+ (c) C+B-S-

(d) C+B+S- (e) C+B+S+ (f) C+B-S+

Figure 3.6.2: 3D printed prototype model variations with (a) C-B+S-, (b) C-B+S+, (c) C+B-S-, (d) C+B+S-, (e) C+B+S+ and (f) C+B-S+

Chapter 4

Fan noise evaluation and analysis

4.1 Introduction

Two standards were incorporated to assess and record fan noise: namely ISO 10302 (ISO, 2011) and ISO 3745 (ISO, 2012). ISO 10302 provided standardised procedures that were followed to record sound measurements for small air moving devices. Used in conjunction with ISO 10302, ISO 3745 facilitated a precision method for making sound measurement inside an anechoic chamber. Fan noise measurements were used to quantify the noise in terms of psychoacoustic metrics while also obtaining sound recordings to perform subjective evaluation tests. Fan rotor models were assembled onto a test platform, as shown in Figure 4.1.1, which facilitated an adjustable design allowing various rotor models to be tested.

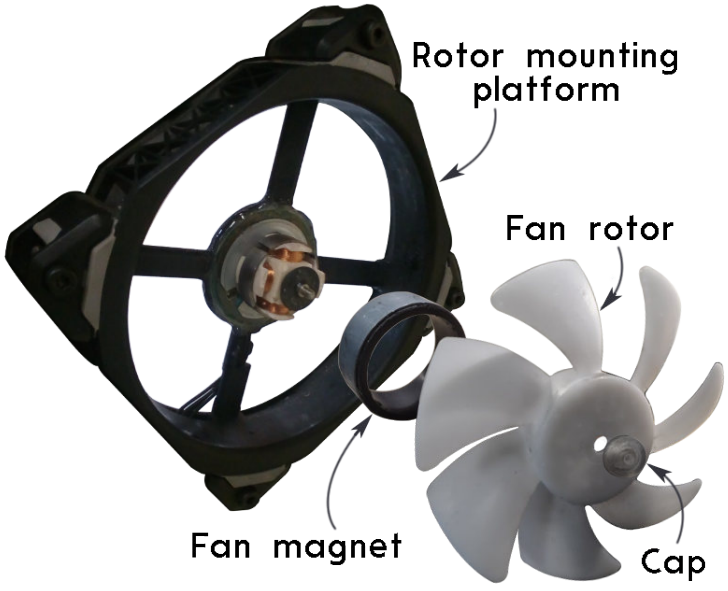

Figure 4.1.1: Fan components for assembly

4.2 Experimental setup

Figure 4.2.1 shows the design setup used to test fan prototype models. A 12V DC power supply was used to operate the fan with a Pulse Width Modulation unit (PWM) used to regulate the fan speed. A signal generator was incorporated in the design outputting a 1 kHz square wave voltage signal for which the duty cycle was altered to change the speed of the fan. Due to the floating signal of the tachometer output, it was necessary to incorporate a pull-up resistor to allow for a pulse reading measured using an oscilloscope. Two square wave pulses were generated by the tachometer per revolution of the fan. As such, the speed of the fan could be determined through the frequency of the square wave output by the tachometer.

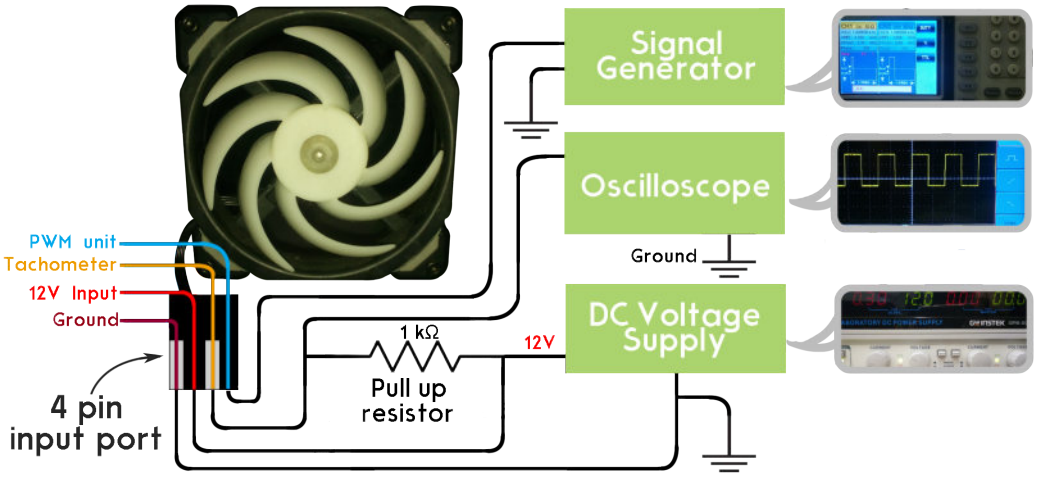

Figure 4.2.1: Fan operation diagram

A test plenum was built using design instructions as provided by ISO 10302 (ISO, 2011). The plenum, as shown in Figure 4.2.2 was used to make sound recordings as well as make fan performance measurements. The measurement box allowed for the operating region of fans to be altered by adjusting the resistance provided by the system using a slider to control the level of airflow and static pressure rise. Pressure was measured by use of a piezometer pressure ring built into measurement box. The box was covered by a layer of polyester film sealed with a silicone lubricant making the chamber airtight. With a rubber panel used to hold fans being tested in place, vibration-induced noise from structural resonance was mitigated. The plenum provided a flow resistance to the air-moving device but was designed in accordance with ISO 10302 to permit sound from the AMD to radiate freely into the test room with minimal levels of attenuation (ISO, 2011:3). The test plenum size was scaled accordingly, making considerations for fan dimensions.

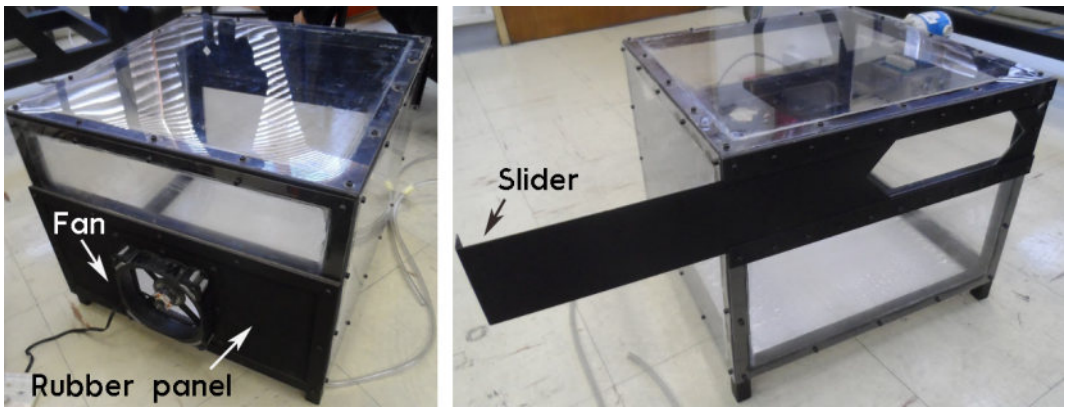

Figure 4.2.2: Fan testing plenum (ISO 10302) with, (a) plenum front view showing fan mounting configuration, (b) plenum rear view with adjustable slider used to vary airflow and pressure rise

The AMD in consideration consist out of computer cooling fans with a casing dimension of 120 mm × 120 mm. The technical data sheet provided the maximum airflow of the base fan of 74 CFM (0.035 m^3/s). ISO 10302 recommends that the smallest scaled plenum size be applied for the purpose of the standard where the original plenum dimensions are scaled according to the equation as given by equation 4.2.1.

$$q_{V,max} = q_{V,0} \times V/V_0 \tag{4.2.1}$$

For equation 4.2.1, $q_{V,max}$ denotes the maximum flow rate of the scaled plenum measured in cubic meters per second; $q_{V,0}$, the maximum flow rate of the full-size unscaled plenum having a value of 1 m^3/s; V_0, the nominal air volume of the full size plenum equal to 1.2 m×1.2 m×0.9 m = 1.296 m^3 and V, the nominal air volume of the scaled plenum. The final scaled plenum had dimensions as given in Figure 4.2.2 had dimensions 0.4 m×0.4 m×0.3 m = 0.048 m^3 designed to operate at a maximum airflow of 78.48 CFM (0.037 m^3/s).

The equipment used to make performance measurements in terms of airflow and pressure rise is shown in Figure 4.2.2. Ten discrete measurement points were determined according to ISO 10302, which reduced interference effects caused by plane reflection and also avoided intake or exhaust air streams from the test plenum. The 10 locations were associated with equal areas on the surface of the hemisphere as described by ISO 3745, where the coordinates (x, y, z) are presented in Table 4.2.1. Airflow was measured using an anemometer connected to a vane probe. The vane probe was mounted inside the test plenum placed behind the fan making measurement for air blown into the plenum chamber. A pressure transducer was used to make static pressure readings connected to a piezometer pressure ring placed behind the rubber panel on which fans being tested were mounted.

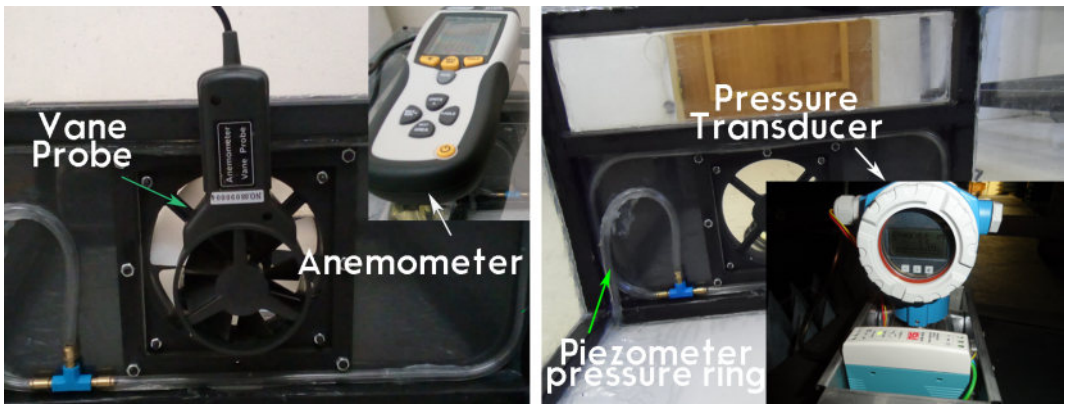

Figure 4.2.3: Measurement tools used to make performance measures using a test plenum using an anemometer (left) and a pressure transducer (right)

In accordance with ISO 10302, the measurement region as shown by a hemispherical dome in Figure 4.2.4 was used to record measurements. The plenum box was positioned in the centre of the anechoic chamber room for testing due to instructions as specified by ISO 10302. The standard ISO 10302 specifies that the test sound source needs to be located as close as possible with the geometric centre of the measurement sphere preferably located in the centre of the anechoic chamber (ISO 10302, 2011:32). The design region, as specified by the standard indicates that a scaled radius value can be used, but the radius considered needs to be greater than 0.5 m. Although the radius for the test hemisphere could be reduced, the standard specifies that a value less than 1 m could impose a limit on the frequency range for which tests are performed. As such, a radius value of 1.02 m was chosen for the hemispherical dome as given in Figure 4.2.4. Table 4.2.1 lists coordinates for microphone positions as shown in Figure 4.2.5. Figure 4.2.3 shows an example setup for one microphone position (position no. 5).

Table 4.2.1: Microphone measurement positions (ISO 10302, 2011:21)

Measurement position No.	x/r	y/r	z/r
1	-0.16	0.96	0.22
2	-0.78	0.60	0.20
3	-0.78	-0.55	0.31
4	-0.16	-0.90	0.41
5	0.83	-0.32	0.45
6	0.83	0.40	0.38
7	0.26	0.65	0.71
8	-0.74	0.07	0.67
9	0.26	-0.50	0.83
10	-0.10	0.10	0.99

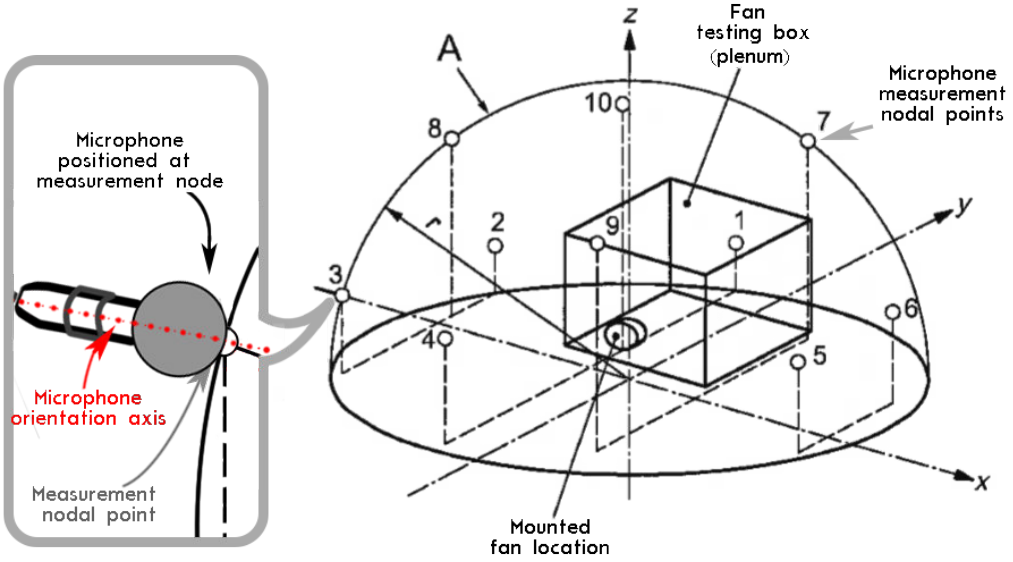

Figure 4.2.4: Hemi-spherical measurement surface(ISO 10302, 2011:21)

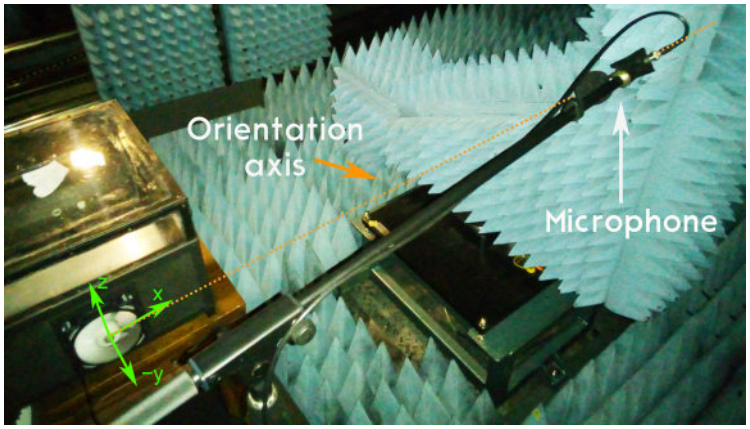

Figure 4.2.5: Microphone position no. 5, as shown in Figure 4.2.4 and Table 4.2.1

The selection of the operation point for a fan is case-specific (Zulovich *et al.*, 2008), with fan performance data used to select fans for specific applications and situations. When considering computer cooling fans, cooling fans are categorised to be either a static pressure fan or a high airflow fan (Edmonds, 2018). The type of fan considered as well as the decision made as to select performance criteria governs the operating point (Osawa, 2015). The operating point, as seen on performance curves, is a point where the system resistance curve meets the fan performance curve. Different operation points can be reached by varying the system resistance. The system resistance was changed by adjusting the slider position such that the area in comparison to the full open plenum was reduced by the percentage specified. Adjusting the area of the slider also

increased system resistance. As such, the speed of the fan operating had to be readjusted to operate at the desired speed.

A selection had to be made for an operating condition to be used to test fan prototype models. ISO 10302 (ISO, 2011) identified three possible operating points that can be considered; with the adjustable exit port (slider) completely open, 80% open or 20% open. The baseline 3D scanned fan was identified to be a high airflow fan (Corsair, 2019). Therefore a selection was made to make the plenum operate with the slider 80 % open. Compared to the fully open case, the 80 % open case made considerations for higher system resistance. Computer fans are usually operated within enclosures, as such fans are expected to operate with increased impedance (Osawa, 2015) giving a reason to rather consider the operating condition with the slider 80% open.

It is well known that the speed of the fan has a great influence on the noise emission of fans. Due to the study being focused on how the blade metrics affect the sound, it was necessary to keep the fan operating at a constant speed throughout the test for each rotor model being tested. As such a speed of 1800 rpm was selected, making considerations as to ensure that the fan is not operated for airflows which the test plenum was not designed for. As it was not possible to operate fans with an exact speed of 1800 rpm, a tolerance of $\pm$ 15 rpm was used in which the fan could vary from the operation fan speed. This value was determined by inspecting the readings obtained from the oscilloscope's maximum and minimum frequency readings describing fan speed.

4.3 Data processing

Sound recordings were made for 15 different fans over the selected ten different microphone positions as given by Table 4.2.1 for which the SPL readings were A-weighted. The recordings were made with three different slider position setups. As it was not possible to evaluate every recording position one specific microphone recording position had to be selected as a base for which sound recordings will be made which can be used as stimuli for which jurors can evaluate and compare sound stimuli.

ISO 10302 provides a useful measure namely the directivity index for sound which gives a measure of the extent to which a noise source under test radiates sound in the direction of the ith microphone position on a measurement surface (ISO 10302, 2011:7). By using the directivity index as a guideline, it can be determined how sound is directed towards a specific microphone position for each fan sound relative to the overall averaged SPL reading. By comparing the magnitude difference in dBA, how much variation as to the sound at a specific measurement node can be determined. As the directivity index

changes for a specific microphone position considered for all 15 fan variations, the microphone position with the least variation as to the directivity index could be used as the measurement node for sound recordings. The equation used to calculate the directivity index (D_{IAi}) is given by equation (4.3.1) where L_{pAi} is the background noise corrected sound pressure level for the ith microphone measured in dBA, and $\overline{L_{pA}}$ is the mean surface sound pressure level over the hemispherical dome (ISO, 2011:7). The mean surface SPL value in dBA can be calculated using equation (4.3.2) where the notation N_M stands for the number of microphone positions and L_{pAi} the background noise corrected time-averaged sound pressure level for the ith microphone position with the noise source under test in operation.

$$D_{IAi} = L_{pAi} - \overline{L_{pA}} \tag{4.3.1}$$

$$\overline{L_{pA}} = 10log[\frac{1}{N_M}\sum_{i=1}^{N_M} 10^{0.1L_{pAi}}]\text{dBA} \tag{4.3.2}$$

Variable L_{pAi} can be calculated using (4.3.3), where L'_{pAi}(ST) is the time averaged A-weighted sound pressure level measured at the ith microphone position with the noise source under test (ST) in operation measured in dBA and K_{1Ai} a background noise correction value at the ith microphone position which can be calculated using equation 4.3.4 and 4.3.5, where L_{pAi}(B) is the time averaged sound pressure level of the background noise (B) measured at the ith microphone position measured in dBA.

$$L_{pAi} = L'_{pAi}(\text{ST}) - K_{1i} \tag{4.3.3}$$

$$K_{1Ai} = -10log(1 - 10^{-0.1\Delta L_{pAi}}) \tag{4.3.4}$$

$$\Delta L_{pAi} = L'_{pAi}(\text{ST}) - L_{pAi}(\text{B}) \tag{4.3.5}$$

For $\Delta L_{pAi} \geq 15$ dB, ISO 3745 specifies that the background correction value K_{1Ai} can be assumed to be zero rather than using equation 4.3.5. The equipment used to make measurements for the fan sounds consisted out of the usage of a Head Acoustics Squadriga (Head Acoustics, 2010) and a microphone setup where the microphone was held in place using a stand. Markers were made to ensure a degree of consistency when relocating microphone stands, this is to say that the floor board was marked with tape indicating the x and y coordinates of microphone positions for which microphones need only be relocated with a set height from marked positions.

It was first necessary to calibrate the equipment to ensure precision as to the sound levels measured. A Larson Davis CAL200 calibrator was used to calibrate the microphone. The calibrator was used to output a discrete 1 kHz tone which had a specific dB value of either 94 dB or 114 dB. Equipment was calibrated by recording the sound output by the calibrator which would be attached to the microphone head. For a specified microphone sensitivity rating

given in units of V/Pa a reading would be obtained using Squadriga giving an SPL reading (L_{cal}) relative to the sensitivity rating used. With the calibrator chosen to output a tone that is 94 dB loud, if the measure value for L_{cal} varies from the true value of 94 dB the equation $L_{cal} = 20log(P_{meas}/(20\mu Pa))$ would be used to determine a new value for the sensitivity rating. The notation P_{meas} denotes the pressure reading determined by dividing the measured voltage by the sensitivity rating. Table 4.3.1 shows the directivity index calculated for each fan at different microphone measurement positions.

Table 4.3.1: Directivity index, change in dBA value for fans at measurement nodes

Fan no.	**Microphone measurement position no.(ith position)**									
	1	**2**	**3**	**4**	**5**	**6**	**7**	**8**	**9**	**10**
1	0.230	0.046	0.398	0.086	-0.427	-0.165	-0.791	-0.088	0.354	0.214
2	0.189	0.369	0.536	0.074	-0.398	-0.313	-0.503	-0.558	0.594	-0.188
3	-0.349	-0.235	0.495	0.180	0.108	-0.318	-0.396	0.024	0.441	-0.059
4	-0.132	-0.090	0.383	-0.296	-0.098	0.105	0.056	0.208	0.345	-0.564
5	0.231	0.268	0.400	0.038	-0.724	-0.048	-0.101	-0.380	0.500	-0.332
6	-0.281	-0.030	0.994	-0.371	0.163	-0.025	-0.266	-0.399	0.588	-0.641
7	0.021	0.094	0.669	0.240	-0.401	-0.813	-0.170	-0.326	0.578	-0.103
8	-0.301	-0.031	0.704	-0.493	-0.259	0.149	-0.067	-0.001	0.702	-0.618
9	-0.377	0.299	0.615	0.114	-0.083	-0.481	-0.702	-0.174	1.023	-0.558
10	-0.142	-0.560	0.792	0.277	-0.320	0.373	-0.699	-0.546	0.740	-0.228
11	0.028	0.103	0.610	0.087	-0.003	-0.057	-0.872	-0.139	0.285	-0.183
12	-0.677	-0.533	0.391	-0.213	-0.347	0.013	0.776	0.027	0.184	0.176
13	0.265	0.034	0.791	-0.278	-0.425	0.191	-0.797	-0.628	0.607	-0.300
14	-0.255	-0.446	0.806	-0.263	-0.137	-0.185	-0.716	0.399	0.803	-0.289
15	-0.182	-0.041	0.540	-0.439	0.039	0.080	-1.082	0.188	0.716	-0.071

The directivity index gave an indication of how much the sound levels deviated from $\overline{L_{pA}}$. This is to say that if a value of $\overline{L_{pA}}$= 49 dBA was determined over N_M microphone positions and a value of L_{pAi} = 50 dBA was determined for one specific microphone position(e.g. i=4), a directivity index of 1 dBA would be determined. It is commonly known in literature that a change in dB level of 1 dB is barely perceptible, 3 dB to be noticeable, 6 dB to be clearly noticeable and 10 dB perceived as a doubling in sound level. This still holds for A-weighted sound levels. Table 4.3.2 shows the range of directivity index obtained from Table 4.3.1. The microphone position with i= 4 had the smallest directivity index with a minimum variation from the mean surface sound pressure level measured over the hemispherical dome as denoted in Table 4.3.2. An A-weighted SPL difference of maximum 0.277 dBA and a minimum of -0.493 dBA was recorded, indicating that people assessing the sound as measured at microphone position 4 would barely perceive a difference in the loudness levels

between sounds being compared. The sound as measured can be simplified in analysis to be a point source due to the analysis of the directivity index. As such, the use of any single microphone position was determined to be sufficient for making sound recordings with.

Table 4.3.2: Directivity index

ith microphone position *no.*	$L_{pAi}(B)$	D_{IAi}	
		min	*max*
1	22.43	−0.677	0.265
2	22.45	−0.560	0.369
3	22.44	0.383	0.994
4	22.45	−0.493	0.277
5	22.84	−0.724	0.163
6	22.65	−0.813	0.373
7	22.51	−1.082	0.776
8	22.23	−0.628	0.399
9	22.33	0.184	1.023
10	22.78	−0.641	0.214

4.4 Results

4.4.1 Fan performance

An important design criterion considered for fan design is fan performance. It is known that fan parameters influence performance which also affects noise emission. Fan performance is also one major factor which needs to be considered to see whether the fan is sufficient in fulfilling a desired task. It is therefore important to consider fan performance as it has implications to both noise and usefulness in providing cooling. Certain performance measures such as fan power is known to have a trade-off with noise (Subagyo *et al.*, 2019). Therefore, it is often most difficult to create an optimal design for both performance and noise as often increasing a fans power levels also increases broadband noise emissions. A more efficient fan would reduce noise levels while increasing performance but the purpose of this study was not directed towards determining a design for the most efficient fan but to rather study how blade metrics as common in literature affect the subjective evaluation of sound. This is to say that by considering the fan power differences for varied blade parameters operating at the same speed, the pleasantness of the noise is rather assessed. Measurements were made only for airflow and static pressure for prototype models. The following sections describe the methods used to

determine the performance of measured fans. The performance curve for the commercial fan selected as a baseline model was compared to the 3D printed fan replica which was 3D printed.

With the speed unknown, there was uncertainty towards how the performance curves should have aligned. Figure 4.4.1a shows the performance curve for the fan running at 1800 rpm in comparison to the fan curve for the original 3D scanned fan. Although it is assumed that the performance curve, as measured by manufacturers, were provided at the fans maximum speed operated at 2400 rpm, this was not clear. The fan laws, used to scale for pressure measured in units of pascal and airflow measured in CFM is given in equation (4.4.1) and (4.4.2). The notation Q_1 and H_1 denote the airflow and static pressure reading measured at a speed of N_1 which is scaled to airflow and static pressure readings of Q_2 and H_2 measured at the speed of N_2.

$$\frac{Q_1}{Q_2} = (\frac{N_1}{N_2}) \tag{4.4.1}$$

$$\frac{H_1}{H_2} = (\frac{N_1}{N_2})^2 \tag{4.4.2}$$

The measured readings for the fan running at 1800 rpm were scaled using the fan laws to the speed of 2400 rpm to try and compare the distributions. It was determined that although it was not an exact fit, a similar trend was visible between the scaled and original fans performance curves. With a comparison made between the original and recreated fan models performance curves, each other fans performance running at the same speed and operating conditions were compared with the original fan model. The readings obtained for each fan tested at the same speed show that the maximum airflow did not exceed 70 CFM (0.033 m^3/s). As such, the plenum used for testing was applicable as identified for ISO 3745.

Due to the primary objective of the fan being focused on airflow rather than static pressure, low-pressure readings were obtained. The influence of each blade parameter to the measured performance for each fan can bee seen visually, given in Figure 4.4.1b, Figure 4.4.1c and Figure 4.4.1d. The primary factor which contributed to fan performance seems to mainly depend on the fan blade angle as seen in Figure 4.4.1d where increasing blade angle seems to increase fan airflow. It was also seen that static pressure also rises marginally with increasing blade angle. The change as to airflow between the worst and best-performing fan was determined to be about 23 CFM (0.011 m^3/s) running with constant conditions being maintained as to system resistance and blade speed.

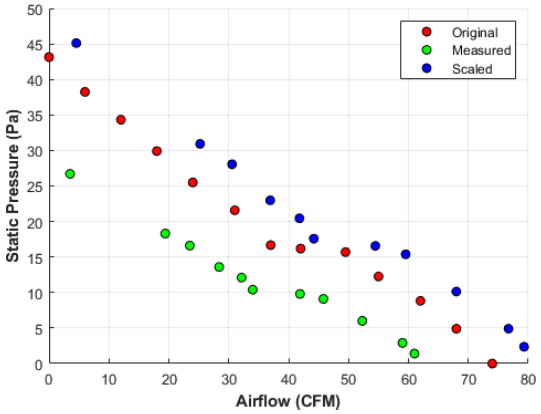

(a) Performance curve comparison (Corsair, 2018)

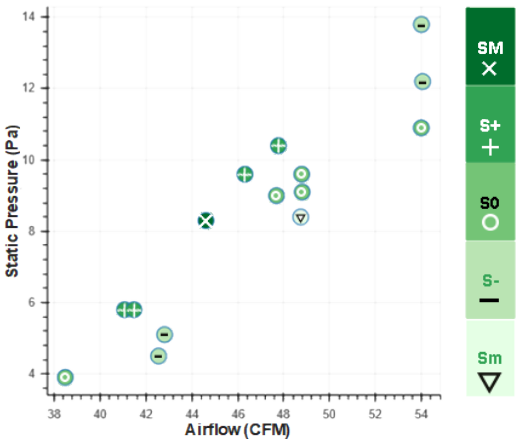

(b) influence of sweep on performance

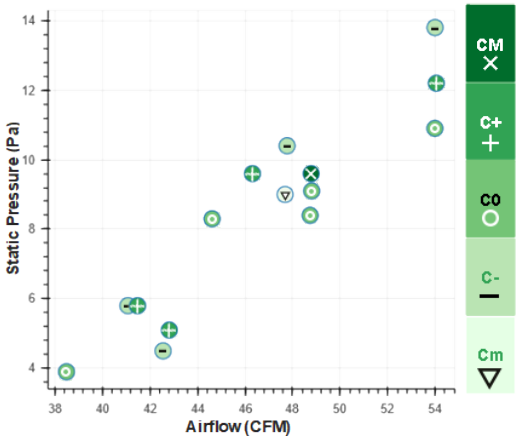

(c) influence of chord on performance

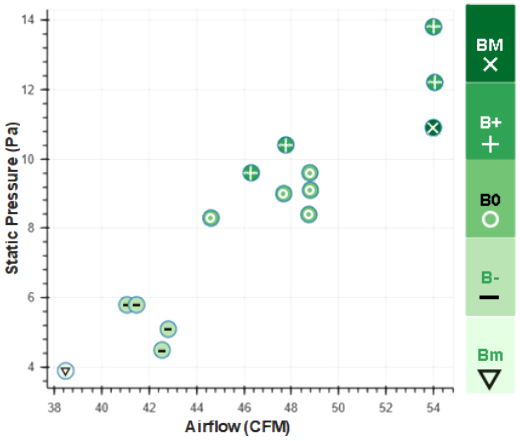

(d) influence of blade angle on performance

Figure 4.4.1: Performance measures for fans with (a) baseline fan performance curve comparison with original fan (fan no. 9); performance measures for prototype fan models as seen by (b) altered sweep, (c) altered chord, and (d) altered blade angle

4.4.2 Fan noise

Standard octave or third-octave bands are most commonly used in industry to make analysis in the frequency domain. This is especially so for continuous noise sources such as fan noise. Octave bands are used to create segments of frequency bins where noise around a certain frequency is expressed as a single number. The true frequency response was of interest. As such, no weighting was applied to the octave bands (Swart, 2018). All fans were operated at the speed of 1800 rpm.

Fan noise is characterised mainly by broadband noise and a discrete tone which is present at the blade pass frequency located at 210 Hz. Muiyser *et al.* (2018) showed broadband noise for fans to be typically expected between the frequency range of 900 Hz to 4 kHz where human hearing is quite sensitive. Harmonics or additional tones are also expected to be present. By analysis of magnitude levels displayed over frequency bins, the effects of blade metrics on frequency content were identified. The 3^{rd} octave analysis for prototype fan models SM, Sm, BM, Bm is shown in Figure 4.4.2. An interesting finding was the observed change as seen in Figure 4.4.2a and 4.4.2b showing how SPL levels changed over frequency bins with altered blade angle. The expected finding for an increase in broadband noise as seen in Figure 4.4.2a was identified for increased blade angle alone, supported by Glegg and Devenport (2008) and Filleul (1966).

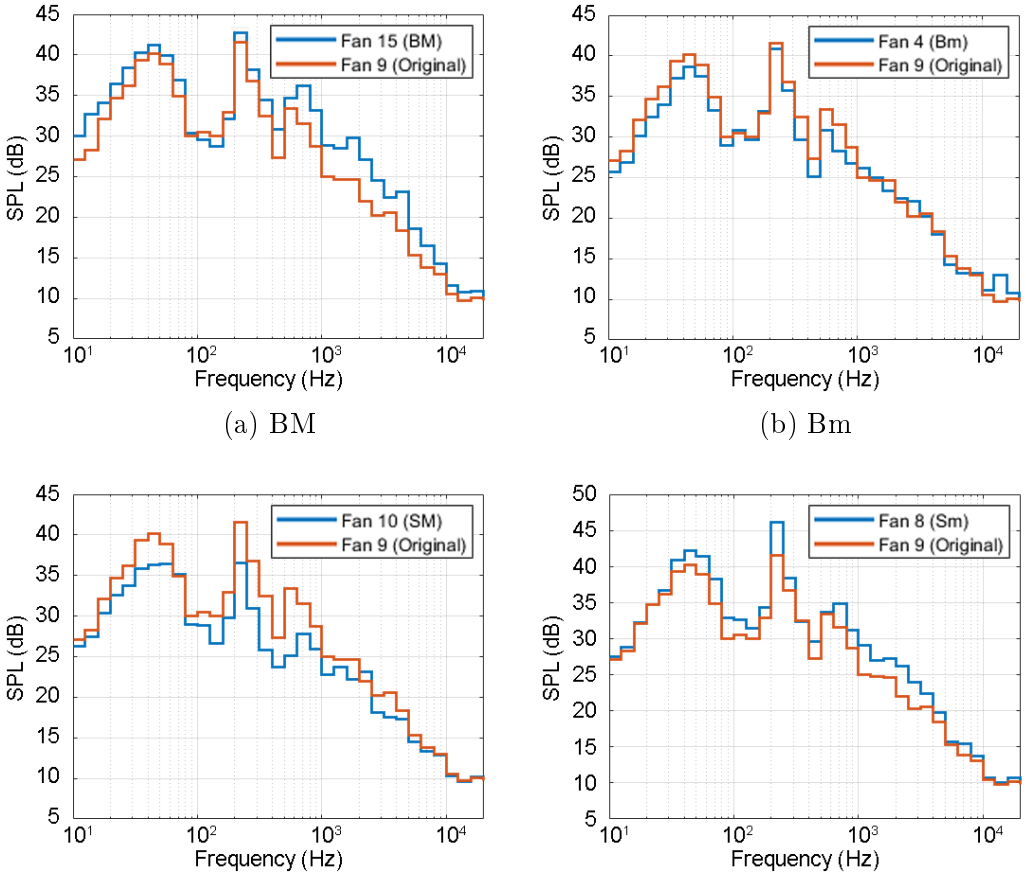

(a) BM (b) Bm

(c) SM (d) Sm

Figure 4.4.2: 3^{rd} octave band analysis shown for (a) fan prototype BM, (b) fan prototype Bm, (c) fan prototype SM and (d) fan prototype Sm

Equal amounts of blade angle were added and subtracted to create the rotor models BM and Bm, but changes, as observed over the frequency domain for decreased blade angle, had a significantly less impact as compared to increasing blade angle as shown in Figure 4.4.2b which was unexpected. It was also interesting to observe that the bands near BFP showed very little change for altered blade angle.

Alterations made to blade sweep is show in Figure 4.4.2c and 4.4.2d. A substantial change to broadband noise encompassing frequency content near BPF was observed. Changing blade sweep independently showed results as expected by Wright and Simmons (1990:7) where reduced magnitudes of noise were observed to be significant, especially for the bin encompassing BPF. An additional observation was made respect to blade metrics sweep and angle where increasing either parameter resulted in noticeable changes in magnitude for higher frequency content. Blade harmonics were identified to change as well where additional peak other than the one present at BPF was observed to change. Both increasing and decreasing blade sweep showed significant contributions to the broadband noise and discrete tones.

Altering blade chord individually is shown in Figure 4.4.3a and 4.4.3b. An expected trend is observed as identified by Wright and Simmons (1990:193) and Cumpsty (1977); where increased blade chord seems to increase SPL levels over most bins marginally, but the effect was quite minor. Higher frequency broadband noise seems to be impacted much less in comparison other blade parameters for altered chord. Decreasing blade chord had significant effects on frequency bins near 600 Hz. Magnitude levels were also observed to remained similar for the BPF octave bin.

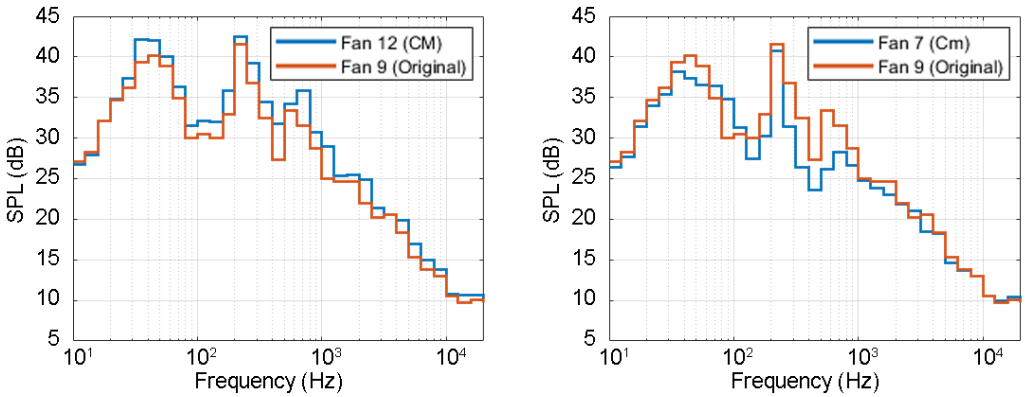

(a) CM (b) Cm

Figure 4.4.3: 3^{rd} octave band analysis shown for (a) fan prototype CM and (b) fan prototype Cm

Fan rotors with interactive changes made to blade metrics are shown in Figure 4.4.4a, 4.4.4b, 4.4.4c and 4.4.4d. Blade chord and angle are both known to increase SPL levels as such it was of interest how destructive interactions between the latter parameters would affect noise. Sweep was also considered for both interactions. As shown in Figure 4.4.4b, it was observed that fan model C-B+S- had a very similar magnitude distribution over frequency bins as compared to the original model. An observation was made for Figure 4.4.4a to 4.4.4d where lesser changes in magnitude was present for higher frequency bins. For the plots as given in Figure 4.4.4c and Figure 4.4.4d, effects to harmonic components was observed to be significant for C+B- for the frequency bins near 600 Hz whereas C-B+ showed almost no changes made in this identified region for S+ and S-.

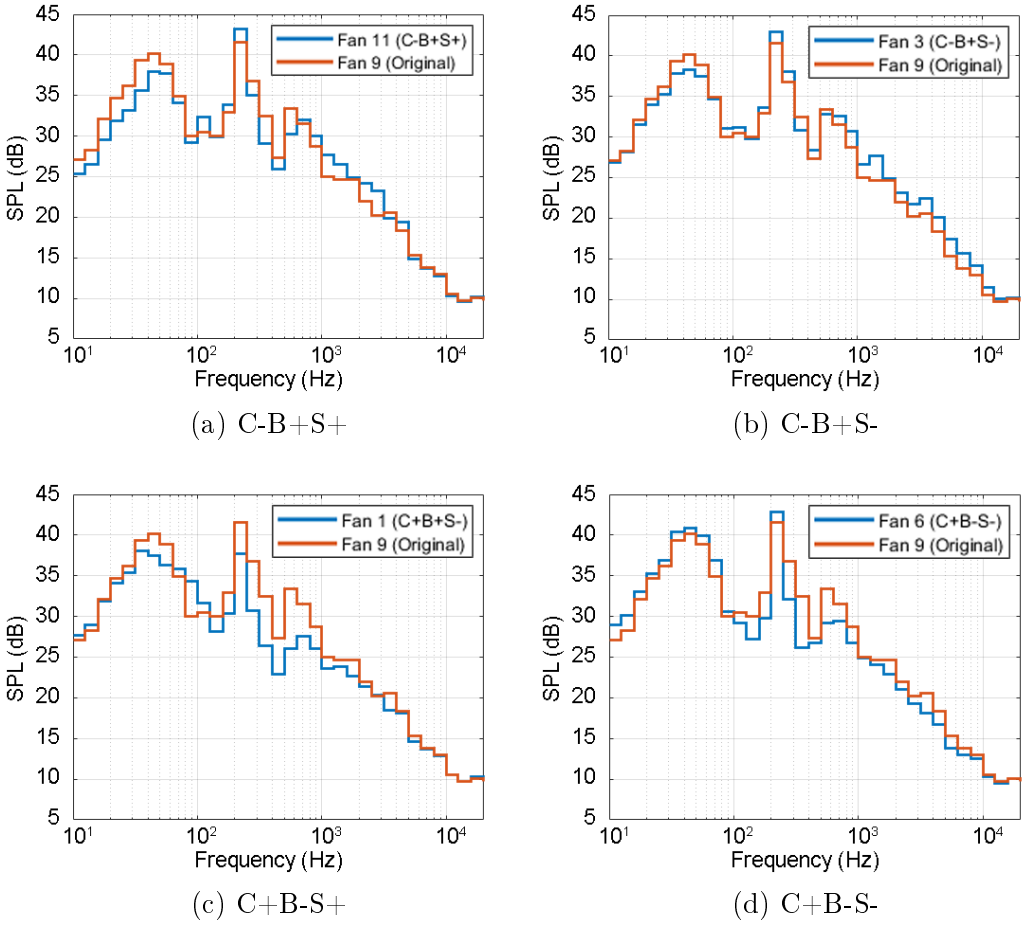

(a) C-B+S+ (b) C-B+S-

(c) C+B-S+ (d) C+B-S-

Figure 4.4.4: 3^{rd} octave band analysis shown for (a) fan prototype C-B+S+, (b) fan prototype C-B+S-, (c) fan prototype C+B-S+ and (d) fan prototype C+B-S-

Fukano *et al.* (1978) identifies sweep to have considerably more significant effects to noise with increased chord length. It was interesting to observe for C+B-S+ that a degree of decreased noise encompassing harmonic and BFP bins was present. It was also assumed that decreased blade angle also had an effect contributing to a more considerable decrease to noise. In contrast to observations made by Fukano *et al.* (1978), C-B+S- did not show almost any change to noise. This was largely unexpected because if increasing blade chord and sweep showed large changes to noise as observed by literature, doing the reverse would be expected to show similar results but with opposite effects.

In contrast to observations made by Fukano *et al.* (1978), C-B+S- did not show almost any change to noise. If increasing blade chord and sweep presented larger changes to noise as observed by literature, it would be assumed that doing the reverse would be expected to show similar results but with opposite effects. It was deduced that the effect of increasing blade angle might have contributed to the unexpected finding for C-B+S-. Also, Fukano *et al.* (1978) only considered the effect of increasing chord with sweep. As such, considering the performance of decreasing sweep and chord may be expected to present unexpected results.

Figure 4.4.5a to 4.4.5b shows fans considering constructive interactions between blade chord and angle (C+B+). Fan C+B+S- seem to show the largest increase in magnitude level especially at BFP. This was expected as the blade parameters were altered such that each parameter would contribute to an increase in noise for rotor model C+B+S-. Broad band noise was largely affected for rotor models as shown in Figure 4.4.5b, 4.4.5c and 4.4.5d. Lesser effects to the BFP was observed for rotor models with chord and angle decreased (C-B-).

Prototype model C+B+S+ shown in Figure 4.4.5c, was identified to have decreased sound pressure levels around BFP and blade harmonics positioned at 600 Hz. In contrast, prototype model C-B-S- showed almost no change to magnitude levels near BFP and harmonics. Instead, higher frequency broadband noise larger than 1 kHz was identified to be primarily influenced, which was an interesting comparison. Literature identifies that magnitude for frequency bins near BFP, and discrete tones have a significant contribution to the overall fan noise levels. Prototype model C+B+S+ was identified to have a significant effect to magnitude levels near BFP and harmonics. By analysis of the 3^{rd} octave plots the blade metrics angle and sweep seem to have the greatest influence as to noise but the overall response considering all combinations showed much variability.

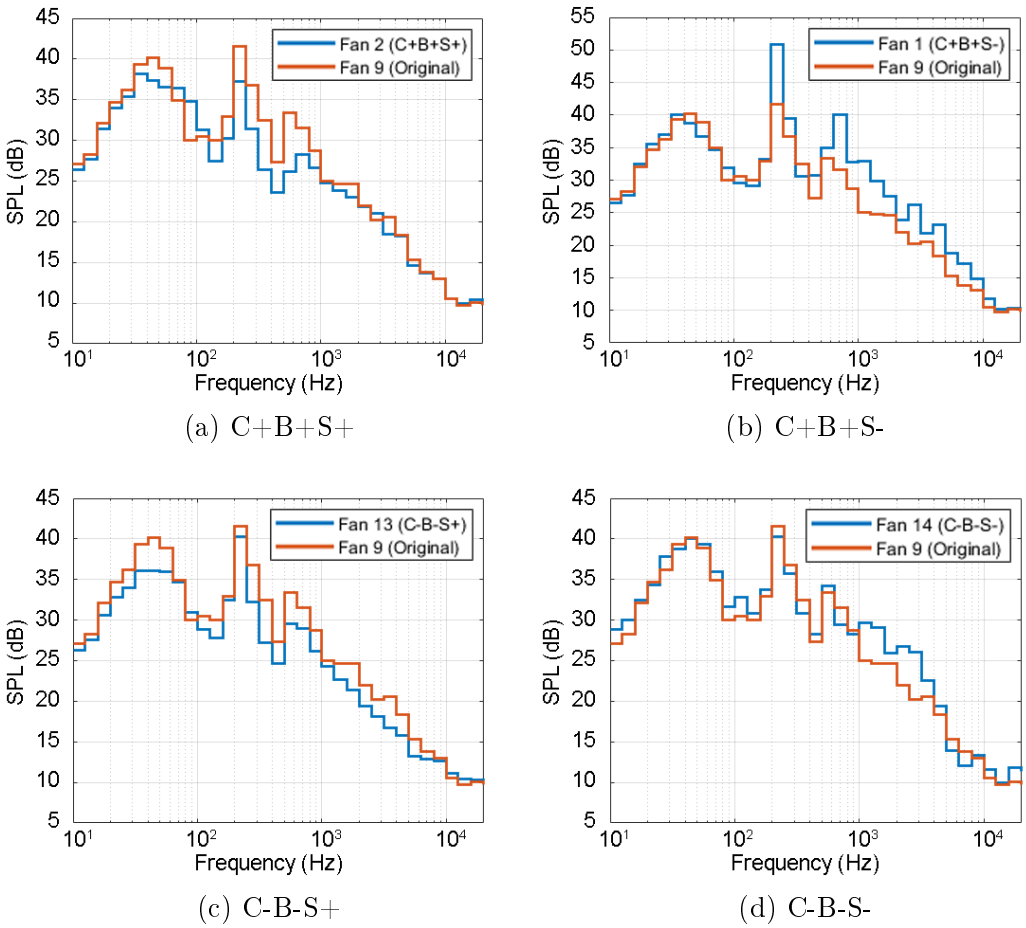

(a) C+B+S+ (b) C+B+S-

(c) C-B-S+ (d) C-B-S-

Figure 4.4.5: 3^{rd} octave band analysis for (a) fan prototype C+B+S+, (b) fan prototype model C+B+S-, (c) fan prototype model C-B-S+ and (d) fan prototype model (C-B-S-)

By analysis of the 3^{rd} octave plots the blade metrics angle and sweep seem to have the greatest influence for noise but the overall response considering all combinations showed much variability. The overall SPL readings for each fan was determined as shown in Table 4.4.1. The A-weighted and unweighted overall SPL measurements are shown.

Table 4.4.1: Comparison made between unweighted and A-weighted sound pressure levels for noise created by prototype fan models

Fan name	Overall SPL level		**Fan name**	Overall SPL level	
	dB	dBA		dB	dBA
Original	48.71	35.32	Original	48.71	35.32
Sm	51.10	38.24	SM	45.28	33.49
BM	50.05	39.67	Bm	47.34	34.38
CM	49.37	37.29	Cm	47.15	34.10
C+B+S-	52.66	40.14	C+B+S+	46.76	33.65
C+B-S-	49.17	35.53	C+B-S+	46.56	34.21
C-B-S-	48.30	34.45	C-B-S+	46.35	32.91
C-B+S-	48.82	36.83	C-B+S+	47.91	36.59

The overall SPL difference between the loudest fan (C+B+S-) and quietest (SM) in dBA was 6.65 dBA characterised by a doubling of sound level. Blade chord was identified to have the least effect on increasing the overall weighted SPL level with a difference of 3.19 dBA. Sweep had a noticeable change to the sound with an overall change of 4.75 dBA, and blade angle had an even greater noticeable change of 5.21 dBA.

4.4.3 Psychoacoustics metrics

The next step of considering the study of psychoacoustics, necessary to create a link between the measured pure sound and the subjective response was taken. It is true that the level of sound pressure in respect to frequency content is often sufficient to describe the continuous steady-state sound but to describe more complex sound quality attributes it is often lacking. The study of psychoacoustics provided a means to quantify sound in terms of metrics that describe a broader range of sound quality traits. Four psychoacoustic metrics, namely sharpness, roughness, loudness and fluctuation strength, are commonly used to determine what is called the 'Psychoacoustic Annoyance' which gives a measure of the unpleasantness of a sound sample. The fundamental theory that governs analysis as to determining psychoacoustic metrics will be discussed.

The psychoacoustic metrics are often used to determine for a unit which gives a description as to how annoying a sound is perceived. This unit as described in the literature by Zwicker and Fastl (2006) is known as the psychoacoustic annoyance (PA) value which provides a unit describing how annoying a sound is in comparison to other stimuli.

The equation used to calculate for the psychoacoustic annoyance (PA) value is given by equation 4.4.3.

$$PA = N_5(1 + \sqrt{w_S^2 + w_{FR}^2}) \tag{4.4.3}$$

$$w_S^2 = (\frac{S}{\text{acum}} - 1.75) \times 0.25 \times \text{lg}(\frac{N_5}{\text{sone}} + 10) \text{ for } S > 1.75\,\text{acum} \tag{4.4.4}$$

$$w_{FR}^2 = \frac{2.18}{(N_5/\text{sone})^{0.4}}(0.4\frac{F}{\text{vacil}} + 0.6\frac{R}{\text{asper}}) \tag{4.4.5}$$

Equation 4.4.4 and 4.4.5 is used to determine relevant parameters as identified in equation 4.4.3. With sharpness values equal or less than 1.75, the effect of sharpness is known to be negligible with $w_S^2 = 0$ (Park *et al.*, 2015; Rossi and Nicolini, 2010). The psychoacoustic metrics determined for prototype fan models is given by Table 4.4.2. Table 4.4.2 was ordered in increasing magnitude of the PA value. A difficulty arises when trying to visualise what is considered to be a large change for psychoacoustic measures. To deal with this problem, values obtained from literature were referred to. As in the case of loudness, SPL analysis was also determined to have beneficial implications, which can be used to determine the effect of the loudness metric.

The sharpness value as shown in Table 4.4.2 ranged between values of 1.19 and 1.38 acum. When compared to the sharpness value of 1.17 acum as determined by Yang and Zhu (2016b) and 1.75 acum for one select fan for Novak *et al.* (2005); the values were determined to be quite similar in contrast to higher sharpness values obtained by Muiyser *et al.* (2018), ranging between 4.1 - 5.7 acum. An interesting observation was made using Table 4.4.2 with sharpness playing no role in the equation for PA due to sharpness values being lower than 1.75 acum as seen by Table 4.4.2. Values, as obtained for the metric loudness, presented a range of values (2.29 - 4.46 sone); close to the loudness value obtained by Yang and Zhu (2016b) measured to be 3.73 sone. Measures of loudness obtained were much lower when compared to loudness values obtained by Muiyser *et al.* (2018) ranging between 90 - 190 Sone. Possible reasons for higher measures for sharpness and loudness as obtained by Muiyser *et al.* (2018) was identified to be due to larger-scale fans being considered with blade diameters of 630 mm.

Values obtained for roughness and fluctuation strength, as shown in Table 4.4.2 were compared to the roughness value of 0.174 asper and 0.0186 vacil obtained by Yang and Zhu (2016b). Due to measurements being made in an anechoic chamber, the influence of background noise is reduced drastically. This is to say lower readings of fluctuation strength and roughness were observed due to the modulation effect of background noise being reduced.

Table 4.4.2: Psychoacoustic analysis for noise created by prototype fan models sorted in levels of increasing levels of PA

Fan name	**Loudness** (Sone)	**Sharpness** (acum)	**Roughness** (asper)	**Fluctuation Strength** (vacil)	**Psychoacoustic Annoyance** (PA)
C+B+S–	4.46	1.26	0.0536	0.0134	5.41
BM	4.45	1.31	0.0495	0.0111	5.35
Sm	3.72	1.19	0.0553	0.00958	4.53
CM	3.45	1.27	0.054	0.0106	4.21
C-B+S–	3.31	1.18	0.0497	0.00903	4.01
C+B–S–	3.27	1.16	0.0510	0.01012	3.98
C–B–S–	3.15	1.3	0.0483	0.0112	3.83
C-B+S+	3.14	1.3	0.0508	0.00966	3.82
Original	3.06	1.26	0.0485	0.00844	3.71
Bm	2.90	1.25	0.0476	0.00882	3.52
Cm	2.63	1.2	0.0432	0.00887	3.18
C–B–S+	2.60	1.30	0.0461	0.00824	3.16
C+B+S+	2.38	1.19	0.0453	0.0091	2.90
SM	2.29	1.38	0.0455	0.00689	2.79
C+B–S+	2.29	1.38	0.043	0.00912	2.78

The loudness levels observed in Table 4.4.2 for values higher than 3.45 Sone present A-weighted SPL measurements between 37.29 - 40.41 dBA; with loudness values lower than 2.6 Sone presenting values between 32.91 - 34.21 dBA. A maximum difference of 7.5 dBA in the A-weighted SPL readings was comparable to a difference in loudness value of 2.17 Sone. The values obtained for loudness and sharpness seem to show a similar conclusion as made by Muiyser *et al.* (2018) stating that fan noise is dominated by loudness with sharpness showing lesser implications for fan noise. This was further supported by the high correlation as observed between loudness measures when compared to PA values given in Table 4.4.2. It was an interesting finding to observe the influence of altered chord, angle and sweep to be similar as compared to when considering sweep alone as in the study by Muiyser *et al.* (2018).

A general trend was identified where the PA value showed decreasing magnitudes for annoyance levels with increased sweep and decreasing blade angle and chord length. Blade sweep was identified to have the strongest correlation to the PA values with the influence of chord having lesser implications. Fukano *et al.* (1978) mention increased chord to have a significant effect on blade sweep. It was interesting to determine that increased chord with sweep contributed largely to obtaining the lowest obtained PA values. Blade parameter combinations show to have interesting results as to the deviation caused, but the statistics analysis on how the blade metrics relate to other metrics need to be first investigated to verify observations made.

Chapter 5

Subjective evaluation of fan noise

The following sections will describe the methods which were used to collect data on the subjective metrics, which consist of data as obtained by the response of people to different fan noises. Two tests have been noted to be most prominent for collection of data consisting out of a forced pairwise comparison test as well as a bipolar semantic differential test. Two GUI interfaces have been designed for which automated tests will be used to determine preference ranking and semantics for fan sounds as perceived by jurors. As the test will be conducted on people, it was necessary to obtain ethical approval for the project to be able to commence. The project reference number approved by the Research Ethics Committee is ING-2018-7882.

5.1 Test setup

The setup, as shown in Figure 5.1.1 was used to perform jury testing. Recorded fan sounds were output via a pair of Sennheizer HD6 Mix headphones. The pair of headphones used was known to reduce background noise emission through partial noise-cancelling traits (Sennheiser, 2018).

Figure 5.1.1: Jury evaluation test setup showing (left) computer, Xonar Essence DAC and headphone setup and (right) jury evaluation tests being conducted

The quality of sound output from a pair of headphones is determined by the precision of the DAC converter. As such, outputting a signal through a computers sound card was identified to be insufficient. Sound was therefore output through a Xonar Essence STU USB DAC (Digital to Analog Converter). To ensure that the sound output from the headphones was of the same level of loudness as measured using the calibrated microphones, a 1 kHz tone signal as output by the Larson Davis CAL200 calibrator was recorded using a Head Acoustics Squadriga (Head, 2010) and microphone setup. The recorded noise sample was output and measured using a binaural HATS (Head and Torso Simulator) system. The volume of the computer was adjusted until a reading of 94 dB was obtained.

5.1.1 Forced pairwise comparison test

The algorithm used to code for the forced pairwise comparison test compared each fan sound sample to one another where jurors needed to choose between two samples on their perceived preference in sound quality. The matrix used to keep track of comparisons made is shown in Figure 5.1.2, using the pairwise comparison tests as mentioned by Dieter and Schmidt (2013) with adaptations for the test to be made into a 2AFC as proposed by Bi (2015:5).

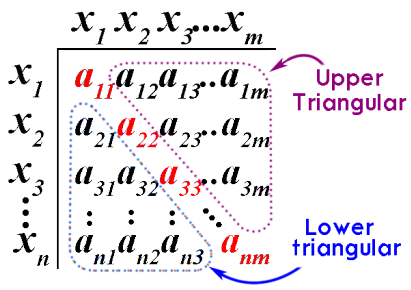

Figure 5.1.2: Forced pairwise comparison test matrix adaptations from Dieter and Schmidt (2013) with x_n independent variables; a_{nm} comparisons; n and m used as indices for the rows and columns and comparisons only made in the upper triangular region

Figure 5.1.2 shows a matrix which shows the orientation of stimuli being compared with one another. For convenience, the notation n was used for the number of rows and m denotes the number of columns. The maximum value which both n and m could have was 15 as 15 fan stimuli were being compared with one another. The notation x_n and x_m both represent the sound stimuli for the nth or mth fan being compared. The variable n is used as a row index while m is used as a column index. Each fan sound stimuli being compared had a chance to obtain a tally for each comparison adding up to a maximum of 14 tallies if one specific fan sound was preferred over all the other stimuli.

Figure 5.1.3 shows the GUI interface which was used for the forced pair comparison test. The test was initiated with a start button for which jurors were asked to listen to sound stimuli being compared using a replay button.

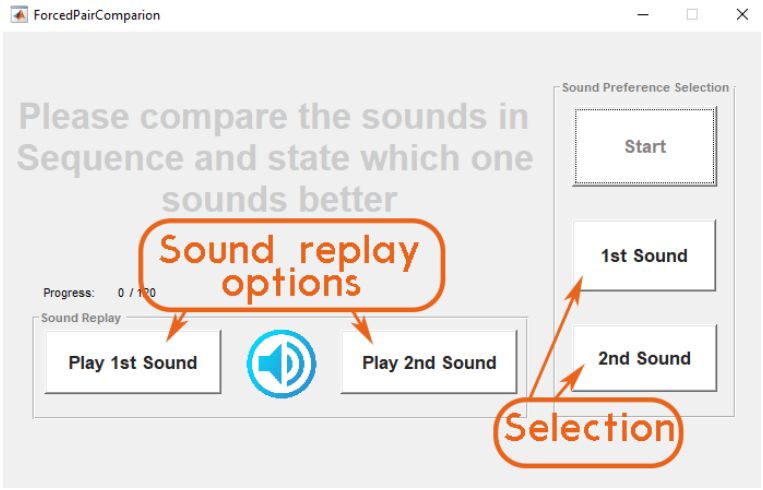

Figure 5.1.3: GUI used to conduct a forced pairwise comparison test

A total of 105 comparisons were made between fan sounds for which a progress bar would indicate the number of samples which still needed to be compared for jurors. A selection was made by the juror where the juror would press the button for either the 1^{st} or 2^{nd} sound stimuli, whichever the juror preferred in regards to sound quality. With a selection being made the program would increment the tally number for the fan stimuli selected by 1 unit and would move onto the next sample being compared until all samples in the upper triangular region have been compared. The samples being tested were shuffled in the output to ensure that jurors will perceive stimuli to be randomly selected. A flow diagram describing the algorithm used for the forced pairwise comparison is given in Appendix B.1.

5.1.2 Semantic differential test

The semantic differentials test was conducted using 10 established semantic adjective used inside a bi-polar semantic differential scale (Likert scale), used to describe fan noise in the paper published by Schneider and Feldmann (2015:2). The semantic adjectives considered as listed as shown by Table 5.1.1, with the bi-polar counterparts, also listed.

Table 5.1.1: Adjectives used to conduct the semantic differential test

Bi-polar semantic adjectives	
Semantic adjective	**Bi-polar counterpart**
Strong	Weak
High quality	Low quality
Quiet	Loud
Pleasant	Annoying
Without tones	With tones
Non-humming	Humming
Non-droning	Droning
Non-whooshing	Whooshing
Low tone	High tone
Non-fluctuating	Fluctuating

Figure 5.1.4 shows the GUI interface used to evaluate each fan noise according to semantics. Each adjective had an integer weight value ranging from -3 to 3 measuring either a positive or negative response for an adjective statement. A value of 3 indicates a positive response towards the semantic adjective being considered indicates a bias towards a specific trait of noise quality. The semantic GUI interface was initiated by pressing the 'Start' button, as shown in Figure 5.1.4.

Figure 5.1.4: GUI used to conduct a bipolar semantic differential test

Jurors were asked to listen to fan noise stimuli for each fan and determine the weighting for each semantic adjective. The response for each fan sound was recorded for which jurors filled in radio buttons to describe the weighting. A 'Next' and 'Previous' button facilitated transfer between fan sound stimuli being compared and the filled in the response of the jurors for the bi-polar Likert scale. Each sound was evaluated by pressing a 'Replay' button which would output a fan sound for a specific fan being evaluated. After jurors completed filling in the information related to the semantics for each prototype fan model the test was completed. An average time of 30 minutes was taken for jurors to complete both tests.

5.2 Results

A total number of 51 jurors were asked to collect data where an average test lasted 30 minutes. All jurors except 2 jurors fell into the age group of 19-26 years of age where 22 jurors were female and 29 jurors male. The full list of polar and violin plots describing data collected is given in Appendix B.

5.2.1 Forced pairwise comparison test results

The violin plots, as given in Figure 5.2.1 shows the statistical distribution for the data obtained from the forced pairwise comparison test. The abscissa gives the number of tallies assigned to each violin plot. The maximum number of tallies which each fan could obtain was 14 as 15 fans were evaluated with one another. The notation Q denotes quartiles with $Q0$ denoting the lower limit, $Q4$ the upper limit, $Q1$ representing the lower quartile, and $Q3$ the upper quartile. With the median shown, the skewness of the distribution can be determined. Gaussian distributions with skew was observed with very few bi-modal distributions present. To get a better idea of the perception of jurors semantic radar in conjunction with comparative violin plots were used. The mean value was used to make radar plots while violin plots presented quartile ranges as while showing the distribution of data.

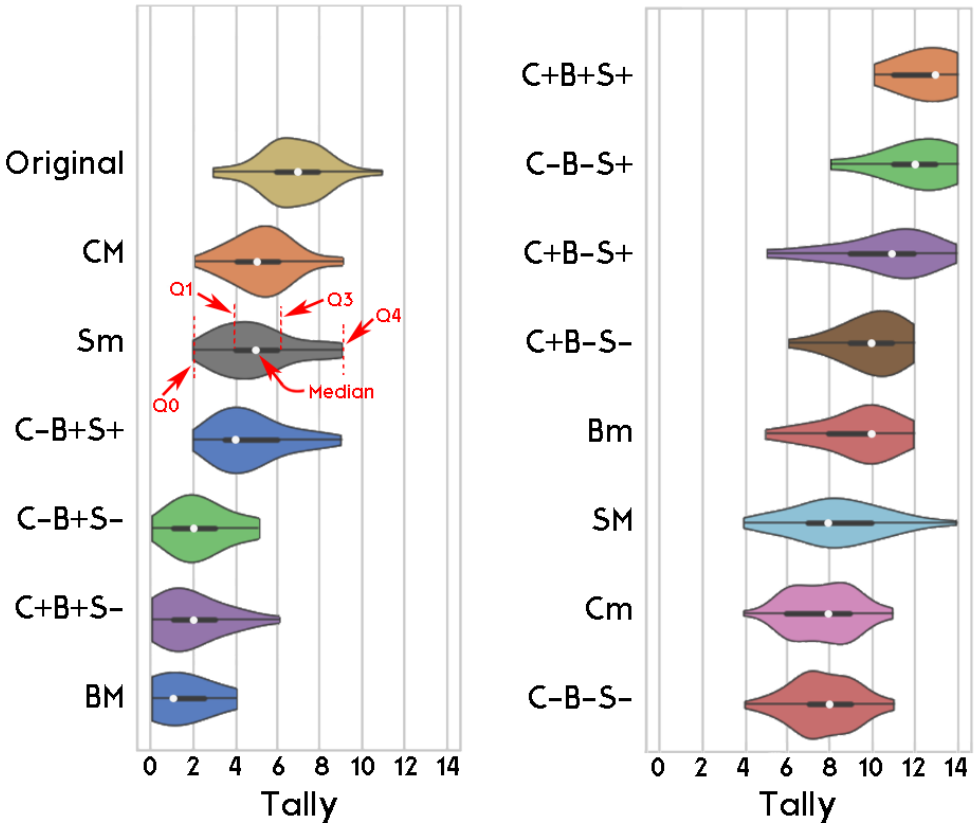

Figure 5.2.1: Violin plots showing the distribution of tallies assigned with (left) lower-ranking fans and (right) higher-ranking fans

5.2.2 Semantic differential test results

With ranking for jury preferences determined from the forced pair comparison test, the bi-polar semantic differential test was used to visualise how jury perceived noise. Figure 5.2.2 shows the results obtained for the bi-polar semantic differential test; comparing the top three ranking fans C+B+S+ (highest ranking), C–B–S+ (2^{nd} highest) and C+B–S+ (3^{rd} highest) to the three lowest-ranking fans being BM (lowest ranking), C–B+S– (2^{nd} lowest) and C+B+S– (3^{rd} lowest); shown in Figure 5.2.2a and Figure 5.2.2b. The baseline fan was also displayed, used as a means to compare between higher and lower-ranking fans. The mean value for jury response for each semantic adjective is displayed on the polar plots.

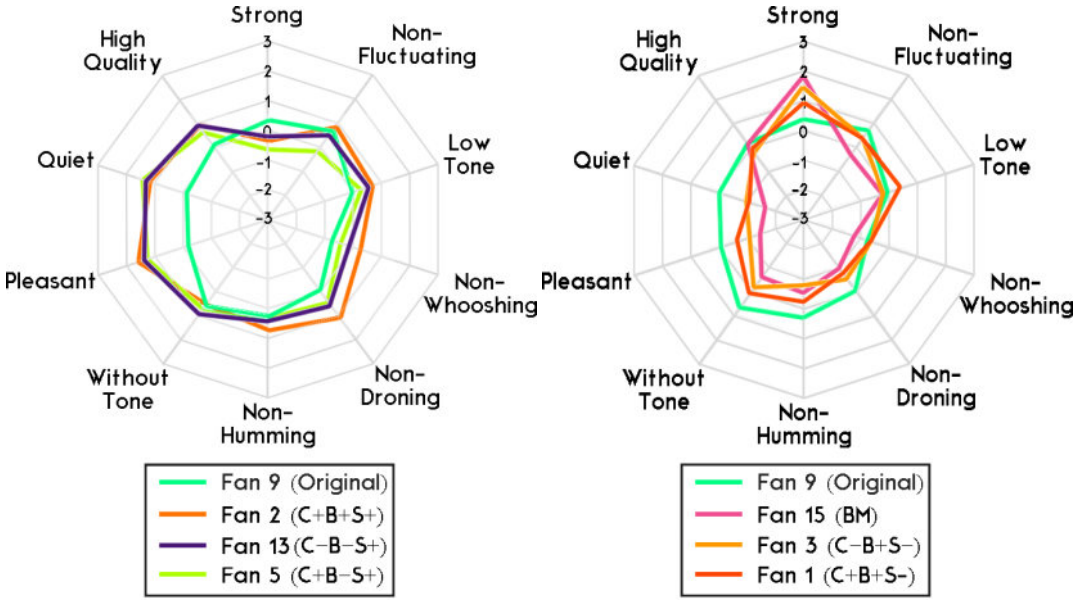

(a) Highest ranking fans (b) Lowest ranking fans

Figure 5.2.2: Radar plot comparison made to baseline fan with (a) highest ranked fans, (b) lowest-ranked fans

Semantic adjectives expected to have a positive influence as to a sound trait were displayed on the outer rims of the polar plot with a magnitude of 3. Conversely, the magnitude value –3 describes the polar plot position representing the bi-polar counterparts. Two things were mainly looked at, namely analysing how much magnitude levels differ in comparison to the baseline fan, for each semantic adjective; and whether a gradual increase in magnitude was present, relating fan ranking to identified changes made. Violin plots were used in conjunction to polar plots to visualise the data distributions as only using the mean value limited evaluation to an averaged reading. Figure 5.2.3 shows split violin plots used to visualise the spread of data obtained from the semantic differential test for jurors, comparing the highest-ranking fan (Figure 5.2.2a) to the lowest ranking fan (Figure 5.2.2b). The key points used to understand the data obtained will be mentioned only.

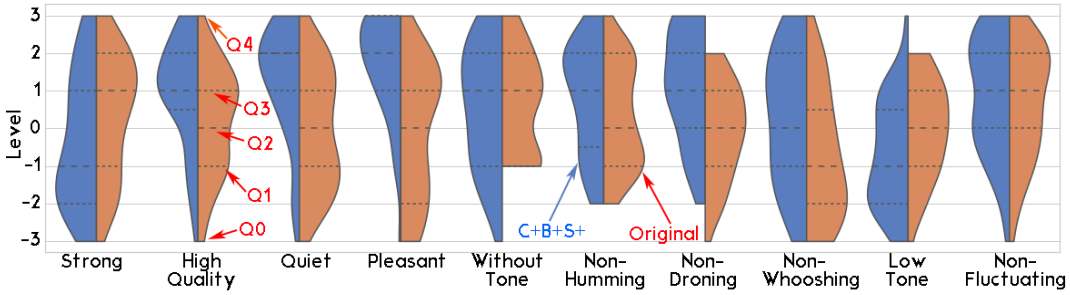

(a) Distribution of semantic data for fan model C+B+S+ (highest ranked fan), showing half violin plots; comparing fan model C+B+S+ (left) to the original fan model (right) for each semantic adjective

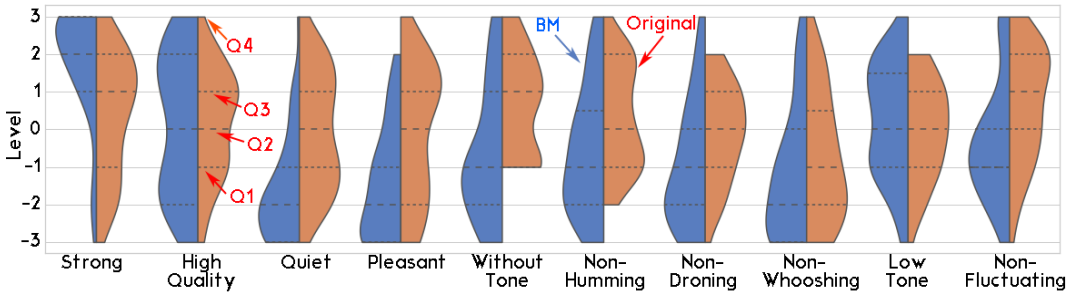

(b) Distribution of semantic data for fan model BM (lowest-ranked fan), showing half violin plots; comparing fan model BM (left) to the original fan model (right) for each semantic adjective

Figure 5.2.3: Half violin plots showing semantic adjective data distributions for (a) prototype fan model C+B+S+ and (b) fan prototype model BM

A comparison was made using data obtained from the baseline prototype fan, showing as split violin plot distribution on the left for each semantic adjective considered for Figure 5.2.3a and Figure 5.2.3b. The other fan being compared is presented on the left for each violin split plot. When considering the baseline fan (right distribution for each violin plot) in Figure 5.2.3, a bi-modal distribution was often seen. This indicated that two distinct populations could be identified for jurors, with opinions to semantic adjective being divided. With increased fan rank indicating jury preference, it can be seen that most bi-modal responses change to a skewed distribution often with a single-mode having a high magnitude value. This indicated that the divided jury opinion started to become less variable. The rest of the polar and violin plots giving insight to all other prototype models is given in Appendix B.2 and Appendix B.3.

Chapter 6

Statistical analysis and optimisation

6.1 Introduction

The following section describes the methods used for statistical analysis. The procedures used aimed at determining the relationship between blade parameters, psychoacoustic metrics and the subjective response of jurors. First and second-order regression models considering main and interaction effects between variables were considered. The focus of this study was to determine the relationship between blade parameters, psychoacoustic metrics and the subjective response of jurors. For convenience the terminology used for various parameters considering the main and interaction effect within a regression model will be stated. Parameters considering main effects for 1^{st} order equations are represented by the notation $\beta_a x$ where x denotes a specific independent variable and β_a its coefficient. For 2^{nd} order models, parameters considering the main effect are represented using the expression $\beta_b x^2 + \beta_c x$ where the variable x once again denotes an independent variable with coefficients β_b and β_c. Parameters considering two and three way interaction effects between variables is the same for both 1^{st} and 2^{nd} order equations. Namely, the notation $\beta_d x_i x_j$ represents a two way interaction effect ($i \neq j$) with a constant β_d and $\beta_e x_i x_j x_k$ representing a three way interaction ($i \neq j \neq k$) effect with a constant β_e will be used.

6.2 ANOVA

A decomposition of the total variability present will be given in response of a dependant variable using the ANOVA method (Iversen *et al.* , 1987). The ANOVA method gave a means to determine the sensitivity of a model towards the variability present for data (Myers, 2013). This allowed for different models to be evaluated giving insight on how well the model can predict for a dependant variable. The equations representing a generic first and second or-

der model for k independent variables is given by equation (6.2.1) and (6.2.2). The equations make considerations as to the main and two,three way interactions between variables. The independent variables $(x_1, x_2, x_3 ... x_k)$ will be referred to as the regressor variables and the dependant variable $(\hat{y})$ the response variable.

$$\text{Generic } 1^{st} \text{ order model:} \quad \hat{y} = \beta_0 + \sum_{i=1}^{k}(\beta_i x_i) + \sum_{i<j=2}^{k}\sum (\beta_{ij} x_i x_j) + \sum_{i<j<m=3}^{k}\sum\sum (\beta_{ijk} x_i x_j x_m) + \epsilon \tag{6.2.1}$$

$$\text{Generic } 2^{nd} \text{ order model:} \quad \hat{y} = \beta_0 + \sum_{i=1}^{k}(\beta_i x_i) + \sum_{i=1}^{k}(\beta_{ii} x_i^2) + \sum_{i<j=2}^{k}\sum (\beta_{ij} x_i x_j) + \sum_{i<j<m=3}^{k}\sum\sum (\beta_{ijk} x_i x_j x_m) + \epsilon \tag{6.2.2}$$

$$H_0 : \beta_1 = \beta_2 ... = \beta_n = 0 \tag{6.2.3}$$

$$H_1 : \beta_j \neq 0 \qquad \text{for at least one j} \tag{6.2.4}$$

The test for significance of regression is a test used in ANOVA, which is used to determine if there is a linear relationship between a response variable and a number of regressor variables. The appropriate null and alternative hypothesis are given by equation 6.2.3 and 6.2.4 where n denote the number of parameters included in the model. The p-value statistic will be used to determine a criterion to reject the null hypothesis (H_0) where a p-value smaller than a select criterion α_c indicates that the regression model is significant and H_1 can be accepted. Although a typical selection of p$<$0.05 is commonly used, arguments, as given by Fisher (1959), gives indications as to select higher p-value thresholds when considering jury response. Measured values were evaluated using the threshold of p$<$0.05 while the response from jurors was evaluated using a higher threshold of p$<$0.2. In analysis of data obtained, the Pearson's r, R squared, adjusted R squared, and p-value was used.

Pearson's product-momentum correlation is often used to determine the strength and direction of a linear relationship between two continuous variables (Myres, 2013). The coefficient used is called the Pearson's correlation coefficient, also called the Pearson's r value.The value can range between -1 for a perfect negative linear relationship to $+1$, indicating a perfect positive linear relationship. A value of 0 indicates that there was no linear correlation present between the two variables. The Pearson's r value will be used to identify the linear correlations present between blade parameters, psychoacoustic metrics and the

subjective response respectively.

The R^2 value describes the percentage of variance explained by the model. Used in conjunction with the Pearson's r value, the percentage of variance explained by the model with visuals as to the contribution of each independent variable can be determined. Typically, the R^2 value is used in conjunction with the adjusted R^2 value due to problems which arise when more independent variables are added to a model. This is to say that the R^2 value is often biased, with the R^2 value increasing every time an independent variable is added, even when it may have been by chance that there was a correlation between variables. A second problem related to R^2 values is also known to arise due to overfitting, where adding more variables to a model will create very high misleading R^2 values. Although there is a degree of criticism linked to the R^2 value, it is still known to be a good starting measure to understand results (Draper and Smith, 1998).

The adjusted R square value explains the percentage of variation explained by the model similar to the R squared value while correcting the above-mentioned positive bias. The adjusted R square compared to the R square value is used to determine what is known as the effect size (R^2 value - adjusted R^2 value = effect size). The effect size is indicative of the medium effect size according to Cohen's(2013) classification indicating the expected range of variability. The medium effect size, in conjunction with the p-value, can be used to give an analysis of the data's statistical significance (p-value) and its substantive significant (effect size).

Table 6.2.2 shows the results obtained for various R square, adjusted R square and p-values for psychoacoustic metrics modelled using fan parameters for 1^{st} and 2^{nd} order equations. Table 6.2.2 was used to identify the effect of adding interaction terms to a regression model. This was necessary as often the influence of adding interaction terms is not always beneficial. Table 6.2.1 denoting the Pearson's correlation table was used in conjunction with table 6.2.2 comparing relationships between regressor (psychoacoustic metrics) and response variables (blade parameters). The notation '**C**' for blade chord, '**B**' for blade angle and '**S**' for blade sweep was used for comparisons made as to the blade parameters. The blade parameters were used as the three regressor variables(x_1, x_2, x_3). Notations of this form with constants will represent model equations β_n for the n^{th} parameter, β_0 the constant term as well as the error term ϵ not shown. The equations considered in table 6.2.2 will be mentioned. The equation $\mathbf{C} + \mathbf{B} + \mathbf{S}$ represents a first-order model considering only the main effects between variables. The equation $\mathbf{C} + \mathbf{B} + \mathbf{S} + \mathbf{CB} + \mathbf{SB} + \mathbf{SC}$ considers main effects and two way interactions between variables. Lastly, $\mathbf{C} + \mathbf{B} + \mathbf{S} + \mathbf{CB} + \mathbf{SB} + \mathbf{SC} + \mathbf{CBS}$ represents the equation considering the main effects between variables and also two way and three-way interactions

between blade parameters.

When considering Pearson's r coefficient, two considerations can be made as to what is regarded as a strong, moderate, and weak correlation. When considering measurements and data generated by mechanical processes, Ratner (2009) mentions that the Pearson's r values are generally accepted to indicate a strong positive (negative) linear relationship for magnitude values between 0.7 and 1 (-0.7 and -1), moderate for values between 0.3 and 0.7 (-0.3 and -0.7) and weak when smaller than 0.3 (-0.3). Data considering the correlation between psychoacoustic metrics and blade parameters can use this criterion, but when considering data obtained from jurors, this criterion is identified to be too strict. When considering jury response, Lantz (2019) identifies that a more lax criterion can be used for the Pearson's r values, with values between 0.3 to 1 (0.3 to 1) being strong, values between 0.1 and 0.3 (-0.1 to -0.3) considered moderate and lastly values between 0 and 0.1 (0 and -0.1) considered weak. The criterion, as mentioned by Ratner (2009), was used to evaluate between blade parameters and psychoacoustic metrics. Blade sweep and blade angle were identified to have a substantial linear correlation as to the PA levels. Increased sweep was identified to decrease levels of PA while increasing blade angle was related to the levels of PA rising. Blade chord also was identified to have some correlation, especially to levels of sharpness and roughness but its overall impact as to the PA levels was minor. A moderate linear correlation was present for blade parameters to psychoacoustic metrics; with exceptions to **B** and **S** when compared to fluctuation strength, and **C** when compared to loudness and the PA levels. The parameters **B** was identified to have a positive linear correlation and **S** a negative linear correlation with psychoacoustic metrics.

Table 6.2.1: Pearson's r correlation table correlating blade parameters to psychoacoustic metrics

Pearson's Coefficient			
$\hat{y}$	**Chord (C)**	**Blade (B)**	**Sweep (S)**
Fluctuation Strength	0.007	0.254	−0.685
Roughness	−0.406	0.384	−0.462
Loudness	−0.151	0.497	−0.517
Sharpness	0.557	0.476	−0.359
Psychoacoustic Annoyance	−0.151	0.485	−0.516

With significant correlations between variables identified using the Pearson's r value, Table 6.2.2 gave indications as to how much variability the combination of blade parameters could account for while indicating as to the significance of the data obtained. The observations made will be briefly mentioned. Adding two-way and three-way interaction effects significantly improved the total variance accounted by sharpness and fluctuation strength while maintaining model significance. Adding interaction effects to model for roughness was identified to be less significant. Lastly, the analysis, as obtained by loudness and PA, showed very similar results compared to blade parameters. Adding interaction terms improved the model, but this effect was questionable when only considering a 2-way interaction with main effects, as a lower adjusted R square value was observed. The p-value was also identified to increase when adding interaction terms for loudness and PA.

Table 6.2.2: Psychoacoustic metrics analysis using blade parameters as regressor variables

	R squared, adjusted R squared(p-value)					
$\hat{y}$	**C+B+S**		**C+B+S+CB +SB+SC**		**C+B+S+CB +SB+SC+CBS**	
	1^{st} **order**	2^{nd} **order**	1^{st} **order**	2^{nd} **order**	1^{st} **order**	2^{nd} **order**
Fluctuation Strength	0.533[a]	0.544	0.829	0.840	0.948	0.960
	0.406[b]	0.203	0.700	0.552	0.896	0.859
	(0.033)[c]	(0.265)	(0.010)	(0.126)	(0.001)	(0.022)
Roughness	0.526	0.706	0.596	0.776	0.637	0.817
	0.396	0.485	0.293	0.373	0.275	0.360
	(0.036)	(0.066)	(0.185)	(0.244)	(0.237)	(0.303)
Loudness	0.537	0.695	0.608	0.765	0.716	0.874
	0.411	0.466	0.313	0.343	0.433	0.560
	(0.032)	(0.075)	(0.169)	(0.266)	(0.122)	(0.168)
Sharpness	0.665	0.728	0.860	0.923	0.861	0.923
	0.574	0.524	0.755	0.783	0.722	0.732
	(0.006)	(0.050)	(0.005)	(0.026)	(0.014)	(0.072)
Psychoacoustic Annoyance	0.524	0.685	0.604	0.765	0.708	0.869
	0.394	0.448	0.307	0.342	0.415	0.540
	(0.037)	(0.083)	(0.174)	(0.267)	(0.133)	(0.181)

Note: a = R squared; b = adjusted R squared; c = p-value

Table 6.2.3 show the results obtained from comparing the blade parameters to the subjective metrics used for jury testing. The variable 'Tally' indicated data, obtained from the forced pairwise comparison test, while other variables were variables used in the semantic test. 'Tally' only indicated a relative measure for perceived preference and nothing more. How strongly each blade parameter correlated with variables was of interest. Low R^2 or adjusted R^2 indicated increased model sensitivity. Increased sensitivity meant models were less likely able to predict for variables. A low R^2, adjusted R^2 or a high p-value gave indications for increased model sensitivity prone to error.

With a small p-value smaller than 0.05 typically The threshold as discussed by Lantz (2019) was used to determine what was considered a strong, moderate and weak correlation using the Pearson's coefficient in Table 6.2.3. The Pearson's coefficient results shown in Table 6.2.3 show that blade angle and blade sweep had the highest contribution towards variable adjectives: strong, quiet and pleasant. This trend was also seen from radar plot analysis indicating that **B** and **S** has a strong to moderate influence to fan sounds being quiet, and associations towards pleasantness. Variable **C** had a weak to moderate correlation, having the least influence when compared to **B** and **S**.

The overall reaction, as determined by variables used in the semantic test, had a moderate to weak correlation (between magnitude values of 0 and 0.3). One interesting observation was that 'Tally' for **B** had a magnitude value of 0.53, which indicated a very strong correlation when considering the response from people. An interesting finding was that all models considering main and interaction effects presented that each respective model using **C B** and **S** could make predictions to variables used for juror testing. However, most models were still sensitive with low R^2 values being present, making models only account for a small amount of variability (less than 0.2).

Table 6.2.4 shows the results linking psychoacoustic metrics to variables which were used to evaluate jury response. The Pearson's coefficient, R^2, adjusted R^2 and p-value are respectively given. Criteria mentioned by Lantz (2019) will be used to evaluate Pearson's r coefficients. The notation **F**, **R**, **L**, **S** was used to notate the four psychoacoustic metrics used to calculate the PA levels. Tally showed very strong correlation with **F**, **R** and **L** shown by Pearson's r values; presenting magnitude levels higher than 0.5. Variable **S** was identified to not correlate with 'Tally'. Variable **S** was identified to have a weak correlation when compared to variables considering jury response. Variable **L**, **R**, **F** presented strong correlations with adjective 'Quiet' and 'Pleasant' supporting the idea that the variables strongly influences annoyance levels.

Variable **L** was identified to have a higher correlation value when compared to **F** and **R**, indicating that **L** may have a stronger influence on levels of pleasantness. Main effects and interaction terms using psychoacoustic metrics were evaluated, used to determine model sensitivity towards jury test results. Most models sensitivity was considered to be high with R^2 values being typically lower than 0.2. It was interesting to see that only semantics, 'Quiet', 'Pleasant' and 'Strong' showed R^2 values which are larger than 0.2. All other semantic adjectives presented R^2 values explaining for only 2% to 7% of the variance. Only models for 'Tally' showed high R square values, considering main and all interaction terms, explaining for over 60 % of the variance with the p-value indicating that the model was capable of explaining for this variance.

The overall analysis, as obtained by the subjective response, showed that models considered for semantic variables accounted very little of the variability. Most results obtained, as shown by Table 6.2.3, indicated that models considered were significant. Semantics 'Quiet', 'Pleasant' and 'Strong' had R square and adjusted R square values which were more meaningful as compared to other semantics considered. The subjective variable which accounted for the largest amount of variability was the variable 'Tally' with R square and adjusted R square values larger than 0.5. This indicated that **C**, **B** and **S** predicted more than 50% of the variability in 'Tally'. It was also quite interesting to note that the difference in R^2 and adjusted R^2 between the 1^{st} and 2^{nd} order model for 'Tally' was less than 2% for the model considering the main and two-way, three-way interactions between variables. The main objective of the statistical analysis was to identify a model which can be used for optimisation as to jury preference. From an analysis of different metrics being compared, the PA value and 'Tally' was identified to be the most relevant. With interest being focused towards jury preference, the model for 'Tally' was select as the model to be optimised as it considered the largest degree of variability with the p-value indicating that the parameters **C**, **B** and **S** is able to predict for 'Tally'.

Table 6.2.3: ANOVA method comparing blade parameters to the jury test results

	Pearson's coefficient			R squared, adjusted R squared(p-value)					
$\hat{y}$	Chord (C)	Blade (B)	Sweep (S)	C+B+S		C+B+S+CB +SB+SC		C+B+S+CB +SB+SC+CBS	
				1^{st} order	2^{nd} order	1^{st} order	2^{nd} order	1^{st} order	2^{nd} order
Tally	0.070	–0.530	0.390	0.436[a] 0.434[b] (<0.001)[c]	0.453 0.449 (<0.001)	0.493 0.489 (<0.001)	0.509 0.504 (<0.001)	0.553 0.549 (<0.001)	0.570 0.564 (<0.001)
Strong	–0.183	0.299	–0.209	0.167 0.163 (<0.001)	0.172 0.165 (<0.001)	0.191 0.184 (<0.001)	0.196 0.186 (<0.001)	0.197 0.189 (<0.001)	0.202 0.191 (<0.001)
High Quality	0.057	–0.112	0.099	0.026 0.022 (<0.001)	0.030 0.022 (<0.001)	0.33 0.026 (<0.001)	0.037 0.026 (<0.001)	0.037 0.029 (<0.001)	0.042 0.029 (<0.001)
Quiet	0.122	–0.332	0.333	0.235 0.232 (<0.001)	0.249 0.244 (<0.001)	0.261 0.255 (<0.001)	0.275 0.266 (<0.001)	0.282 0.275 (<0.001)	0.296 0.287 (<0.001)
Pleasant	0.131	–0.275	0.301	0.183 0.180 (<0.001)	0.194 0.188 (<0.001)	0.200 0.194 (<0.001)	0.211 0.202 (<0.001)	0.222 0.215 (<0.001)	0.233 0.223 (<0.001)
With Tone	0.026	–0.113	0.166	0.041 0.037 (<0.001)	0.043 0.0359 (<0.001)	0.052 0.044 (<0.001)	0.054 0.043 (<0.001)	0.054 0.045 (<0.001)	0.056 0.044 (<0.001)
Non-Humming	0.056	–0.080	0.171	0.039 0.035 (<0.001)	0.044 0.036 (<0.001)	0.043 0.036 (<0.001)	0.048 0.037 (<0.001)	0.047 0.038 (<0.001)	0.052 0.039 (<0.001)
Non-Droning	0.010	–0.142	0.219	0.068 0.064 (<0.001)	0.075 0.067 (<0.001)	0.094 0.086 (<0.001)	0.100 0.089 (<0.001)	0.109 0.101 (<0.001)	0.116 0.104 (<0.001)
Non-Whooshing	0.024	–0.067	0.066	0.009 0.006 (0.064)	0.015 0.007 (0.070)	0.016 0.008 (0.058)	0.022 0.010 (0.056)	0.022 0.013 (0.017)	0.028 0.015 (0.018)
Low Tone	0.056	–0.036	0.038	0.006 0.002 (0.211)	0.022 0.014 (0.011)	0.012 0.004 (0.159)	0.028 0.016 (0.011)	0.017 0.008 (0.079)	0.032 0.019 (0.006)
Non-Fluctuating	0.014	–0.008	0.004	0.001 0.001 (0.006)	0.006 0.002 (0.050)	0.007 0.001 (0.005)	0.013 0.001 (0.026)	0.014 0.005 (0.014)	0.020 0.007 (0.072)

Note: a = R squared; b = adjusted R squared; c = p-value

Table 6.2.4: ANOVA method comparing psychoacoustic metrics to jury test results

	Pearson's Coefficient				R squared, adjusted R squared (p-value)							
$\hat{y}$	Fluctuation Strength (F)	Roughness (R)	Loudness (L)	Sharpness (S)	F+R+L+S		F+R+L+S +FR+RL+LS		F+R+L+S +FR+RL+LS +SF+FRL+RLS LSF		F+R+L+S +FR+RL+LS +SF+FRL+RLS +LSF+FRLS	
					1^{st} order	2^{nd} order	1^{st} order	2^{nd} order	1^{st} order	2^{nd} order	1^{st} order	2^{nd} order
Tally	-0.588	-0.519	-0.652	-0.05	0.4759[a] 0.4732[b] (<0.001)[c]	0.5872 0.5828 (<0.001)	0.5828 0.5784 (<0.001)	0.6178 0.6117 (<0.001)	0.6245 0.6185 (<0.001)	0.6294 0.6225 (<0.001)	0.6294 0.623 (<0.001)	0.6294 0.6225 (<0.001)
Strong	0.231	0.26	0.3	-0.0541	0.09137 0.08659 (<0.001)	0.1266 0.1173 (<0.001)	0.1316 0.1224 (<0.001)	0.1991 0.1863 (<0.001)	0.2053 0.1927 (<0.001)	0.2223 0.2077 (<0.001)	0.2204 0.2069 (<0.001)	0.2223 0.2077 (<0.001)
High Quality	-0.123	-0.158	-0.156	0.0278	0.02785 0.02274 (<0.001)	0.04239 0.03225 (<0.001)	0.03711 0.02692 (<0.001)	0.0449 0.0296 (0.001)	0.04519 0.02995 (<0.001)	0.04571 0.02789 (0.001297)	0.04539 0.02887 (<0.001)	0.04571 0.02789 (0.001297)
Quiet	-0.358	-0.368	-0.435	0.076	0.1916 0.1873 (<0.001)	0.2464 0.2384 (<0.001)	0.2356 0.2275 (<0.001)	0.3232 0.3124 (<0.001)	0.3222 0.3114 (<0.001)	0.3259 0.3133 (<0.001)	0.3259 0.3142 (<0.001)	0.3259 0.3133 (<0.001)
Pleasant	-0.331	-0.333	-0.384	0.0654	0.1532 0.1487 (<0.001)	0.2245 0.2163 (<0.001)	0.2122 0.2038 (<0.001)	0.2724 0.2608 (<0.001)	0.2746 0.2631 (<0.001)	0.2754 0.2618 (<0.001)	0.2753 0.2627 (<0.001)	0.2754 0.2618 (<0.001)
With Tone	-0.134	-0.124	-0.165	0.0175	0.02748 0.02236 (<0.001)	0.0471 0.0370 (<0.001)	0.04604 0.03595 (<0.001)	0.0723 0.0576 (<0.001)	0.07213 0.05732 (<0.001)	0.07488 0.05761 (<0.001)	0.07218 0.05612 (<0.001)	0.07488 0.05761 (<0.001)
Non-Humming	-0.167	-0.118	-0.15	0.0411	0.02906 0.02395 (<0.001)	0.0457 0.0356 (<0.001)	0.0473 0.03722 (<0.001)	0.06985 0.05501 (<0.001)	0.07357 0.05879 (<0.001)	0.07537 0.05811 (<0.001)	0.07382 0.05778 (<0.001)	0.07537 0.05811 (<0.001)
Non-Droning	-0.25	-0.157	-0.252	0.0509	0.07437 0.0695 (<0.001)	0.1108 0.1013 (<0.001)	0.1069 0.0974 (<0.001)	0.1401 0.1263 (<0.001)	0.138 0.1243 (<0.001)	0.1413 0.1253 (<0.001)	0.1409 0.126 (<0.001)	0.1413 0.1253 (<0.001)
Non-Whooshing	-0.1	-0.0703	-0.117	0.00431	0.01509 0.00991 (0.02)	0.0344 0.0241 (<0.001)	0.03106 0.02081 (0.002)	0.03927 0.02394 (0.002491)	0.03871 0.02338 (0.003)	0.03937 0.02144 (0.006791)	0.03909 0.02246 (0.005)	0.03937 0.02144 (0.006791)
Low Tone	-0.0535	-0.0835	-0.0785	-0.0078	0.008711 0.003494 (0.1551)	0.0445 0.0343 (<0.001)	0.04292 0.0328 (<0.001)	0.05397 0.0389 (<0.001)	0.05053 0.03538 (<0.001)	0.05635 0.03874 (<0.001)	0.05635 0.04001 (<0.001)	0.05635 0.03874 (<0.001)
Non-Fluctuating	-0.0619	-0.00042	-0.0646	-0.0221	0.01129 0.006085 (0.07078)	0.0215 0.0111 (0.03615)	0.02276 0.01242 (0.02552)	0.02388 0.008308 (0.1069)	0.0249 0.009339 (0.08646)	0.0297 0.01159 (0.06374)	0.02491 0.008033 (0.1205)	0.0297 0.01159 (0.06374)

Note: a = R squared; b = adjusted R squared; c = p-value

6.3 Optimisation

This section describes the optimisation done to the empirical model considered for the subjective variable 'Tally' for a model considering main and two-way,three-way interactions between variables. The first order system was identified to have a very slight difference as compared to the second order model in terms of R^2 and adjusted R^2 values. The 1^{st} order model for 'Tally' was therefore used as the optimisation model as lower order models are less prone to numerous local maximas. With polynomial problems known to be closed form, the optimisation of the function can be determined by equating the partial derivatives of the function and equating them to zero to find the critical points. The optimum of the final model can be determined by considering the determined critical points. The final equation was converted from a maximisation problem $f(\boldsymbol{x})$ to a minimisation problem $F(\boldsymbol{x}) = -f(\boldsymbol{x})$ where the equation used to convert $F(\boldsymbol{x})$ back to the original problem is given by $\max_{\boldsymbol{x}} f(\boldsymbol{x}) = -\min_{\boldsymbol{x}}\{\ f(\boldsymbol{x})\} = -F(\boldsymbol{x})$. This was necessary as the algorithms used consisted out of minimisation techniques. The final equation which was minimised is given by equation 6.3.1 where the variable $\boldsymbol{x}$ denotes a vector (x_1, x_2, x_3). The notation x_1 represents a variable for blade chord; x_2 blade angle and x_3 blade sweep. The equation was subject to inequality constraints given by equation 6.3.2, 6.3.3 and 6.3.4.

$$F(\boldsymbol{x}) = \beta_0 + \beta_1 x_1 + \beta_2 x_2 + \beta_3 x_3 + \beta_4 x_1 x_2 + \beta_5 x_1 x_3 + \beta_6 x_2 x_3 + \beta_7 x_1 x_2 x_3 \tag{6.3.1}$$

$$\beta_0 = 21.0522,\ \beta_1 = -1.0063,\ \beta_2 = -1.24509,\ \beta_3 = -1.33607$$
$$\beta_4 = 0.04753,\ \beta_5 = 0.06024,\ \beta_6 = 0.04004,\ \beta_7 = -0.00191$$

$$29\,mm \leq x_1 \leq 39\,mm \tag{6.3.2}$$
$$10.21^\circ \leq x_2 \leq 40.21^\circ \tag{6.3.3}$$
$$9.47^\circ \leq x_3 \leq 59.47^\circ \tag{6.3.4}$$

The equation considered was parabolic for which well known solutions exist. To find the optimum value, partial derivatives were taken for equation 6.3.1 with regards to x_1, x_2 and x_3 and critical/saddle points were determined by equating each partial derivative to zero and solving for the equations. Equation 6.3.5 to 6.3.6 show the partial derivatives which have been equated to zero to find the critical/saddle points. Equations 6.3.5 to 6.3.7 were rearranged to obtain expressions for x_1, x_2 and x_3 as given by equation 6.3.8. By substituting the expression for x_3 into x_1, and thereafter substituting the obtained expression into x_2 as given by equation 6.3.8; the critical/saddle points for the system can be determined by solving for the quadratic expression, determining values for x_2 as shown by equation 6.3.9 and thereafter resubstituting into equation

6.3.8 to determine for x_3 and x_1.

$$\frac{dF}{dx_1} = \beta_1 + \beta_4 x_2 + \beta_5 x_3 + \beta_7 x_2 x_3 = 0 \tag{6.3.5}$$

$$\frac{dF}{dx_2} = \beta_2 + \beta_4 x_1 + \beta_6 x_3 + \beta_7 x_1 x_3 = 0 \tag{6.3.6}$$

$$\frac{dF}{dx_3} = \beta_3 + \beta_5 x_1 + \beta_6 x_2 + \beta_7 x_1 x_2 = 0 \tag{6.3.7}$$

$$x_1 = \frac{-\beta_2 - \beta_6 x_3}{\beta_4 + \beta_7 x_3}, \quad x_2 = \frac{-\beta_3 - \beta_5 x_1}{\beta_6 + \beta_7 x_1}, \quad x_3 = \frac{-\beta_1 - \beta_4 x_2}{\beta_5 + \beta_7 x_2} \tag{6.3.8}$$

$$Ax_2^2 + Bx_2 + C = 0 \tag{6.3.9}$$

$$A = (\beta_4\beta_6\beta_7 - \beta_2\beta_7^2)$$
$$B = (2\beta_4\beta_5\beta_6 - 2\beta_2\beta_5\beta_7)$$
$$C = (\beta_1\beta_5\beta_6 - \beta_1\beta_3\beta_7 + \beta_3\beta_4\beta_5 - \beta_2\beta_5^2)$$

For polynomial optimisation the absolute minimum, maximum can be determined by determining values for positions located at the boundaries of the design space and comparing these values with values obtained at the critical/saddle points (Stewart, 2015:198). The absolute minima/maxima is determined by the value which is determined to be smallest or largest which is of interest. The critical points have been determined to be at (0.1946, 22.1867, 20.643) and (62.884, 19.740, 29.127) which give magnitude values -6.563 and -7.806. Both points have been identified to be saddle points with both co-ordinates located outside the design space. As such, the minimum value for 'Tally' was determined by using the values located in the boundary conditions as given by equation 6.3.2 to 6.3.4. The minimum was determined to be at (39, 40.21, 59.47) with a value of -14.389. Two more computationally expensive algorithms were used to validate this value optimise for the function by using a Genetic algorithm code and a Nelder-Mead simplex algorithm implemented in MATLAB. The GA algorithm which converged after 50 generations with a final fitness value of -14.3903. The parameters for used to obtained the minimal fitness value had co-ordinates $\boldsymbol{x} = (39.001, 40.211, 59.471)$. Substituting this value into the original maximisation equation a total rounded number of 14 tallies were expected. The Nelder-Mead simplex algorithm produced the same co-ordinates as determined by the GA. Contour plots are given in Figure 6.3.1 mapping the response for changes made to blade metric. For each contour plot only two blade parameters were used to make each plot where the omitted variable was kept constant with a value as obtained by the optimisation. The contour plots provided a visual means as to check for the optimum solution obtained.

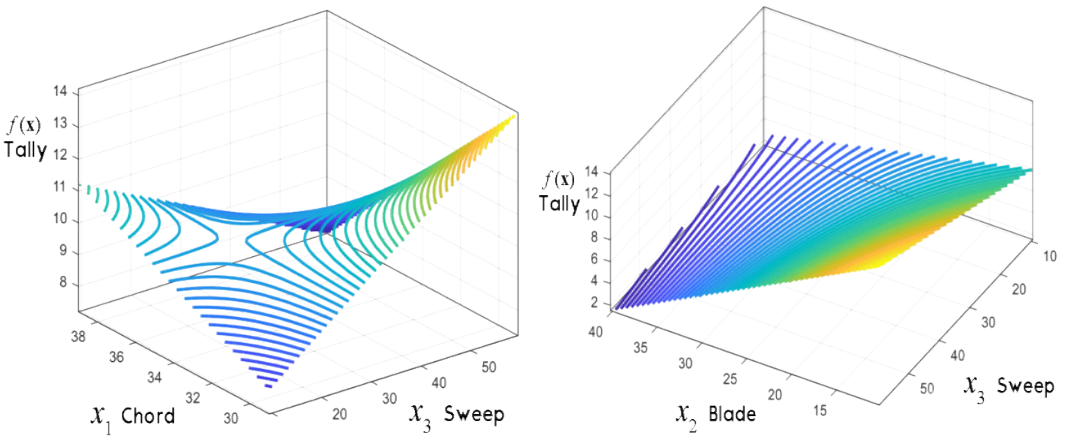

(a) Chord and Sweep distribution (Blade = 40.211°)

(b) Blade and Sweep distribution (Chord = 39 mm)

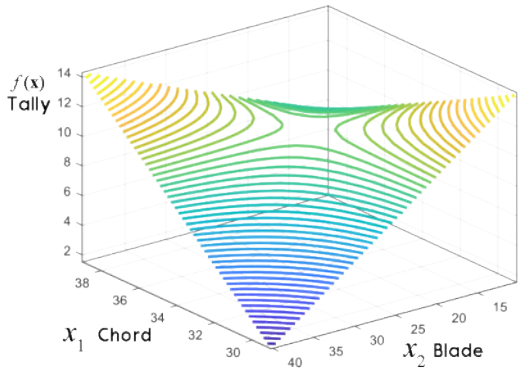

(c) Blade and Chord distribution (Sweep = 59.47°)

Figure 6.3.1: Optimisation function contour plots

6.4 Results

The predicted optimal blade parameters were used to 3D print and test a final rotor model. An additional 20 jurors were asked to partake in the test with the optimised model included in the subjective evaluation test. The subjective and psychoacoustic evaluation of the optimised fan noise is given in Table 6.4.1. Table 6.4.1a shows the measured psychoacoustic values for the optimised fan model while table 6.4.1b and 6.4.1c showing the optimised fan models ranked according to the forced pair comparison test data. The final optimised model was ranked 3^{rd} in the forced pair comparison test. The final optimised model did not perform the best but a high ranking was still obtained using the 1^{st} order empirical model considering main and two-way, three-way interactions between the blade parameters. It was interesting to find

that similar ranking was observed for the 20 jurors who were asked to validate the optimised fan model, when compared to the previously tested 51 jurors response. The psychoacoustic annoyance values were also close to the highest ranked fans sound. A picture of the final 3D printed optimised fan model is given in Appendix C.3.

Table 6.4.1: Psychoacoustic measures and forced pair comparison test data

(a) Psychoacoustic measures for optimised fan noise showing, (a) psychoacoustic metric values, (b) higher ranking fans in validation set and (c) lower ranking fans for validation set

Fan name	**Loudness** (*Sone*)	**Sharpness** (*acum*)	**Roughness** (*asper*)	**Fluctuation Strength** (*vacil*)	**Psychoacoustic Annoyance** (*PA*)
Optimised	2.41	1.39	0.0461	0.00677	2.93

(b) Higher ranking fan sounds

Top ranking fan sounds for forced pair comparison test									
Ranking	1^{st}	2^{nd}	3^{rd}	4^{th}	5^{th}	6^{th}	7^{th}	8^{th}	9^{th}
Fan no.	2	13	16	5	4	6	10	14	7
Fan name	C+B+S+	C–B–S+	Optimised	C+B–S+	Bm	C+B–S–	SM	Cm	C–B–S–
Total tally	239	235	226	214	184	184	183	155	140
PA	2.90	3.16	2.93	2.78	3.52	3.98	2.79	3.83	3.18

(c) Lower ranking fan sounds

Lower ranking fan sounds for forced pair comparison test							
Ranking	10^{th}	11^{th}	12^{th}	13^{th}	14^{th}	15^{th}	16^{th}
Fan no.	9	8	12	11	3	1	15
Fan name	Original	Sm	CM	C–B+S+	C–B+S–	C+B+S–	BM
Total tally	130	119	109	104	86	81	61
PA	3.71	4.53	4.21	3.82	4.01	5.41	5.35

The semantic radar plot comparing the best and worst fans for the optimised model validation set given in Figure 6.4.1a and 6.4.1b. A similar trend was identified when compared to the original 51 jury testing results. Higher ranked fans showed increased magnitude levels for most semantic adjectives excluding 'Strong' while lower ranked fans showed the opposite response. It was interesting to see that according to the radar plot, the predicted optimal fan presented higher magnitude values compared to the first ranking fan. This may have indicated that not much of a difference was observed between higher ranking fans. Split violin plots showing the predicted optimal fan compared

to the original fan for the 20 jury validation set is shown in Figure 6.4.1c giving a better description of the spread of data as opposed to only looking at the mean value. Normal and skewed distributions were observed for the predicted optimised fan leaning to higher magnitude values, indicating that most jurors had a similar opinion for semantics 'High Quality', 'Quiet', 'Pleasant' and 'Non-Humming'. Bimodal responses were also observed indicating either uncertainty or divided opinions towards the fan noise. The rest of the results obtained from the 20 jurors is given in Appendix C.

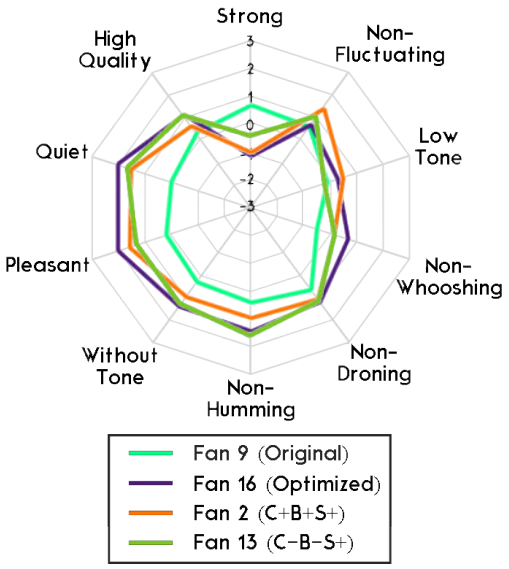

(a) Highest ranking fans

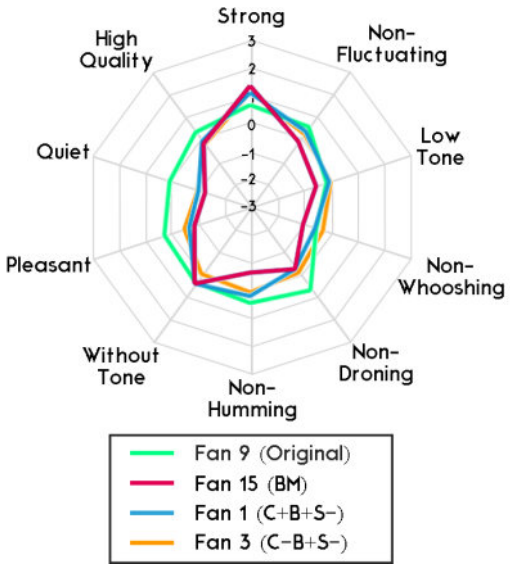

(b) Lowest ranking fans

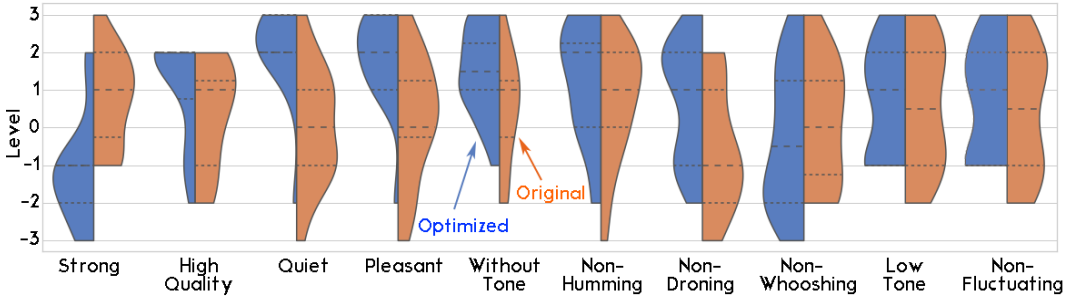

(c) Split violin plots showing data distribution for semantic adjectives used to describe sound traits for predicted optimal fan (left = optimised fan; right = original fan)

Figure 6.4.1: Semantic test evaluation for optimised fan

Chapter 7

Conclusion

The study was aimed at conducting an investigation on how a select number of blade parameters influenced the subjective evaluation of noise. Prototype models were created to determine the influence of varying blade parameters of blade sweep, blade angle and chord. Geometry morphing techniques were used to create 15 variations of prototype fan models, designed according to a central composite design (Myres, 2008). Data collection to make up to a 2^{nd} order polynomial fit was possible with the select design strategy. More specifically, minimal points necessary to fit regression models containing main and two-way, three-way interaction were obtained by using the CCD configuration. Well defined simple models could be used to fit data to learn about the process. The necessary steps used consisted of doing a set of experiments, fitting a polynomial to the data and determining the sensitivity and optimum of the system. Performance measures were made for fan prototypes measuring the airflow and static pressure. No drastic decrease in static pressure readings was observed for increased blade angle. The static pressure ranged between 4 and 14 Pa with no evident decline present with increasing blade angle. A slight started to show with the maximum blade angle showing a difference of 4 Pa, but no drastic decrease was observed. As such, although it was uncertain whether stall was avoided, design regions were considered acceptable in terms of the changes present.

Standard 3^{rd} octave band analysis was used to analyse the unweighted and A-weighted sound pressure levels. The expected trends identified in literature was compared to the noise SPL results. After validating that sound pressure levels change according to the expected trend as identified in literature, psychoacoustic metrics were used to quantify the expected annoyance for sound. Psychoacoustic metrics of loudness, sharpness, roughness and fluctuation strength were used to determine for the psychoacoustic annoyance measures. Measures of psychoacoustic metrics obtained for prototype fan noise was compared to psychoacoustic measures used by Yang and Zhu (2016b). This provided a means to compare the measure of magnitude value presented. Sharpness was

identified to have no influence on the psychoacoustic annoyance for fans, due to sharpness levels lower than 1.75 acum being present. This trend was further clarified in the jury testing procedures, which showed that sharpness did not have a trend as followed by fan ranking.

Fluctuation strength and roughness showed a trend that seemed to increase with increased loudness. Lower levels for fluctuation strength and roughness were measured for fan prototype noise than by Yang and Zhu (2016b). Yang and Zhu (2016b) identified that fluctuation strength and roughness did not have a significant influence to fan noise. With fan prototype noise identified to have lower levels of fluctuation strength and roughness, a deduction was made that the difference in magnitude observed may indicate that the latter may also not have a major influence to fan noise. The psychoacoustic metric loudness was identified to be the primary contributing factor to psychoacoustic annoyance with fluctuation strength and roughness also increasing slightly in proportion to loudness. Subjective jury evaluation tests were thereafter used to evaluate fan noise as perceived by people.

Two jury evaluation tests were performed consisting out of the forced pairwise comparison test and the semantic differential test. The forced pairwise comparison test was used to obtain a ranking for each fan sound, giving a relative measure of perceived preference to noise; while the adjectives used in the semantic differential test gave insight as to how jury perceived noise quality. Violin and polar plots were used to visualise the distribution of data obtained from jury testing. The violin plots showing fan ranking presented Gaussian, and bi-modal distributions for data often presented skew. The response from violin plots showed how distributions aligned with fan ranking more dominantly, represented by the position of the median showing the position dividing data sets into halves. The interquartile range for most data distributions showed values between 2 to 3 counts of the 'tally' for the forced pairwise comparison test.

The alignment of data distributions showed how results could be used to assess how blade parameters influenced the subjective response from jurors. Semantic differential test data distributions were compared, used to visualise the spread of data for higher and lower ranked fans. The mean values for polar plots were shown. This allowed violin plots to represent a better insight into the actual distribution of data. The mean value on polar plots indicated that jurors associated higher fan rank with a more quiet, high-quality sound with fans being ranked higher often with increased semantics as to the humming, droning, whooshing and low tone traits of noise. Violin plots were used in conjunction with the mean value to observe the differences in data spread. In contrast to expecting most values to be around the mean, the influences of varied opinion were identified to be the major factor which contributed to the

position of the mean value. With higher-ranked fans, the opinion towards a fans sound was less variable with a bimodal response seen shifting to a single-mode which identified that opinions for jurors shifted more to a single opinion.

ANOVA models were used to determine the relationship between blade parameters, psychoacoustic metrics and jury testing data. The Pearson's r value was used to determine the degree of correlation between variables while the R^2, adjusted R^2 and p-value indicated whether empirical models would be able to make predictions. The variable Tally, giving a relative measure of perceived preference for jurors, was determined to be able to make predictions for jury preference explaining about 50 % of the total variance using blade parameters. A final prototype model was made optimised according to the 'Tally' model, attempting to relate blade parameters directly to the subjective response of jurors. The results obtained for the final prototype fan model was ranked third used in a validation set of 20 jurors. The study showed that jury preference is most variable and statistical models were only able to explain for a moderate amount of variance - the study aimed at mapping the relationship between blade parameters to the subjective response of jurors. The analysis of psychoacoustic metrics was used in conjunction with jury evaluation to compare the expected and actual evaluation of fan annoyance. The central composite design is used to facilitate data collection up to second-order polynomial models. With only considerations made to second-order models alone, it was determined that the high variability present for jurors could not be sufficiently accounted for.

Shortcomings identified in this study related to the lack of performance analysis made for prototype fan models. Analysis of the amount of warpage present not being made for 3D printed fans was also another shortcoming. It was not possible to determine if stall was present as reduced effects from stall also exist. Performance measures showed that the pressure rise with increased blade angle did not normally drop off, but a slight decreased was observed with the prototype model BM having the largest change to blade angle. With jury testing also being conducted over long periods, this may have made jury subject to fatigue and give less accurate results. The select method of changing for blade parameters was not identified to be the best method but rather was a selection made out of numerous other possibilities. As such, another shortcoming which is presented in this study relates to how there was no way of determining whether the method used to change for blade parameters was the best selection made. It can be recommended to make further studies on the effect of other blade parameters which include parameters such as blade number, thickness and camber.

Appendix A

Detailed geometry morphing

A.1 Construction of modified blade profiles

With sweep removed, and aerofoil profiles for the baseline fan altered i.t.o. chord length and blade angle; some regions of the fan blade needed to be adjusted to maintain the characteristics of the original fan blade geometry. These adjustments were included after making changes to the chord length and blade angle for aerofoil sections. Sweep was thereafter reincorporated into the design to create the final set of prototype blade models.

The following sections describe the methods which were incorporated to morph the fan blade to maintain profiles which deviate from the base aerofoil. A reference aerofoil overlay which overlapped with the base mesh profile was used to create a base mesh over the recreated base fan profile. Figure A.1.1 shows a wireframe view of the base blade with a mesh overlap. A NURBS surface interpolation scheme was used to create segments between aerofoils where each aerofoil profile consisted out of Bezier curves converted to NURBS (Derakhshani *et al.*, 2013).

Altered blade angle and chord would often cause the blade design to extend over and below the blade tip and hub radius. As such a means to preserve the blade's tip to hub ratio was necessary. The aerofoil profiles which was used as a reference projection to the original fan is shown in Figure A.1.2. Interpolated aerofoil sections were determined by following the general trends of previous aerofoil sections for the base blade. The mesh overlay, which was used to wrap the base blade is given in Figure A.1.2.

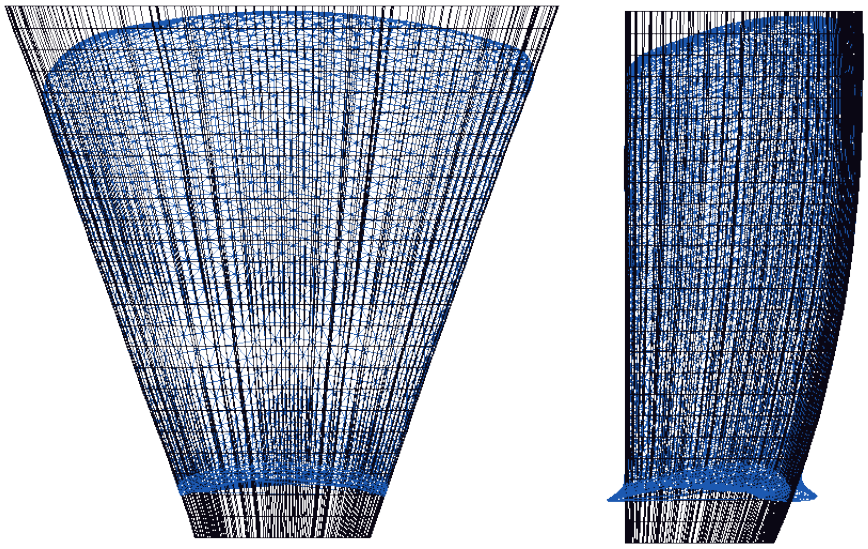

Figure A.1.1: Base blade profile wrapping

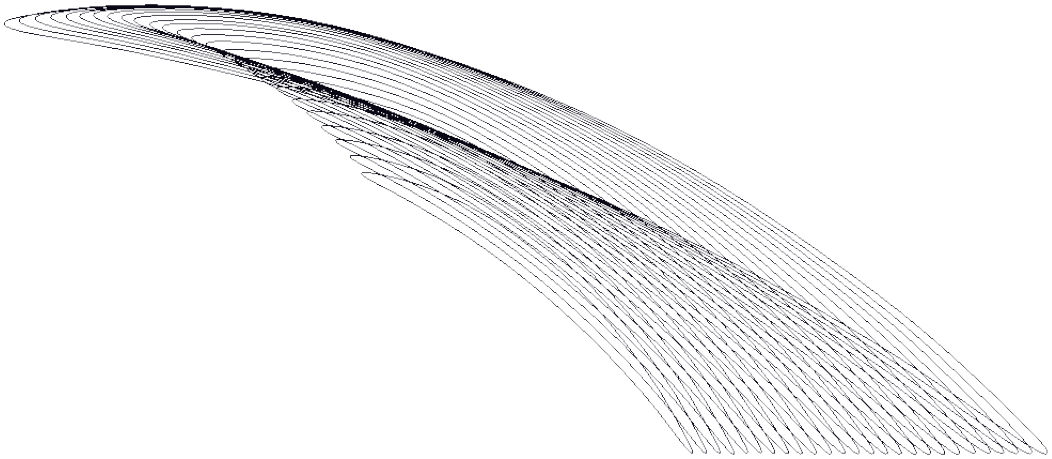

Figure A.1.2: Aerofoil profiles for mesh overlay

With a baseline profile constructed using aerofoil cut-outs, the geometric traits for the fan blade near the hub and tip region needed to be maintained. A morphing technique will be mentioned, using a boolean operand to add and subtract 3D features to the lofted NURBS feature, representing the baseline blade. Figure A.1.3 shows blade regions which need to be preserved. These regions are described as the deviation regions as aerofoil profiles vary for in these blade sections. The regions were identified to be near the blade tip and hub. The following sections will describe the boolean operand which was performed to the 3D geometry to create a set of fan blade incorporating geometrical traits as identified from deviation regions present at the blade hub and tip.

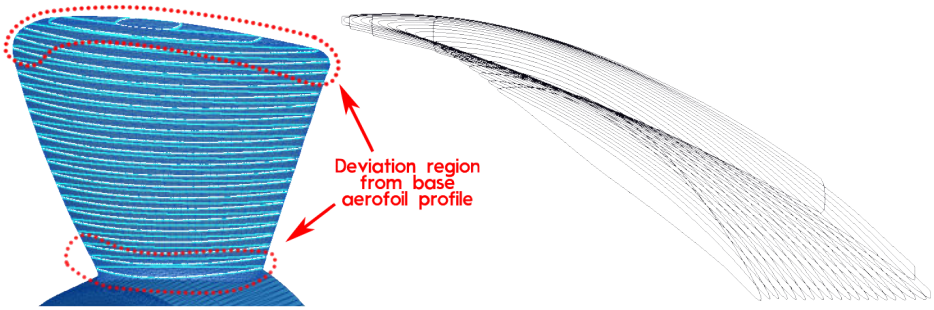

Figure A.1.3: Deviation region inspection

The approach used to alter, match and warp blade segments near the blade tip and hub will be explained, identified to be regions for deviation. The altered aerofoil profile consisted out of modified aerofoil profiles from the base blade with adjustments made to chord and blade angle. The deviation region for the original blade was used as a cut-out and was morphed to match the altered profile. This was achieved by making a reference aerofoil profile, as shown in Figure A.1.3. The reference of the original profile was moved in unison with the cut out from the original mesh to match the altered aerofoil profile. The segments were thereafter combined together to form the final blade incorporating geometry traits from these regions. The region near the fan base was morphed by using boolean cut-outs which allows for 3D geometry addition or subtraction while FFD (Free Form Deformations) vertex controls were used to match the reference to the objective profile. The method of FFD consists out of encasing geometry within an object hull, typically a cube. By altering the cube, the object contained within the hull was also altered proportionally using three-dimensional analogues of parametric curves. As seen in Figure A.1.4, the reference profile is overlapped with a cut out of the original profile near the hub region. The two profiles were morphed together with the reference profile, keeping track of how profiles were deforming.

The transformation made to the blade profile can be seen by referring to Figure A.1.5. A profile with blade angle and chord altered is shown in Figure A.1.5; indicated as the target reference profile. By using vertex positions for the FFD transform the mesh profile can be morphed using a reduced number of vertex positions. Scaling was first applied to the original profile in the x and y axis, with profiles scaled rotationally relative to the trailing edge section. After profiles were matched in the $x - y$ axis plane, the altered profile was further adjusted fit the profile cut out in the z-axis direction as seen in Figure A.1.5. This was done such that the original scaled reference profile would match the altered profile for the blades for the front and back face respectively.

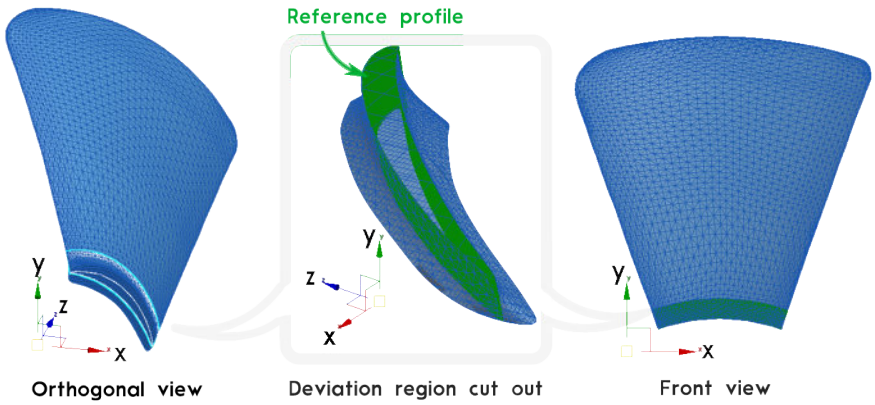

Figure A.1.4: Hub deviation region cut out for original base blade

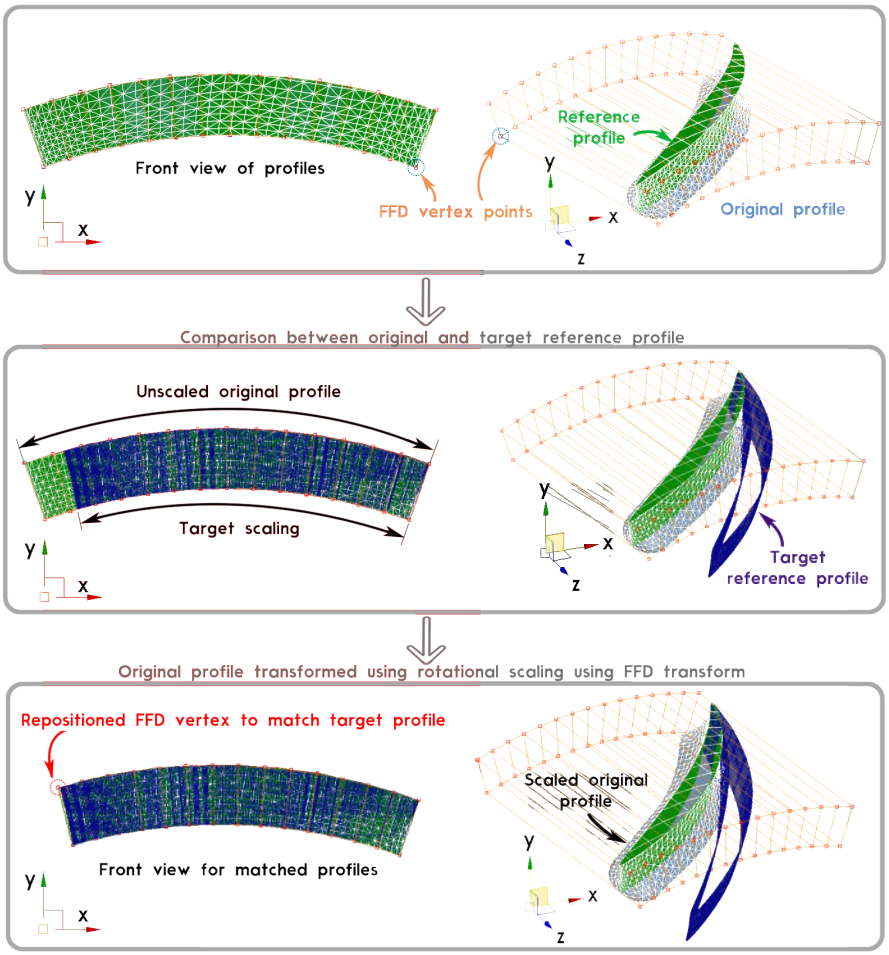

Figure A.1.5: FFD base blade transform near hub

Figure A.1.6 shows the merged profile denoted as the altered profile in comparison to the base blade (original profile), after applying mesh morphing as described in Figure A.1.5.

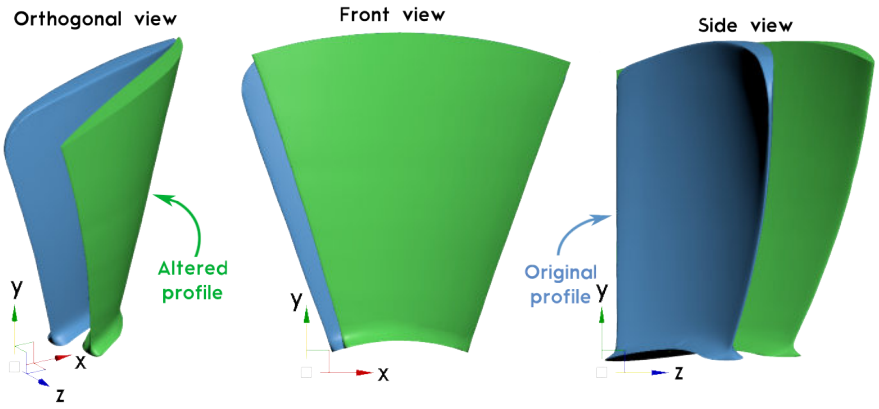

Figure A.1.6: Altered profile merged and compared to original blade

Alteration made to the top region

After the base region has been altered and combined using a Boolean operand, the deviation present in the blade tip region needed to be addressed. FFD transforms were once again used, but cut-out regions near the leading and trailing edge of the blade tip were kept constant in respect to the vertical plane. Motivation to keep the profile the same was obtained by Jian-Hui and Chun-Xin (2008) where a vertical extrusion was present near a CPU cooling fans tip as shown in Figure A.1.7. An extra cut out was identified to be added to the base aerofoil distribution ranging from hub to tip. As such, the geometry extrusion was considered a trait which needs to be preserved. No literature was identified for a standardised method which dictates how cut-out sections for fans should be performed. It was instead determined to be a selection made by designers.

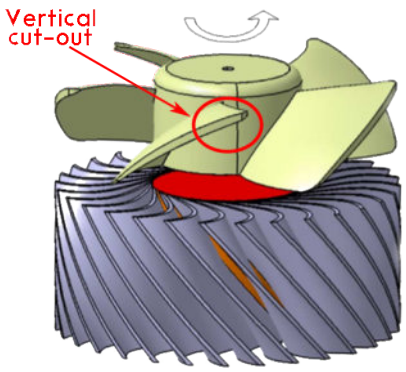

Figure A.1.7: Cut out inspection near blade tip (Jian-hui and Chun-Xin, 2008)

A mesh overlap between the base unswept blade profile and its interpolated aerofoil mesh profile is shown in Figure A.1.8, where cut out profiles for the base blade's tip, leading and trailing edge profiles, were framed. A morphed profile could thereafter be made using the select geometric traits to match altered blade profiles. Figure A.1.9 will be used to explain the steps followed, allowing altered blade profiles to maintain similar geometric traits as compared to the base blade tip region.

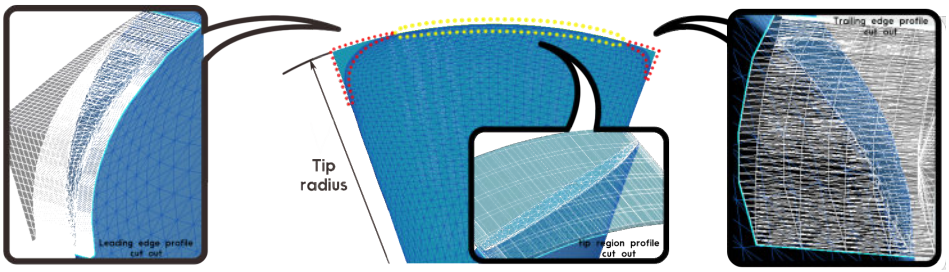

Figure A.1.8: Base blade tip region geometry inspection with (left) leading edge inspection, (centre) tip region inspection and (right) trailing edge inspection

Figure A.1.9 shows a front view comparison made between the original blade profile and a morphed blade which has its chord length and blade angle altered. Profile cut-outs were matched transferred from the original blade profile to the morphed profile. The following notations were used for convenience where ***a*** denoted the profile cut out for the original fan blade near the leading edge; ***b*** denotes the profile cut out located at the blades tip radius for the original fan blade and ***c*** denotes the cut out region for the original fan at the trailing edge region. The following transformations were made in the front view for the fan blade, as shown in Figure A.1.9. The segment ***a*** was rotated a set degree from the origin to arrive at point ***a'*** which aligned the cut out to begin at the edge of the leading edge section for the altered blade. For segment ***b*** the profile was scaled rotationally using FFD transforms to arrive at position ***b'*** wedging the cut out profile between ***a'*** and ***c'***. Lastly, the profile ***c*** defining the trailing edge cut out which was kept constant allowing ***c*** to be equal to ***c'*** the cut out profile for the morphed profile.

With the tip deviation profile regions placed in positioned in the front view, FFD transform was applied in the z-axis direction to relocate the cut-outs to be aligned with the position of the morphed profile as shown in Figure A.1.10. Each profile was moved to match the target profile by relocating FFD control vertex points. Changing the FFD vertex points allowed for the geometry to be morphed in unison for which the top and bottom profiles for each segment was made to align with the morphed fan blade. The desired cut out region

index was determined by creating a cut out from the altered profile located in positions ***a'***, ***b'*** and ***c'***.

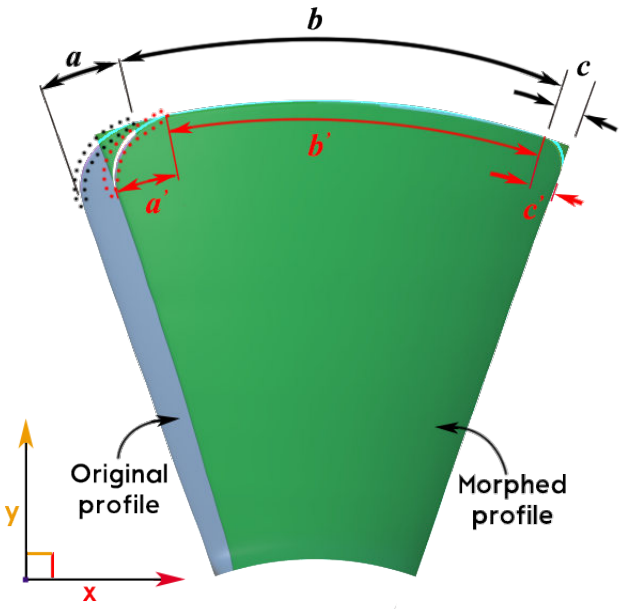

Figure A.1.9: Front view base blade geometry alterations made to match morphed profile with ***a***, ***b***, ***c*** are the original positions transitioned to positions ***a'***, ***b'*** and ***c'***

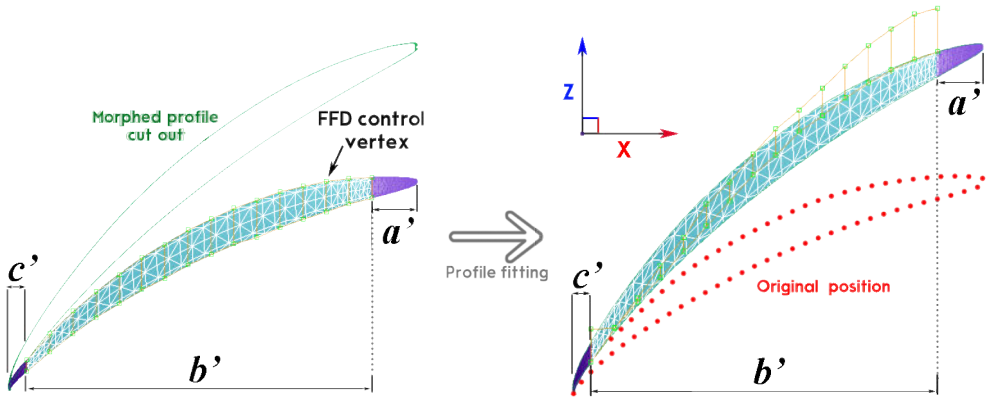

Figure A.1.10: FFD geometry morphing in the z-axis direction showing, (left) unaltered original mesh profile from baseline fan and (right) original mesh morphed to match target profile

Using the profile determined from Figure A.1.10, a boolean cut out operation was used to create a cut-out region from the segments determined. As seen in

Figure A.1.11, a 3D cut out was performed, removing sections of the altered mesh profile to create the final mesh.

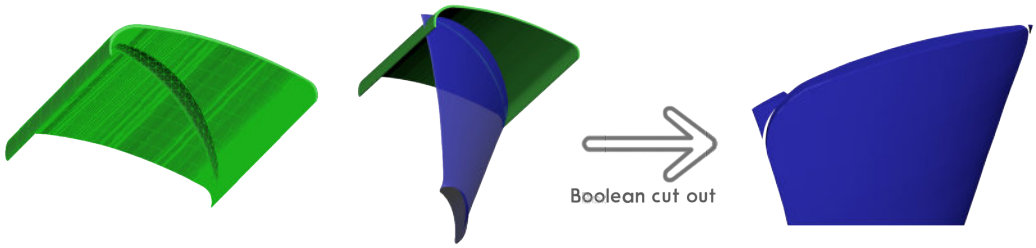

Figure A.1.11: Boolean 3D cut out operand showing, (left) cut out region, (middle) altered blade profile overlapped with cut out section and (right) cut out initiated using boolean operand

The final altered profile for the altered profile of a fan is given in Figure A.1.12 after applying alterations made near the blade tip and hub. After applying a transform to the blade profile with changes made to the blade angle and chord length, forward sweep was reincorporated into the mesh profile. This was achieved by writing a custom script in 3Ds max, which allowed for mesh vertex points and data related to the vertex positions to be exported.

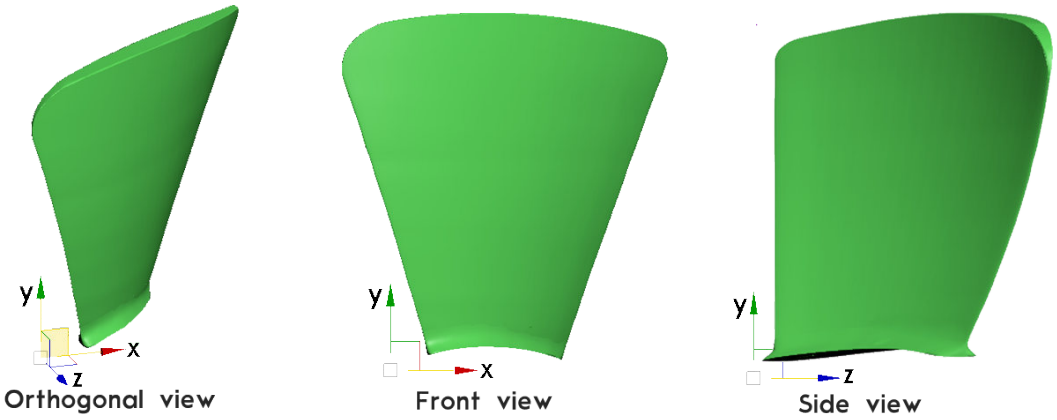

Figure A.1.12: Altered fan blade model

After models with altered chord and blade angle were created, with appropriate boolean operands applied to morph fan blades to be like the original baseline blade, blade sweep was reincorporated into the blade to create the final blade for prototype fans. This was achieved by exporting the vertex coordinates of the mesh and manipulating the coordinates. MATLAB was used to manipulate vertex positions for the altered blade profile using a custom-written code in

Maxscript. Maxcript is a coding platform available in 3Ds Max used to alter geometry (Derakhshani, 2013).

A.2 Geometry of base blade

The dimensions for the base blade which was kept constant as well as the maximum and minimum changes made to blade parameters is given in Table A.1.1 The parameters characterising the geometry at the blade hub and tip is provided for which calculations were made to ensure that design regions were within bounds as identified in the literature study. Using the typical design region for blade solidity ranging between 0.4 and 1.1, it was determined that blade chord needed to range between 14.936 mm and 41.074 mm. By selecting a altered chord length of 5 mm, the chord lengths at the blade hub and tip aerofoils were kept within the boundaries. Selecting a length of 5 mm was a design decision that was made.

Table A.2.1: Baseline fan parameters

Original fan geometry (fan no. 9)	
Variable	**(Value)**
Number of blades	7
Sweep	34.47°
Tip aerofoil chord length	34 mm
Hub aerofoil chord length	19.94 mm
Tip aerofoil blade angle	25.21°
Hub aerofoil blade angle	36.25°

By considering the dimensions of the base blade, the blade angle considered for the hub and tip ranged between 10.21° and 40.21° for the tip aerofoil, and between 21.25° and 51.25° for the hub aerofoil. The aerofoils at the hub and tip described the maximum and minimum changes present for the profiles fan blade. The maximum angle considered was 6.25° larger than the maximum blade angle considered by Van der Spuy *et al.* (1997). The fan blade was identified to be a variable profiled blade. It was necessary to identify which aerofoil profiles need to be primarily considered for design. Huang and Gau (2012) made experimental studies for the design of an axial flow fan blade. Considerations were only made towards the hub and tip aerofoil when determining parameters to be altered. The same design approach of considering the properties of aerofoils located at the blade hub and tip was used to determine feasible design regions for fans.

Appendix B

Subjective jury evaluation test results

B.1 Forced pairwise comparison test

The flow diagram showing the logic used to perform the forced pairwise comparison test is given by Figure B.1.1.

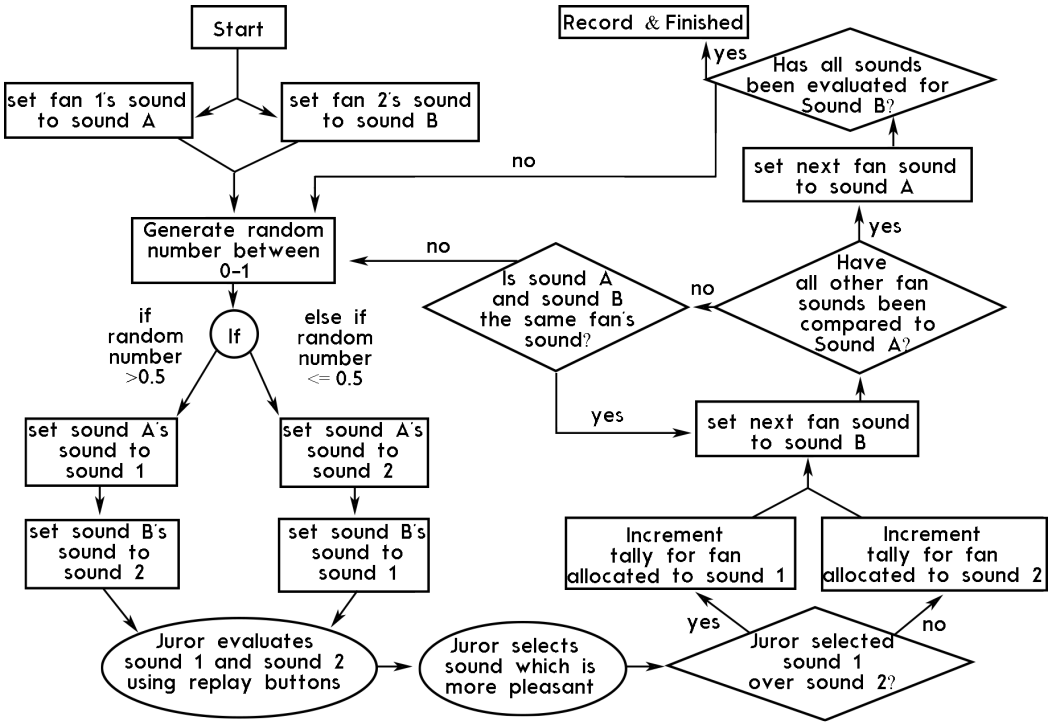

Figure B.1.1: Forced pairwise comparison test flow diagram

B.2 Violin plots showing semantic differential test results

The violin plots describing the distribution of data obtained from the semantic differential test obtained from the group of 51 jurors is given from Figure B.2.1 to B.2.14. Fans were listed in ranking order to see the general trend observed. The original prototype fan was ranked 9^{th} which was compared to every other prototype model.

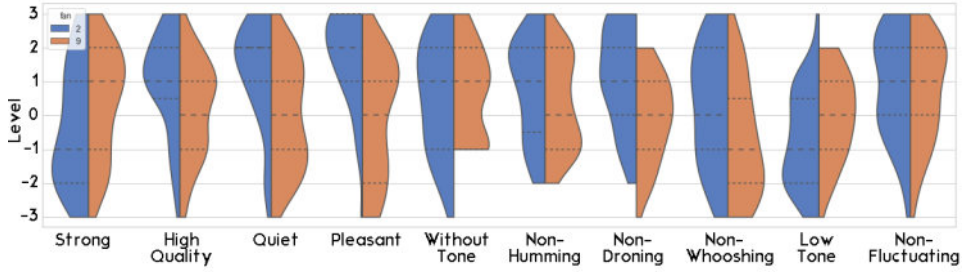

Figure B.2.1: Violin plots for, 1^{st} ranking fan, C+B+S+ (left) compared to original prototype (right)

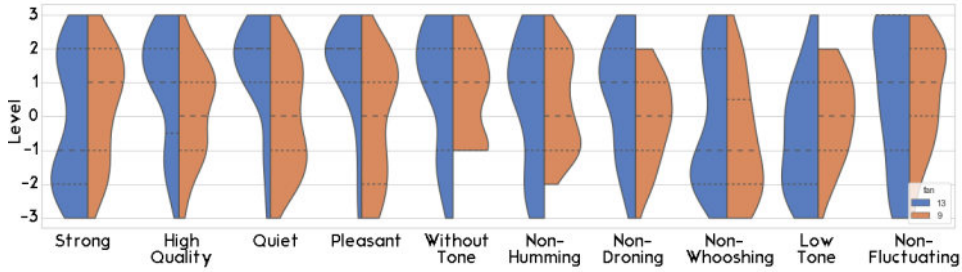

Figure B.2.2: Violin plots for, 2^{nd} ranking fan, C-B-S+ (left) compared to original prototype (right)

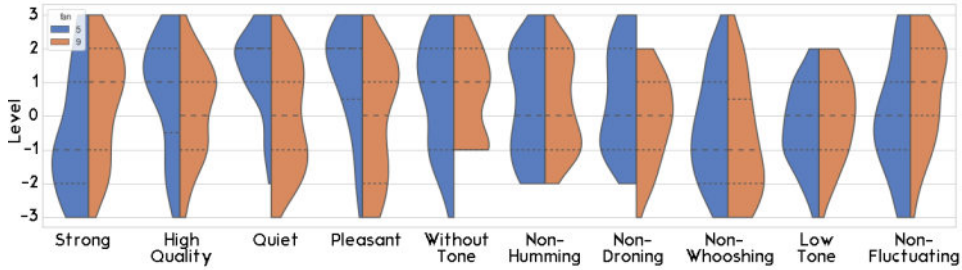

Figure B.2.3: Violin plots for, 3^{rd} ranking fan, C+B-S+ (left) compared to original prototype (right)

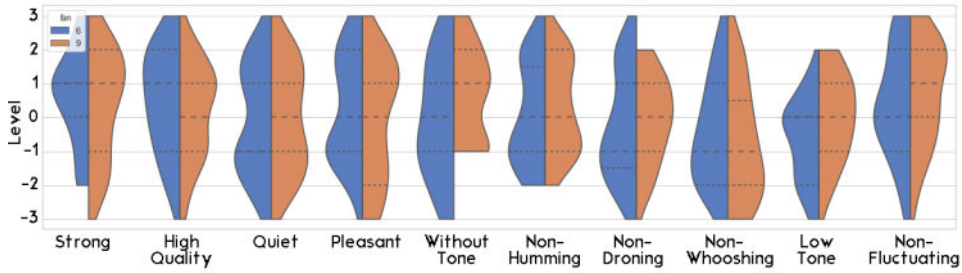

Figure B.2.4: Violin plots for, 4^{th} ranking fan, C+B-S- (left) compared to original prototype (right)

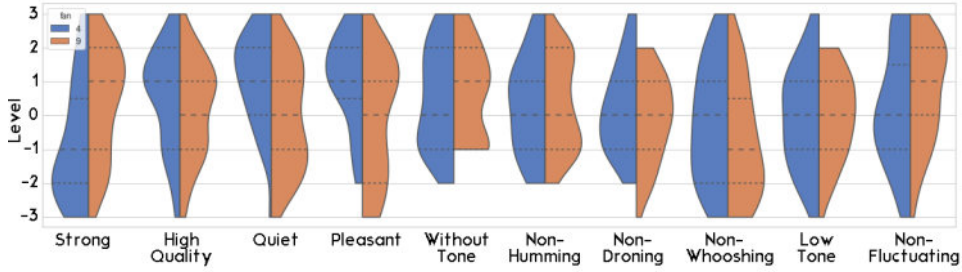

Figure B.2.5: Violin plots for, 5^{th} ranking fan, Bm (left) compared to original prototype (right)

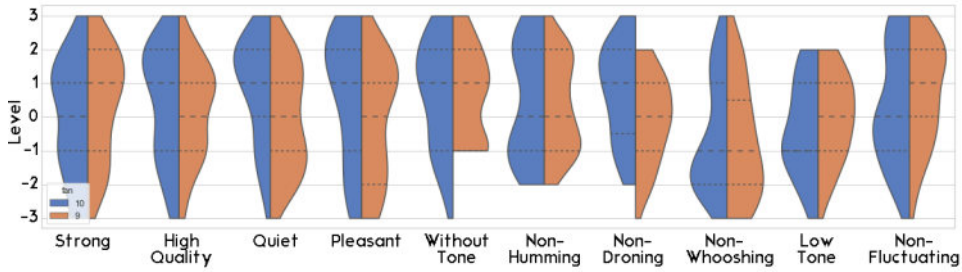

Figure B.2.6: Violin plots for, 6^{th} ranking fan, SM (left) compared to original prototype (right)

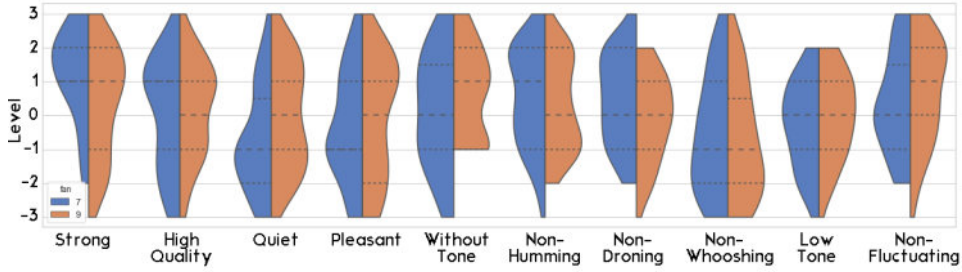

Figure B.2.7: Violin plots for, 7^{th} ranking fan, Cm (left) compared to original prototype (right)

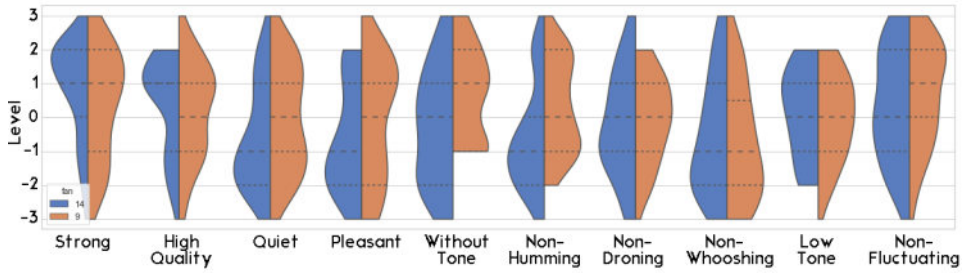

Figure B.2.8: Violin plots for, 8^{th} ranking fan, C-B-S- (left) compared to original prototype (right)

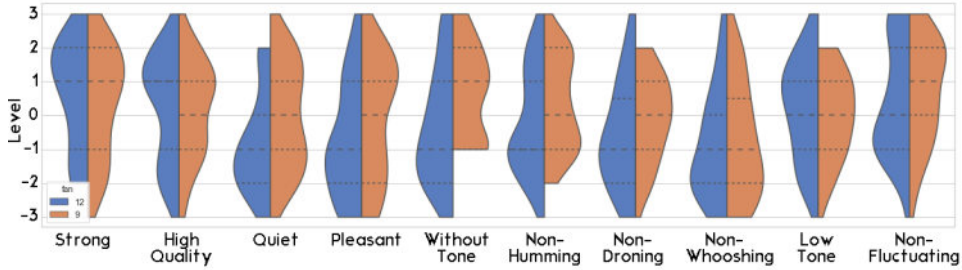

Figure B.2.9: Violin plots for, 10^{th} ranking fan, CM (left) compared to original prototype (right)

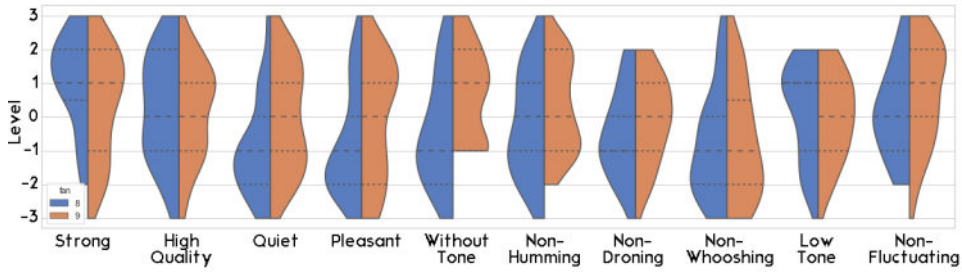

Figure B.2.10: Violin plots for, 11^{th} ranking fan, Sm (left) compared to original prototype (right)

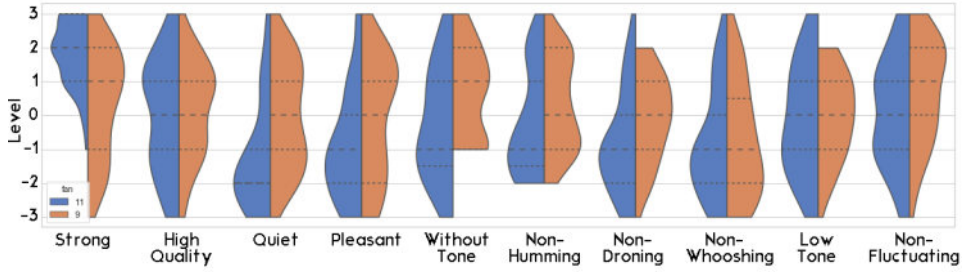

Figure B.2.11: Violin plots for, 12^{th} ranking fan, C-B+S+ (left) compared to original prototype (right)

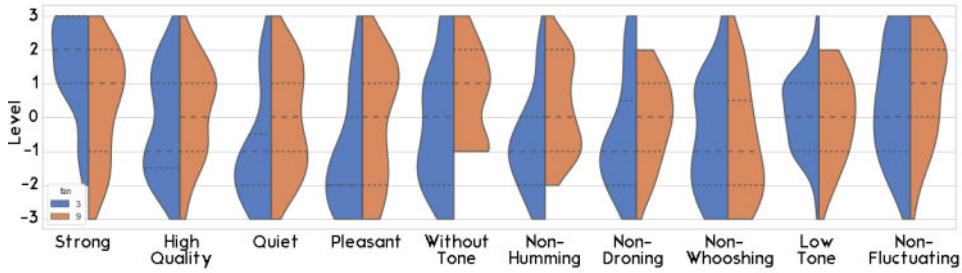

Figure B.2.12: Violin plots for, 13^{th} ranking fan, C-B+S- (left) compared to original prototype (right)

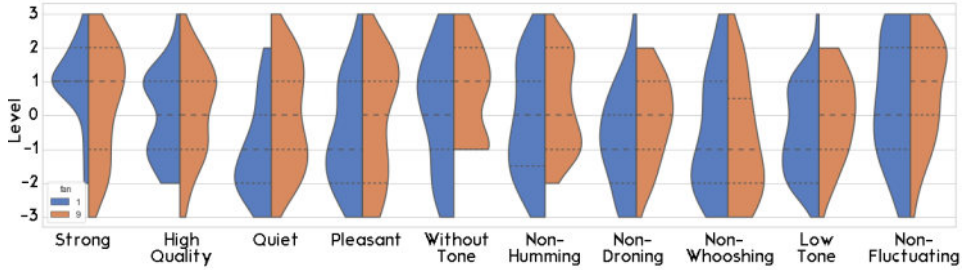

Figure B.2.13: Violin plots for, 14^{th} ranking fan, C+B+S- (left) compared to original prototype (right)

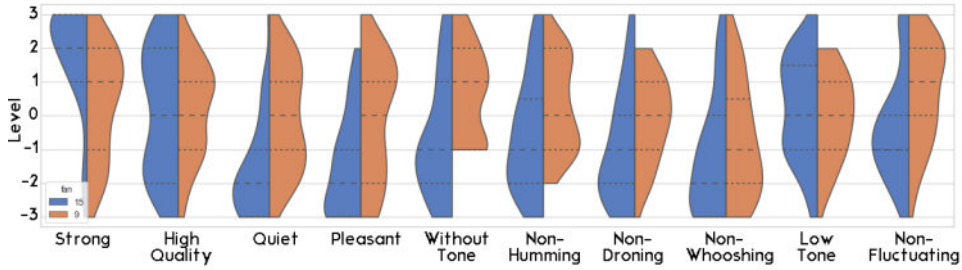

Figure B.2.14: Violin plots for, 15^{th} ranking fan, BM (left) compared to original prototype (right)

B.3 Semantic differential polar plot results

The polar plots showing the mean value obtained for the semantic differential test is given from Figure B.3.1 to Figure B.3.14. Data was collected from 51 jurors. The plots were aligned in terms of model ranking obtained from the forced pairwise comparison test.

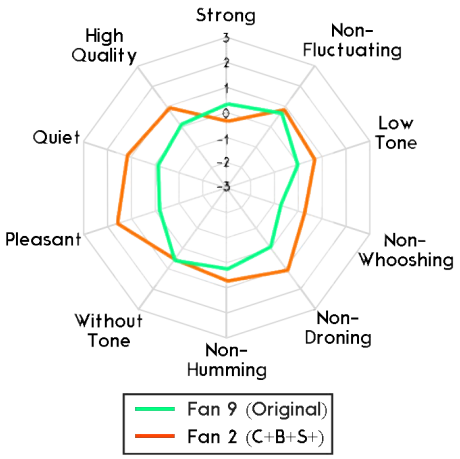

Figure B.3.1: Polar plot for, 1^{st} ranking fan, C+B+S+ (left) compared to original prototype (right)

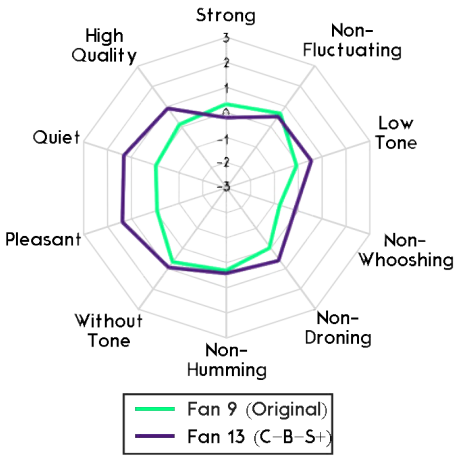

Figure B.3.2: Polar plots for, 2^{nd} ranking fan, C-B-S+ (left) compared to original prototype (right)

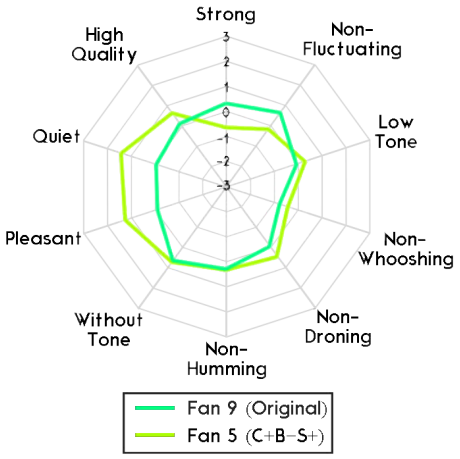

Figure B.3.3: Polar plots for, 3^{rd} ranking fan, C+B-S+ (left) compared to original prototype (right)

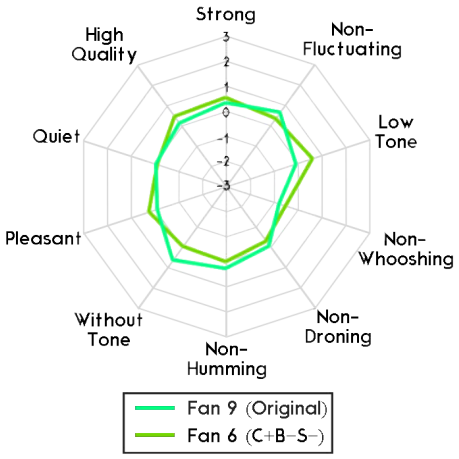

Figure B.3.4: Polar plots for, 4^{th} ranking fan, C+B-S- (left) compared to original prototype (right)

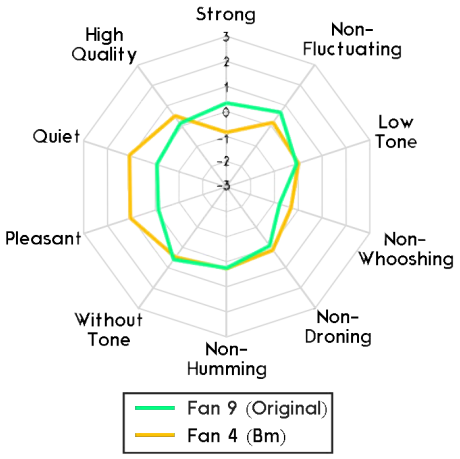

Figure B.3.5: Polar plot for, 5^{th} ranking fan, Bm (left) compared to original prototype (right)

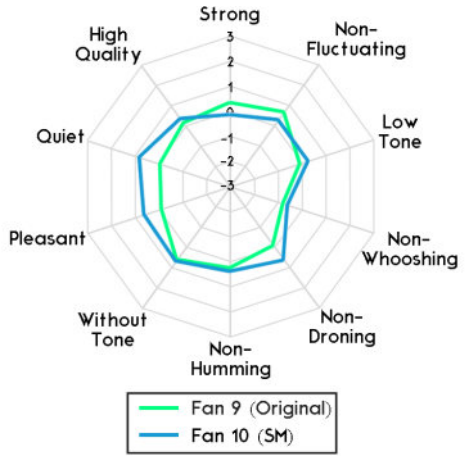

Figure B.3.6: Polar plots for, 6^{th} ranking fan, SM (left) compared to original prototype (right)

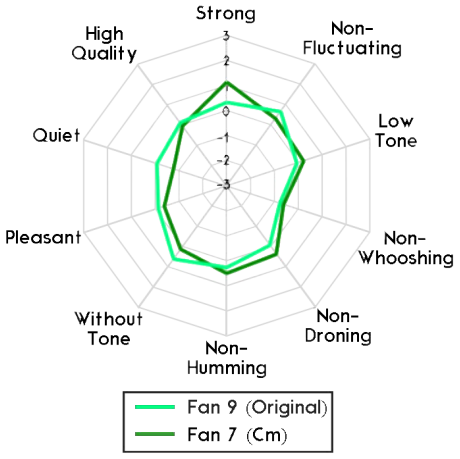

Figure B.3.7: Polar plots for, 7^{th} ranking fan, Cm (left) compared to original prototype (right)

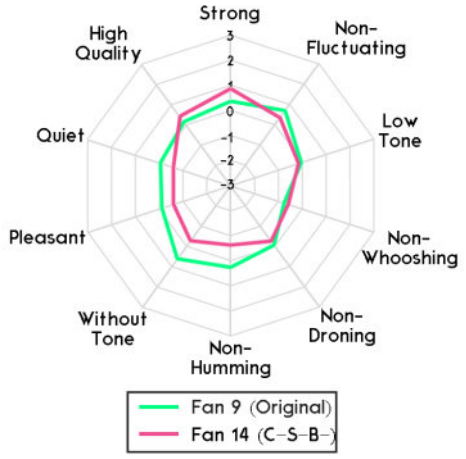

Figure B.3.8: Polar plots for, 8^{th} ranking fan, C-B-S- (left) compared to original prototype (right)

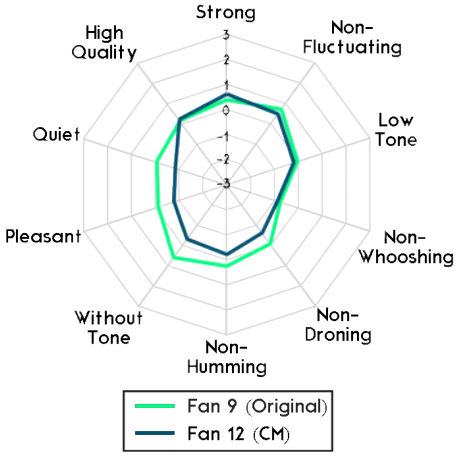

Figure B.3.9: Polar plots for, 10^{th} ranking fan, CM (left) compared to original prototype (right)

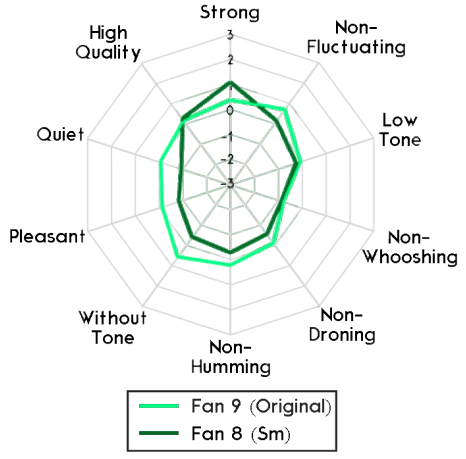

Figure B.3.10: Polar plots for, 11^{th} ranking fan, Sm (left) compared to original prototype (right)

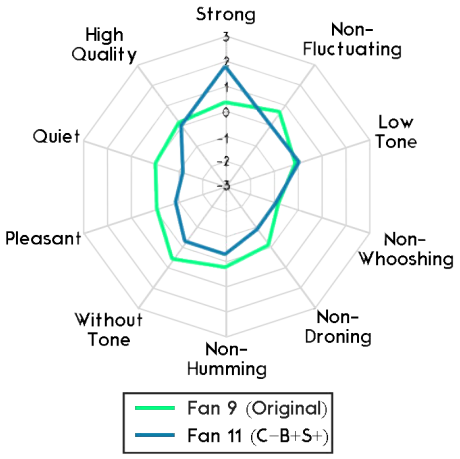

Figure B.3.11: Polar plot for, 12^{th} ranking fan, C-B+S+ (left) compared to original prototype (right)

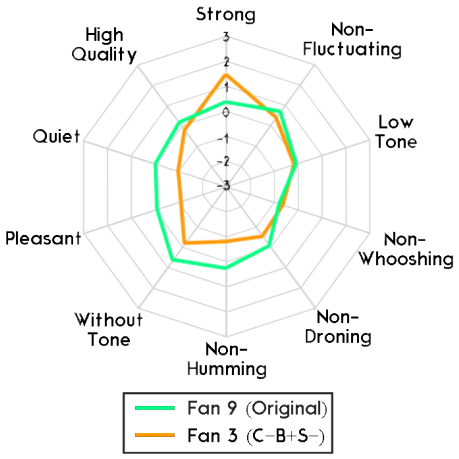

Figure B.3.12: Polar plots for, 13^{nd} ranking fan, C-B+S- (left) compared to original prototype (right)

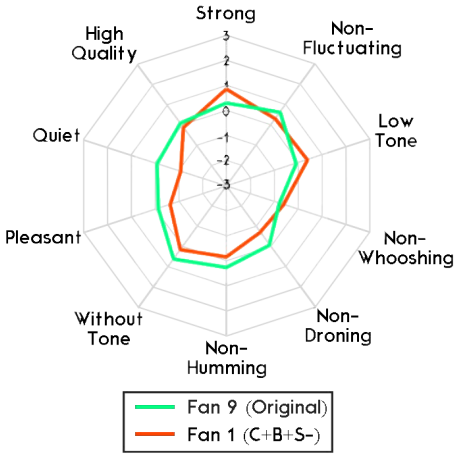

Figure B.3.13: Polar plots for, 14^{nd} ranking fan, C+B+S- (left) compared to original prototype (right)

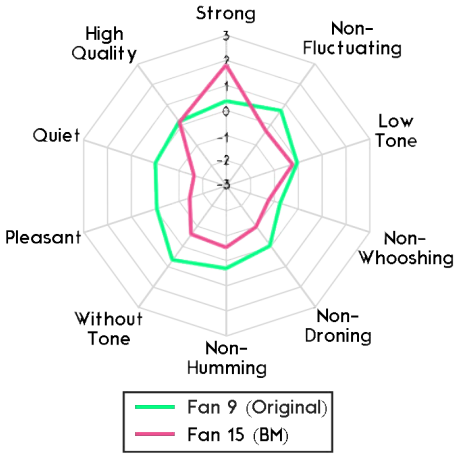

Figure B.3.14: Polar plots for, 15^{nd} ranking fan, BM (left) compared to original prototype (right)

Appendix C

Optimised model jury evaluation results

C.1 Violin plots data distributions for semantic differential test

Violin plots describing results obtained for the semantic differential test, for 20 jurors used to validate the optimised model is given from Figure C.1.1 to C.1.14. The violin plots describing the distribution of data obtained for the forced pair comparison test is also given in Figure C.2.1 and Figure C.2.2. Fans were listed in ranking order to see the general trend observed. The original prototype fan was ranked 10^{th} which was compared to every other prototype model.

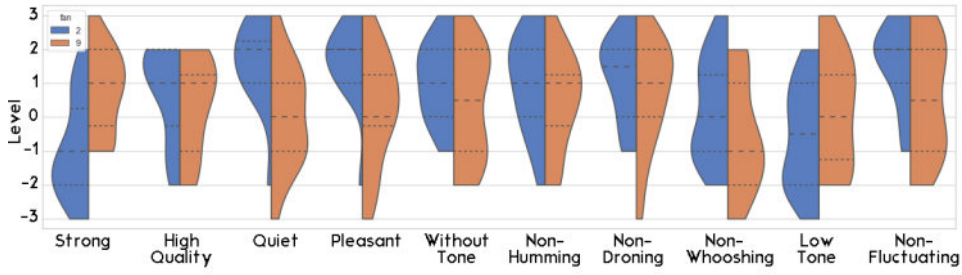

Figure C.1.1: Violin plots for, 1^{st} ranking fan, C+B+S+ (left) compared to original prototype (right)

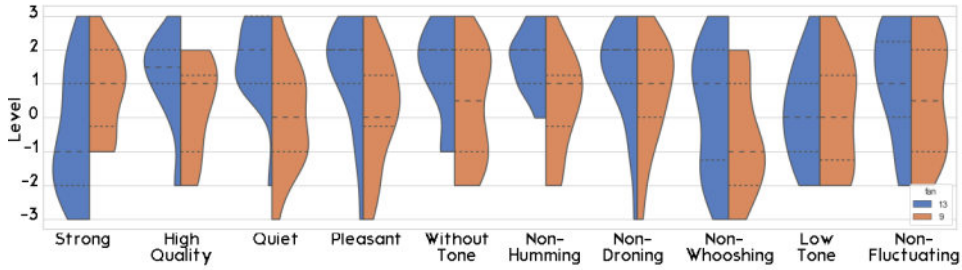

Figure C.1.2: Violin plots for, 2^{nd} ranking fan, C-B-S+ (left) compared to original prototype (right)

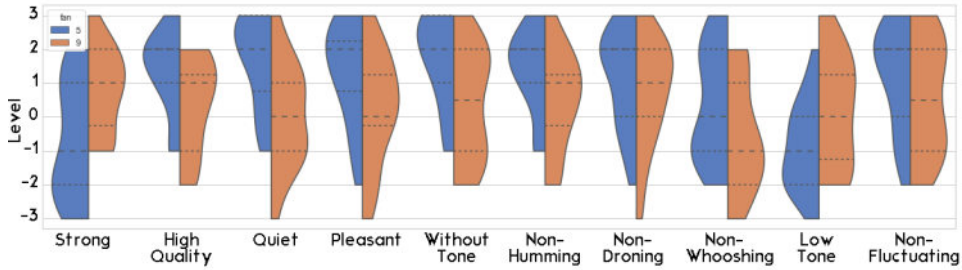

Figure C.1.3: Violin plots for, 4^{rd} ranking fan, C+B-S+ (left) compared to original prototype (right)

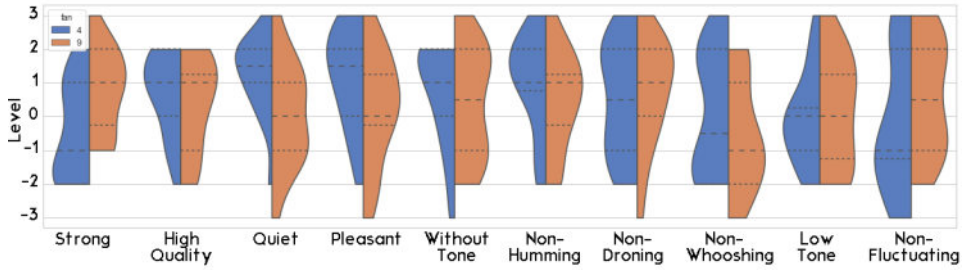

Figure C.1.4: Violin plots for, 5^{th} ranking fan, Bm (left) compared to original prototype (right)

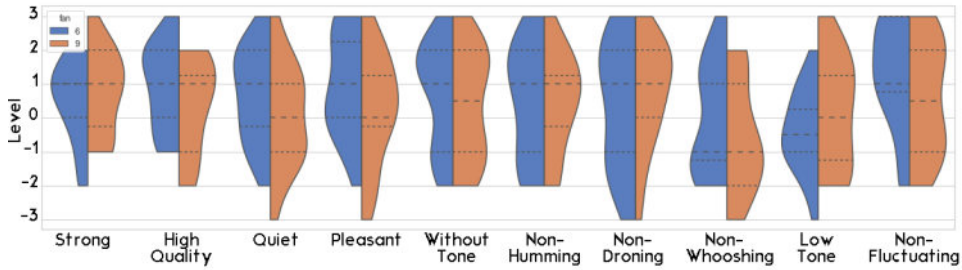

Figure C.1.5: Violin plots for, 6^{th} ranking fan, C+B-S- (left) compared to original prototype (right)

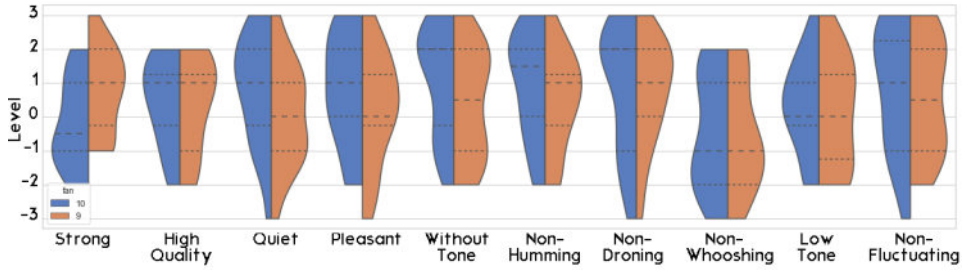

Figure C.1.6: Violin plots for, 7^{th} ranking fan, SM (left) compared to original prototype (right)

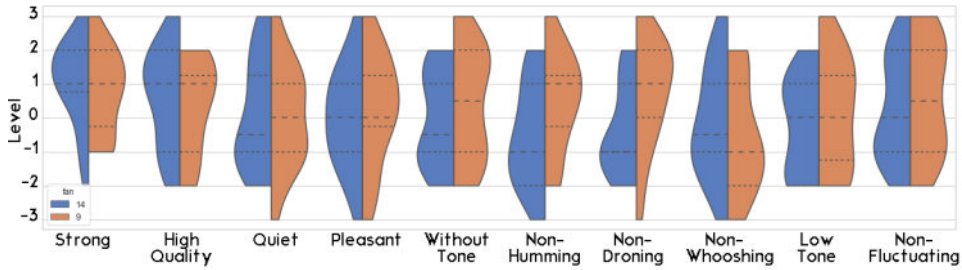

Figure C.1.7: Violin plots for, 8^{th} ranking fan, C-B-S- (left) compared to original prototype (right)

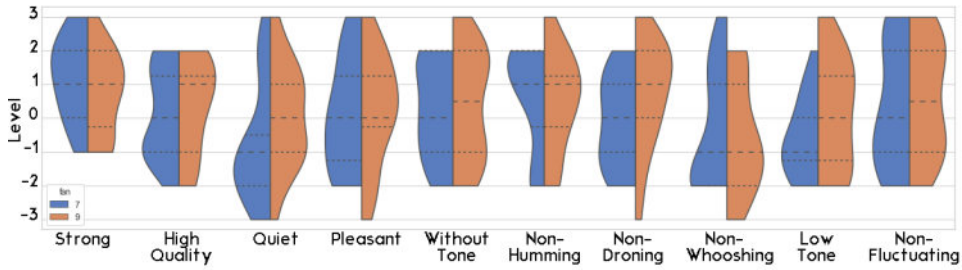

Figure C.1.8: Violin plots for, 9^{th} ranking fan, Cm (left) compared to original prototype (right)

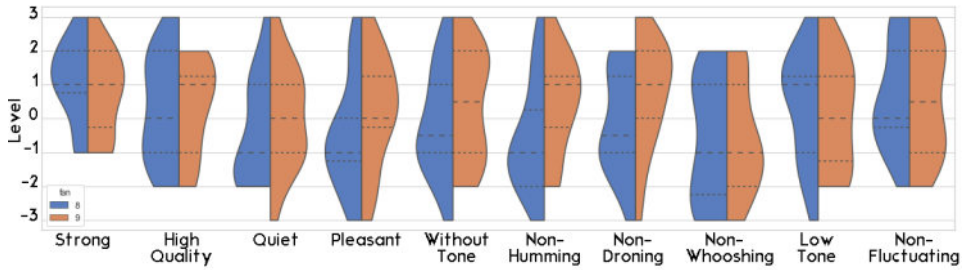

Figure C.1.9: Violin plots for, 11^{th} ranking fan, Sm (left) compared to original prototype (right)

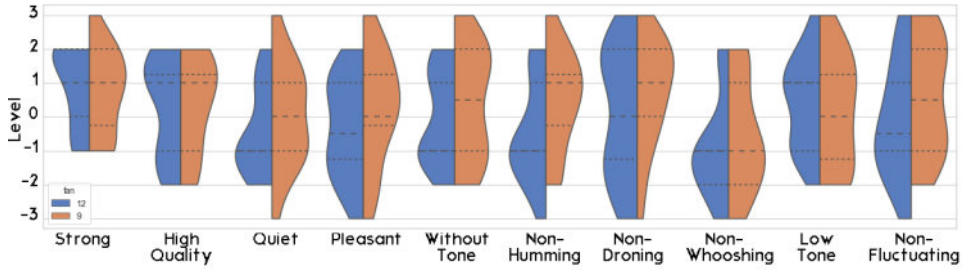

Figure C.1.10: Violin plots for, 12^{th} ranking fan, CM (left) compared to original prototype (right)

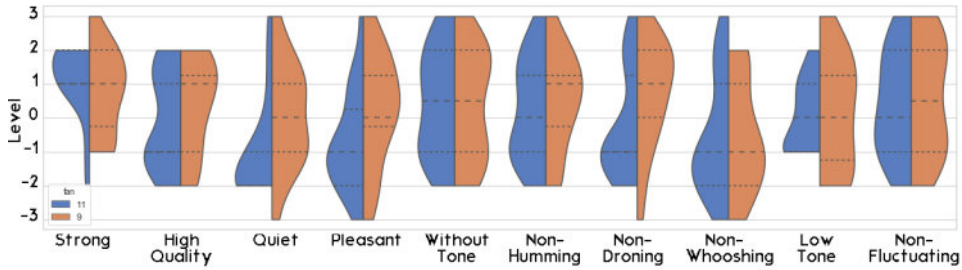

Figure C.1.11: Violin plots for, 13^{th} ranking fan, C-B+S+ (left) compared to original prototype (right)

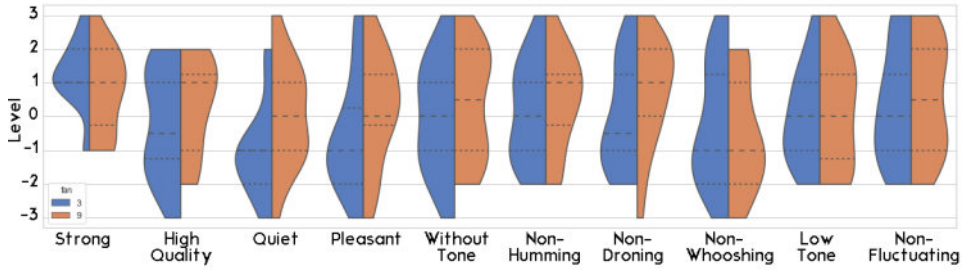

Figure C.1.12: Violin plots for, 14^{th} ranking fan, C-B+S- (left) compared to original prototype (right)

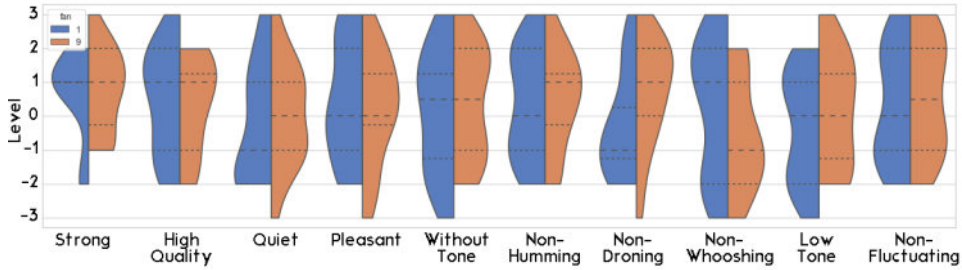

Figure C.1.13: Violin plots for, 15^{th} ranking fan, C+B+S- (left) compared to original prototype (right)

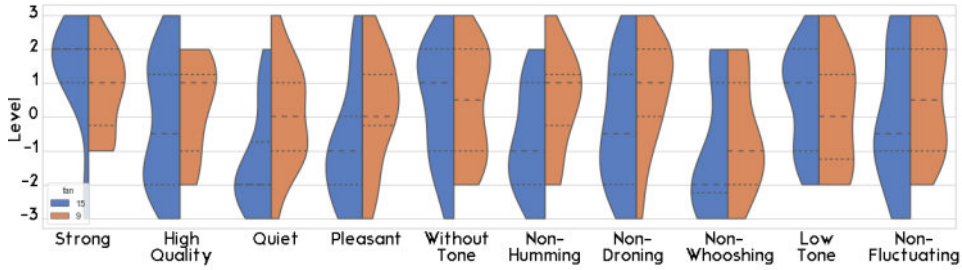

Figure C.1.14: Violin plots for, 16^{th} ranking fan, BM (left) compared to original prototype (right)

C.2 Violin plots showing distribution of tallies

The ranking obtained for the validation set for the forced pairwise comparison test for 20 jurors is given in Figure C.2.1 and Figure C.2.2.

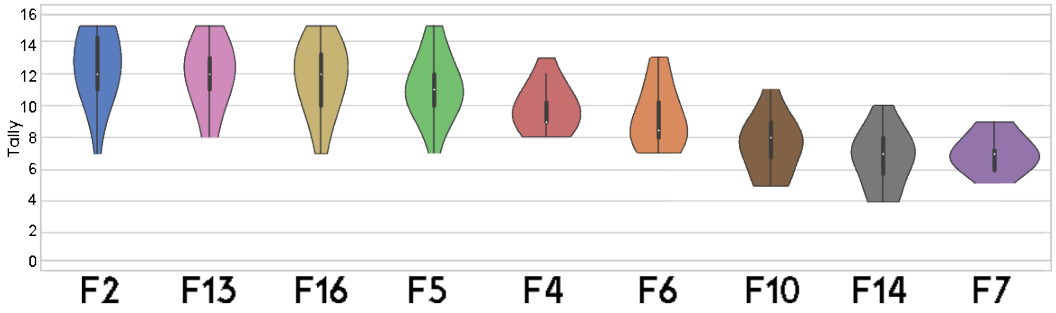

Figure C.2.1: Top ranking fans

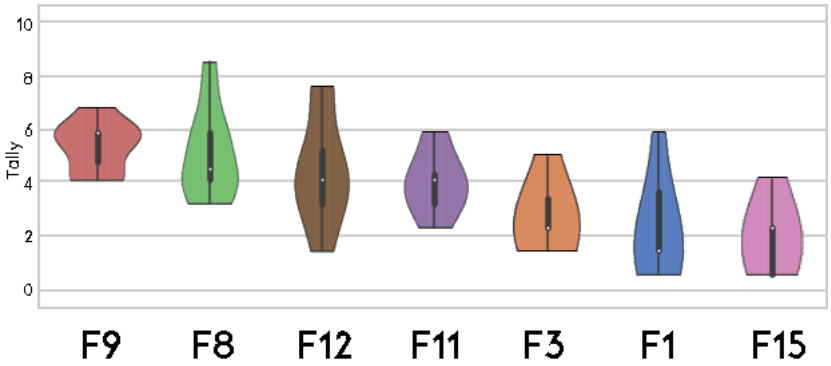

Figure C.2.2: Lower ranking fans

C.3 Optimised fan model

The picture showing the optimised fan model 3D printed and tested is given by Figure C.3.1.

Figure C.3.1: 3D printed optimised fan model

List of References

Amiet, R.K. (1976). Noise due to turbulent flow past a trailing edge. *Journal of sound and vibration*, vol. 47, no. 3, pp. 387–393.

Anghinolfi, D., Canepa, E., Cattanei, A. and Paolucci, M. (2016). Psychoacoustic optimization of the spacing of propellers, helicopter rotors, and axial fans. *Journal of Propulsion and Power*, vol. 32, no. 6, pp. 1422–1432.

Beiler, M. and Carolus, T. (1999). Computation and measurement of the flow in axial flow fans with skewed blades. *Journal of turbomachinery*, vol. 121, no. 1, pp. 59–66.

Bi, J. (2015). *Sensory discrimination tests and measurements: Sensometrics in sensory evaluation*. John Wiley & Sons.

Bianchi, S., Corsini, A., Rispoli, F. and Sheard, A. (2009). Detection of aerodynamic noise sources in low-speed axial fans with tip end-plates. *Proceedings of the Institution of Mechanical Engineers, Part C: Journal of Mechanical Engineering Science*, vol. 223, no. 6, pp. 1379–1392.

Bies, D.A., Hansen, C. and Howard, C. (2017). *Engineering noise control*. CRC press.

Blake, W.K. (2017). *Mechanics of flow-induced sound and vibration, Volume 2: Complex flow-structure interactions*. Academic press.

Box, G.E., Hunter, J.S. *et al.* (1957). Multi-factor experimental designs for exploring response surfaces. *The Annals of Mathematical Statistics*, vol. 28, no. 1, pp. 195–241.

Brown, N.A. (1977). Use of skewed blades for ship propellers and truck fans.

Carter, A., Burrows, R., Sparkes, D. and Turner, R.C. (1960). *The design and testing of an axial-flow compressor having different blade profiles in each stage*. HM Stationery Office.

Clancy, L.J. (1975). *Aerodynamics*. Halsted Press.

Cohen, J. (2013). *Statistical power analysis for the behavioral sciences*. Routledge.

Corsair (2018). Ml120 pro 120mm pwm premium magnetic levitation fan-advertorial-performance curve plots. [Online]. Available: `https://www.corsair.com/corsairmedia/sys_master/productcontent/ML_SERIESadvertorial.pdf` [2019, August 10].

Corsair (2019). Ml120 pro pwm premium magnetic levitation fan - specifications sheet-operating conditions. [Online]. Available: `https://www.corsair.com/us/en/Categories/Products/Fans/Magnetic-Levitation`[2019, August 10].

Cumming, R., Morgan, W.B. and Boswell, R. (1972). Highly skewed propellers.

Cumpsty, N. (1977). A critical review of turbomachinery noise.

Derakhshani, D. and Derakhshani, R.L. (2012). *Autodesk 3ds Max 2013 essentials*. John Wiley & Sons.

Dieter, G.E. and Schmidt, L.C. (2013). *Engineering Design*. Mc Graw Hill.

DIN (2010). 45631/A1, Calculation of loudness level and loudness from the sound spectrum - Zwicker method.

Draper, N.R. and Smith, H. (1998). *Applied regression analysis*, vol. 326. John Wiley & Sons.

Eck, B. (1972). *Fans-Design and operation of centrifugal, axial-flow and cross flow fans*. Pergamon Press.

Edmond, R. (2018). Static pressure vs. high airflow: choosing the right fans for your pc a design guideline for fans. [Online]. Available: `https://www.windowscentral.com/static-pressure-vs-high-airflow-choosing-right-fans-your` -pc.[2019, August 10].

Envia, E. and Kerschen, E. (1984). Noise produced by the interaction of a rotor wake with a swept stator blade. In: *9th Aeroacoustics Conference*, p. 2326.

Envia, E. and Kerschen, E. (1986). Noise generated by convected gusts interacting with swept airfoil cascades. In: *10th Aeroacoustics Conference*, p. 1872.

Fastl, H. and Zwicker, E. (2006). *Psychoacoustics: facts and models*, vol. 22. Springer Science & Business Media.

Feldmann, C., Carolus, T. and Schneider, M. (2017). A semantic differential for evaluating the sound quality of fan systems. In: *ASME Turbo Expo 2017: Turbomachinery Technical Conference and Exposition*, pp. V001T09A001–V001T09A001. American Society of Mechanical Engineers.

Filleul, N.L.S. (1966). An investigation of axial flow fan noise. *Journal of sound and vibration*, vol. 3, no. 2, pp. 147–165.

Fisher, R.A. (1959). Statistical methods and scientific inference. Tech. Rep..

Fletcher, H. and Munson, W.A. (1933). Loudness, its definition, measurement and calculation. *Bell System Technical Journal*, vol. 12, no. 4, pp. 377–430.

Formlabs (2019). 3d printing materials for engineering, manufacturing and product design-rigid-resin material characteristics. [Online]. Available: `https://formlabs.com/materials/engineering/#rigid-resin` [2019, August 10].

Fukano, T., Kodama, Y. and Takamatsu, Y. (1977). Noise generated by low pressure axial flow fans, ii: Effects of number of blades, chord length and camber of blade. *Journal of Sound and Vibration*, vol. 50, no. 1, pp. 75–88.

Fukano, T., Kodama, Y. and Takamatsu, Y. (1978). Noise generated by low pressure axial flow fans, iii: Effects of rotational frequency, blade thickness and outer blade profile. *Journal of Sound and Vibration*, vol. 56, no. 2, pp. 261–277.

Géron, A. (2017). *Hands-on machine learning with Scikit-Learn and TensorFlow: concepts, tools, and techniques to build intelligent systems.* " O'Reilly Media, Inc.".

Glegg, S. and Devenport, W. (2008). The effect of blade thickness and angle of attack on broadband fan noise. *AIAA journal*, vol. 36, no. 93, pp. 1387–1395.

Gudmundsson, S. (2013). *General aviation aircraft design: Applied Methods and Procedures.* Butterworth-Heinemann.

Hanson, D.B. (1985). Near-field frequency-domain theory for propeller noise. *AIAA journal*, vol. 23, no. 4, pp. 499–504.

Head Acoustics (2010). Squadriga ii(code 3320) mobile recording and playback system. [Online]. Available: `https://www.head-acoustics.com/eng/nvh_squadriga_II.htm`[2019, August 10].

HP 3D Scan (2019). Hp 3d scan software pro online instructions. [Online]. Available: `https://support.hp.com/us-en/document/c05286558`[2019, August 10].

Huang, C.-H. and Gau, C.-W. (2012). An optimal design for axial-flow fan blade: theoretical and experimental studies. *Journal of mechanical science and technology*, vol. 26, no. 2, pp. 427–436.

Hutcheson, F.V. and Brooks, T.F. (2006). Effects of angle of attack and velocity on trailing edge noise determined using microphone array measurements. *International Journal of Aeroacoustics*, vol. 5, no. 1, pp. 39–66.

ISO, B. (2011). 10302, acoustics-measurement of airborne noise emitted and structrue-borne vibration induced by small air-moving devices. *International Standard Organization.*

ISO, B. (2012). 3745, acoustics-determination of sound power levels and sound energy levels of noise sources using sound pressure-precision methods for anechoic rooms and hemi-anechoic room. *International Standard Organization.*

Iversen, G.R., Norpoth, H. and Norpoth, H.P. (1987). *Analysis of variance*. 1. Sage.

Jian-Hui, Z. and Chun-Xin, Y. (2008). Design and simulation of the cpu fan and heat sinks. *IEEE Transactions on Components and Packaging Technologies*, vol. 31, no. 4, pp. 890–903.

Kleiner, M. (2011). *Acoustics and audio technology*. J. Ross Publishing.

Lantz, B. (2019). *Machine Learning with R (3rd Edition) - 6.1.3 Correlations*. Packt Publishing.

Li, C., Lin, Q., Ding, X. and Ye, X. (2016). Performance, aeroacoustics and feature extraction of an axial flow fan with abnormal blade angle. *Energy*, vol. 103, pp. 322–339.

McKenzie, A.B. (1997). Axial flow fans and compressors. *Aerodynamic Design and Performance*.

Menus, Q. (2014). Autodesk 3ds max 2014 essentials. autodesk official press.

Metzger, F. and Rohrbach, C. (1986). Benefits of blade sweep for advanced turboprops. *Journal of Propulsion and Power*, vol. 2, no. 6, pp. 534–540.

Minorikawa, G., Yamaguchi, T. and Kihara, M. (2015). Study on evaluation method of tonal noise for small fan. In: *Proc The 22nd International Congress on Sound and Vibration*, pp. 12–16.

Mohammed, K. and Raj, D.P. (1977). Investigations on axial flow fan impellers with forward swept blades.

Muiyser, J., Van der Spuy, J. and A, B. (2018). Comparison of sound quality metrics for axial flow fans with straight and forward swept blades. *Fans 2018*.

Murdock, K. (2015). *Kelly L. Murdock's Autodesk 3ds Max 2016 Complete Reference Guide*. Sdc Publications.

Myers, J.L., Well, A.D. and Lorch Jr, R.F. (2013). *Research design and statistical analysis*. Routledge.

Myres, R. (1976). Response surface methodology, department of statistics, virginia polytechnic institute and state university, blacksburg, virginia, distributed by edwards brothers. *Inc., Ann Arbor, Michigan*.

Nashimoto, A., Fujisawa, N., Nakano, T. and Yoda, T. (2008). Visualization of aerodynamic noise source around a rotating fan blade. *Journal of visualization*, vol. 11, no. 4, pp. 365–373.

Novak, C., Ule, H., Gaspar, R. and Wiley, R. (2005). Use of psychoacoustic metrics for the analysis of next generation computer cooling fan noise. *Canadian Acoustics*, vol. 33, no. 3, pp. 34–35.

Osawa, H. (2015). Fan basics and selection criteria (how to use). *SANYO DENKI Corporation, Ltd., Tech. Rep*, vol. 40.

Osborn, W.M. and Steinke, R.J. (1974). Performance of a 1.15-pressure-ratio axial-flow fan stage with a blade tip solidity of 0.5.

Park, B., Jeon, J.-Y., Choi, S. and Park, J. (2015). Short-term noise annoyance assessment in passenger compartments of high-speed trains under sudden variation. *Applied Acoustics*, vol. 97, pp. 46–53.

Peng, W.W. (2008). *Fundamentals of turbomachinery*. John Wiley & Sons.

Quinlan, D. and Bent, P. (1998). High frequency noise generation in small axial flow fans. *Journal of Sound and Vibration*, vol. 218, no. 2, pp. 177–204.

Ratner, B. (2009). The correlation coefficient: Its values range between+ 1/- 1, or do they? *Journal of targeting, measurement and analysis for marketing*, vol. 17, no. 2, pp. 139–142.

Rossi, F. and Nicolini, A. (2010). Psychoacoustic analysis of squeaking and rattling noises inside vehicle cabins. *Noise Control Engineering Journal*, vol. 58, no. 4, pp. 441–454.

Schneider, M. and Feldmann, C. (2015). Psychoacoustic evaluation of fan noise. *Proc. of Fan 2015*.

Sennheiser (2018). Sennheiser hd6 mix, noise reducing headphones. [Online]. Available: `https://en-uk.sennheiser.com/hd6-mix` [2019, August 10].

Sharland, I.J. (1964). Sources of noise in axial flow fans. *Journal of Sound and Vibration*, vol. 1, no. 3, pp. 302–322.

Smith Jr, L.H. and Yeh, H. (1963). Sweep and dihedral effects in axial-flow turbomachinery.

Snider, J.G. and Osgood, C.E. (1969). *Semantic differential technique; a sourcebook*. Aldine Pub. Co.

Sottek, R. and Genuit, K. (2007). Sound quality evaluation of fan noise based on hearing-related parameters. In: *Proceedings of the Fan Noise Third International Symposium*.

Stewart, J. (2015). Calculus: Metric version.

Sturm, M., Sanjosé, M., Moreau, S. and Carolus, T. (2015). Application of analytical noise models using numerical and experimental fan data. In: *11th European Conference on Turbomachinery, Fluid Dynamics and Thermodynamics, Madrid, Spain, Mar*, pp. 23–27.

Subagyo, A., Basir, B., Malinda, S., Khoerul, A. and Andree, Y. (2019). Performance and noise measurement on the fan cooling system of automotive. *IOSR journal*, vol. 16, no. 1, pp. 01–06.

Swart, D.J., Bekker, A. and Bienert, J. (2018). The subjective dimensions of sound quality of standard production electric vehicles. *Applied Acoustics*, vol. 129, pp. 354–364.

Vad, J. (2008). Aerodynamic effects of blade sweep and skew in low-speed axial flow rotors at the design flow rate: an overview. *Proceedings of the Institution of Mechanical Engineers, Part A: Journal of Power and Energy*, vol. 222, no. 1, pp. 69–85.

Van der Spuy, S.J. (1997). *The design of a low-noise rotor-only axial flow fan series*. Ph.D. thesis, Citeseer.

Wright, T. and Simmons, W.E. (1990). Blade sweep for low-speed axial fans. *Journal of turbomachinery*, vol. 112, no. 1, pp. 151–158.

Yang, L. and Zhu, R. (2016a). Subjective evaluation of cooling fan sound based on grade scoring and paired comparison. In: *2016 International Forum on Energy, Environment and Sustainable Development*. Atlantis Press.

Yang, L. and Zhu, R. (2016b). Research on nonlinear evaluation model of cooling fan sound quality. In: *Proc of the 22nd International Congress on Acoustics; 5-9 September 2016; Beunos Aires, Brazil*. Atlantis Press.

Zenger, F., Münsterjohann, S. and Becker, S. (2017). Efficient and noise reduced design of axial fans considering psychoacoustic evaluation criteria. In: *Applied Mechanics and Materials*, vol. 856, pp. 181–187. Trans Tech Publ.

Zulovich, J., Harner, J., Smith, J. and Pohl, S. (2008). Fans: airflow versus static pressure.